THEORY AND OPERATION OF CAPACITIVE DEIONIZATION SYSTEMS

Ran Zhao

Thesis committee

Promotor
Prof. dr. ir. A. van der Wal
Professor of Electrochemical Water Treatment
Wageningen University

Co-promotors
Prof. dr. ir. H.H.M. Rijnaarts
Professor of Environmental Technology
Wageningen University

Dr. ir. P.M. Biesheuvel
Sub-department of Environmental technology
Wageningen University

Other members
Prof. dr. ir. P.W. Appel, Delft University of Technology
Prof. dr. ir. J. van der Gucht, Wageningen University
Prof. dr. ir. W.T.S. Huck, Radboud University, Nijmegen
Jun.-Prof. dr. V. Presser, Saarland University, Germany

THEORY AND OPERATION OF CAPACITIVE DEIONIZATION SYSTEMS

Ran Zhao

Thesis
Submitted in fulfilment of the requirements for the degree of doctor
at Wageningen University
by the authority of the Rector Magnificus
Prof. dr. M.J. Kropff,
in the presence of the
Thesis Committee appointed by the Academic Board
to be defended in public
on Tuesday 10 September 2013
at 1:30 pm in the Aula.

Table of Contents

List of Publications

In relation to this thesis

Zhao, R., Biesheuvel, P.M., Miedema, H., Bruning, H. & van der Wal, A. *Charge Efficiency: A Functional Tool to Probe the Double-Layer Structure Inside of Porous Electrodes and Application in the Modeling of Capacitive Deionization.* The Journal of Physical Chemistry Letters 1, 205-210 (2010)

Zhao, R., van Soestbergen, M., Rijnaarts, H.H.M., Van der Wal, A., Bazant, M. Z. & Biesheuvel, P.M. *Time-dependent ion selectivity in capacitive charging of porous electrodes.* Journal of Colloid and Interface Science 384, 38-44 (2012)

Zhao, R., Biesheuvel, P.M. & Van der Wal, A. *Energy Consumption and Constant Current Operation in Membrane Capacitive Deionization.* Energy & Environmental Science 5, 9520-9527 (2012)

Zhao, R., Satpradit, O., Rijnaarts, H. H. M., Biesheuvel, P.M. & Van der Wal, A. *Optimization of salt adsorption rate in membrane capacitive deionization.* Water Research 47, 1941-1952 (2013)

Biesheuvel, P.M., Zhao, R., Porada, S. & van der Wal, A. *Theory of membrane capacitive deionization including the effect of the electrode pore space.* Journal of Colloid and Interface Science 360, 239-248 (2011)

Zhao, R., Porada, S., Biesheuvel, P.M., & van der Wal, A. *Energy consumption in Membrane Capacitive Deionization for different water recoveries and flowrates, and comparison with Reverse Osmosis.* Submitted to Desalination (2013)

Other publications

Brogioli, D., Zhao, R. & Biesheuvel, P.M. *A prototype cell for extracting energy from a water salinity difference by means of double layer expansion in nanoporous carbon electrodes.* Energy & Environmental Science 4, 772-777 (2011)

Porada, S., Zhao, R., Van der Wal, A., Presser, V. & Biesheuvel, P.M. *Review on the Science and Technology of Water Desalination by Capacitive Deionization.* Progress in Materials Science, doi: 10.1016/j.pmatsci.2013.03.005 (2013)

Chapter 1   Introduction

Capacitive deionization (CDI) is a newly developed technique for water desalination, where porous carbon is used as electrode material for ion adsorption, which has tremendous potential in desalination of brackish water. However, capacitive deionization is still in its developing stage, of which many aspects need better understanding and in-depth investigation. This thesis deals with characterizing the CDI system, comparing the classical CDI mode with the one with ion exchange membranes (IEMs), i.e. membrane capacitive deionization (MCDI), optimizing the performance of MCDI for different operational modes, and looking into the energy consumption of the MCDI system.

In this introductory chapter, general background information will be given, starting with the challenge to produce fresh water for the world's steadily growing needs, and an overview of the state-of-the-art desalination techniques. Afterwards, it narrows down to the focus of this thesis, i.e. the CDI technology, of which the history and development, and the carbon materials used will be elaborated. Finally the objectives and the outline of this thesis will be depicted.

1.1 The challenge of fresh water supply

Water, H_2O, covering 71% of the earth's surface, is of great importance in maintaining the metabolism of any living creature. Although the total water storage of the earth is 1.4 Gm^3, 97.5% is saline water, and only 2.5% is fresh water. Table 1.1 exhibits a simple classification of natural waters in terms of their saline content, TDS (Total mass of Dissolved Solids) [1].

Table 1.1 Water classification based on salinity content

Type	Total dissolved solids (g/L TDS)
Fresh water	Up to 1.5
Brackish water	1.5–10
Salt water	> 10
Seawater	10–45

Accessible freshwater resources including river, lake and ground water occupy only a tiny fraction of 0.26% of the total freshwater storage [2]**.** Because of the growth of economy and population, withdraw of fresh water for agriculture, industry and daily consumption of humanity is steadily increasing. By 2025, 1.8 billion people will be living in countries or regions with absolute water scarcity, and two-thirds of the world's population could be living under water stress conditions [3]. With increasing groundwater extraction, salt water ingress in wells and aquifers continues. As a consequence, providing clean fresh water in a safe, inexpensive and energy-efficient manner is amongst the most important technological challenges in the coming decades [4-6].

1.2 Desalination technologies

Considering the larger amount of brackish water than that of fresh water in the world, undoubtedly, it is particularly attractive to utilize the various brackish water resources for human consumption in daily use, agriculture, and industry. Over years, a number of desalination technologies have been developed, among which distillation, reverse osmosis, and electrodialysis are the most commonly known and widespread [7]. Here, these widely used techniques will be briefly explained.

1.2.1 Distillation

Distillation occurs on the basis of phase change of water, which requires a significant amount of energy input under ambient conditions (water boiling point=100 ^{o}C at 1 bar). In practice, the boiling point of water can be altered by adjusting the atmospheric pressure to produce the maximum amount of water vapour under controlled conditions. Today, among evaporative desalination processes, Multi Stage Flash (MSF) desalination and Multiple Effect Distillation (MED) are used world widely. In MSF, feed water evaporates in a series of flashing chambers (countercurrent heat exchangers) with decreasing temperature and pressure heated by a steam, which results in the production of large amount of vapour that is then re-condensed on the external surface of a tube bundle. In MED, evaporation occurs on the external surface of a tube bundle which is heated by motive steam condensing inside the tubes. Vapour produced in one effect (stage) then flows into the tubes of the next stage being used to evaporate more water at lower pressure as well as lower temperature. Both MSF and MED can be coupled to vapour recovery devices, in order to enhance the energy efficiency [1].

1.2.2 Reverse Osmosis

Besides the phase change, the separation of fresh water from saline water can also be accomplished by pressure-driven membrane processes. Among these processes, Reverse osmosis is the most widely used, which occupies more than 70% market share for seawater and brackish water desalination in Europe [8]. By pressurizing saline water through a semi-permeable membrane that only allows the permeation of water molecules but not ions or any other dissolved matter, a stream of pure water can be produced as well as a brine stream [1, 8]. Feed pressure is required to overcome the osmotic pressure on the feed side of the membrane. For seawater desalination, the feed pressure commonly ranges from 60-80 bars [9], while for brackish water, the figure is much lower (~20 bar) [10].

1.2.3 Electrodialysis

Like reverse osmosis, electrodialysis [11, 12] is also a membrane based desalination means. However, instead of the usage of semi-permeable membrane, ion-exchange membranes are used. An electrodialysis setup consists of a stack of alternatingly placed anion and cation exchange membranes, with an anode at one end of the stack and a cathode at the other end. During the desalination process, an electrical current is applied between the two electrodes by an external power source, e.g. a battery. Because of the applied electrical current, ions are forced to migrate to their counter-electrode (electrode with the opposite charge, cations to the cathode and anions to the anode). The anions can pass freely through the nearest anion exchange membrane, but their further attempt to reach the anode is blocked by the adjacent cation exchange membrane. Likewise, the cations migrate in the opposite direction, through the nearest cation exchange membrane, but are then blocked by the adjacent anion exchange membrane. As a result, concentrate and dilute streams are formed in the space between the membranes alternatingly.

Electrodialysis is often used for desalinating brackish ground water for use as drinking water [13], and is used in the chemical process industry, in biotechnology and in water pollution control as well [14].

<u>1.2.4 Other desalination technologies</u>

Besides above mentioned desalination means, there are also many novel desalination technologies, and some of them are still in their infancy, for example the production of frozen desalted water by removing the heat from salt solution [1], forward osmosis that utilizes natural osmosis to dilute salt water using a draw solution with higher osmotic pressure than the feed [15], and capacitive deionization.

1.3 Capacitive Deionization

Capacitive deionization (CDI) is a technology for desalination and water treatment in which salts and minerals are removed from salt water by applying an electrical field between two oppositely placed porous carbon electrodes (Fig. 1.1), similar to supercapacitors [16]. Counterions are stored in the electrical double layers (EDLs) which form at the solution interface in the micropores of the porous electrodes, namely cations are stored in the negatively charged electrode (cathode) and anions are stored in the positively charged electrode (anode).

   The employed electrodes in our CDI setup are typically prepared from activated carbon materials with internal areas for ion adsorption in the order of 1000 m^2 per gram (BET area), but other materials are also possible, which will be described in general later in section 1.3.2. The two electrodes are separated by a thin open structured "spacer", or flow channel, through which the water flows. Upon applying an electrical potential difference ("cell voltage") or an electrical current

between the two electrodes, anions are adsorbed into the anode and cations into the cathode, thereby producing a freshwater stream. After the ion adsorption capacity of the electrodes has been reached, the applied cell voltage can be reduced to zero and a small concentrated salt stream is obtained in the ion release-step. In this way the fresh water and the concentrated salt stream are produced intermittently.
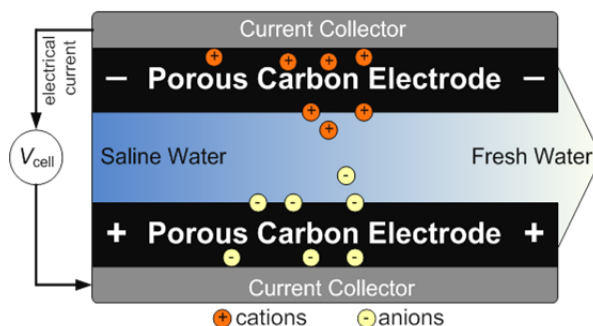
Fig. 1.1. Schematic design of a cell for Capacitive Deionization. Upon applying a voltage difference between two porous carbon electrodes, ions are attracted into the electrode, cations into the negative electrode (cathode, on top), anions into the positive electrode (anode, bottom). As a result, desalinated water is produced. [17]

1.3.1 History of capacitive deionization

In this section an overview of the early phase of CDI development in the 20th century will be given. In 1960s, Blair, Murphy et al., who are the pioneers in the CDI domain, have conceptualized 'electrochemical demineralization of water', [18-21] . During that period, electrodes were classified into cation- and anion-responsive types (analogous to cation- and anion-permeable membranes) according to their "ion-responsiveness", and it was assumed that ions could only be removed from water when specific chemical groups present on the electrode surface are either oxidized to form ionic bonds with cations in the aqueous phase or reduced to

form ionic bonds with anions upon a cell voltage difference is applied. Some years later Evans et al. [22] attempted to explain the fundamental ion removal mechanism of CDI by the electrochemical reactions within the ion exchange mechanism, and it was assumed that the efficiency of the salt removal was determined by the concentration of surface groups.

However, nowadays salt ions being adsorbed in the electrical double layers (EDLs) inside the porous carbon is the most prevalent view on the salt adsorption mechanism of CDI among scientists. Thus, surface groups are considered less relevant, and all electrodes are considered "ion-responsive" for all ions. This modern view has its origin in 1970 when the concept of electrochemical demineralization was made by Johnson et al. [23], where the theory of "potential-modulated ion sorption", similar to the electrical double layer (EDL) theory, was identified as the actual mechanism responsible for ion removal. In the same study the authors stressed that any Faradaic reaction that may occur at the interface between the solid conductive material and the solution side may cause electrode degradation, and from the performance efficiency point of view, these processes are not essential when the current flow is mainly capacitive. A further study by Johnson and Newman [24] described a porous electrode model to analyse ion adsorption in porous carbons, and charge–voltage dependence, which concluded that the ion capacity of the electrode depends on the electrical capacity of the double layer, the available surface area, and the applied cell voltage. Following this concept, extensive studies on this and other topics were initialized by Soffer, Oren and co-workers in the early 1970s, and still continue up to the present time [25-29]. In 1978, Oren and Soffer [26] introduced an idea of "four-action electrochemical parametric pumping cycles" as an effective method to obtain a precise separation between just desalinated water and concentrate (see in Fig. 1.3c).

In 1990s, carbon aerogel materials developed by Farmer et al. drew a lot attention [30]. Since then an increasing number of publications have been focusing on developing effective carbon materials for water deionization. Modern carbon materials for CDI will be briefly introduced in section 1.3.2.

1.3.2 Electrode materials for CDI

As it is the place where ions are stored, electrode plays an important role in the CDI process. In theory electrodes can be fabricated from all conductive and porous materials. However, the selection of electrode materials is normally based on the cost, tunability of porosity, the specific surface area as well as the availability of these materials. In the literature, activated carbons are by far the most used materials due to their low costs (~50 \$/kg), high specific surface area (1000–3500 m^2/g), and high availability (can be derived from natural sources like coconut shells, wood, coal, resins, etc.) [31-35]. Here, in this thesis a commercially available activated carbon material (PAC MM™ 203, Materials and Methods LLC, USA) is used throughout all following chapters. Apart from activated carbon, ordered mesoporous carbons [36, 37], carbide-derived carbons [38, 39], carbon aerogels [27, 30, 40-43], carbon nanotubes [44-46], and graphene [47], etc., can also be used for salt adsorption in the CDI system. Fig. 1.2 provides a selection of images of various carbons used for CDI applications. In Appendix A, we present an overview of salt adsorption in the CDI system with different electrode materials, which exhibits a broad range of salt adsorption capability from 0.6 to 15 mg salt/g electrode weight.
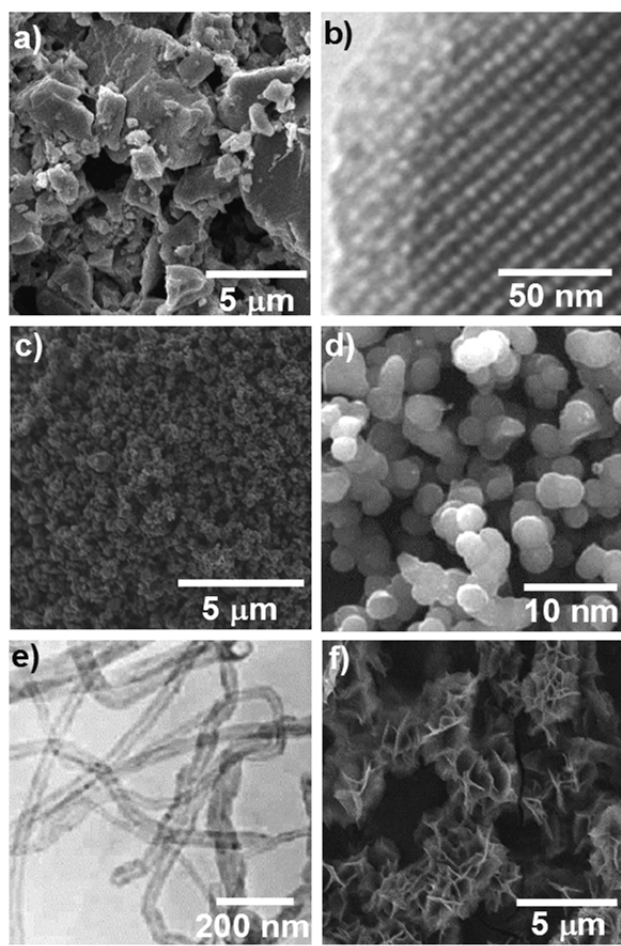
Fig. 1.2. Selection of carbon materials used for CDI. a) activated carbon (Norit DLC Super 30, Norit Nederland B.V., the Netherlands), b) ordered mesoporous carbon [48], c) carbide-derived carbon [49], d) carbon aerogels [50], e) multi-wall carbon nanotubes [44], f) graphene [51].

1.3.3 Geometries for CDI testing based on a two-electrode layout

The classical CDI-geometrical design is comprised of two oppositely placed porous carbon electrodes (between 100 and 500 µm) with a small planar gap in between which allows water flow along the electrodes. This design is known as 'flow-by' CDI, which is schematically sketched in Fig. 1.3. In this geometry, a

typical electrode for laboratory scale experiments is in the range of 5x5 cm^2 to 10x10 cm^2. Such electrodes can be constructed either as freestanding thin films, or can be coated directly onto a flexible current collector such as graphite foil [52, 53]. The planar gap between the electrodes can be an open channel, then typically at least 1 mm in thickness [54], or can be constructed from a spacer material with a high porosity and thickness typically between 100 – 300 µm. The geometry does not strictly require water to enter from one end and to leave at the other. For instance, in this thesis, the water enters from a hole in the centre of a square cell radially, flows outward, and leaves the cell on all four sides, or the reverse.

The second geometry is known as the "flow-through" mode, which directs the water straight through the electrodes, a method applied by Newman and Johnson in Ref. [23, 24] and further developed by Suss et al. [55], see Fig. 1.3b. In this design the feed water is pumped perpendicular to the layered structure, i.e., straight through the larger pores in the electrodes. Compared to the classical "flow-by" mode, this flow pattern can lead to a faster system response (rate of desalination), because ions can direct migrate into the electrodes, instead of diffusing firstly from the spacer channel into the electrodes [55].

The third approach is called "electrostatic ion pumping" [56], see Fig. 1.3c, a method related to the classical technique of "parametric pumping". In electrostatic ion pumping [56], see Fig. 1.3c, feed water is pumped in from the top side, desalinated when passing along the electrodes being stacked in the middle, and the fresh water is then produced on the bottom side. Upon the electrodes are saturated, the system can be regenerated via short-circuiting the electrodes. During the regeneration, the water flow can be reversed, thereby creating a concentrated salt stream (concentrate) on the top side. Thus, the advantage of the electrostatic ion pumping is that always the fresh water and the concentrate can be produced at the same time, unlike in CDI, where those two streams are produced sequentially.

Finally a new design, called "wire-CDI" will be introduced. It employs movable carbon rod electrode wires[57], see Fig. 1.3d. Instead of producing fresh water and concentrate intermittently in the classical "flow-by" or the "flow-through" mode, the fresh water and concentrate streams are separated at all times, right from the start. In the wire-based approach, cell pairs are constructed from wires, or thin rods, with anode wires positioned close to cathode wires. The wire pairs are firstly submerged in the water and upon applying a voltage difference between the anode and cathode wires, salt ions will be adsorbed into their counter electrodes, thereby decreasing the salinity of this stream. After adsorbing salt, the assembly of wires is lifted from the desalinated stream, and immersed into another water stream, upon which the cell voltage is reduced to zero and salt is released. After the salt release, the procedure can be repeated continuously in order to further decrease the salinity in the first stream and increase that in the second stream.
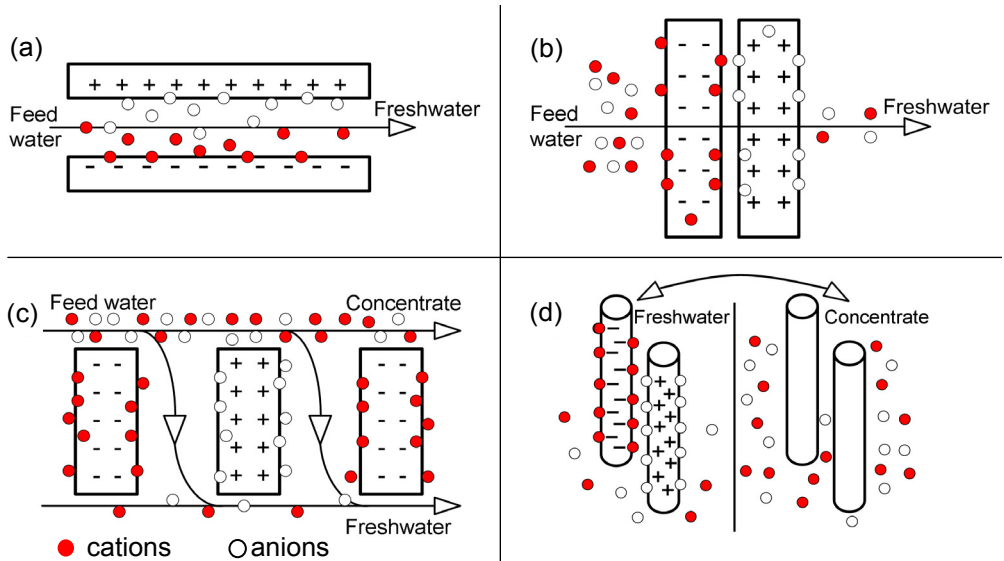
Fig. 1.3. Overview of most relevant CDI system geometries. (a) Flow-by mode, (b) Flow-through mode, (c) Electrostatic Ion Pumping, (d) Desalination with wires. [17]

1.4 Membrane Capacitive Deionization

Membrane Capacitive Deionization (MCDI) is one of the most promising recent developments in CDI, which is also the main focus of this thesis. By definition, MCDI is a combination of conventional CDI with ion-exchange membranes (IEMs) placed in front of the electrodes, see Fig. 1.4. IEMs can be positioned in front of one or both electrodes. IEMs have a high internal charge due to covalently bound groups such as sulfonate or quarternary amines, which allows easy access for one type of ion (the counterion) and block access for the ion of equal charge sign (the co-ion). As will be explained in the thesis (Chapter 3 and 4), addition of IEMs significantly improves desalination performance of the CDI-process, in terms of salt adsorption, charge efficiency and energy consumption. The membranes can be included as stand-alone films of thicknesses between 50 and 200 μm, or can be coated directly on the electrode with a typical coating thickness of 20 μm [52, 58-61].
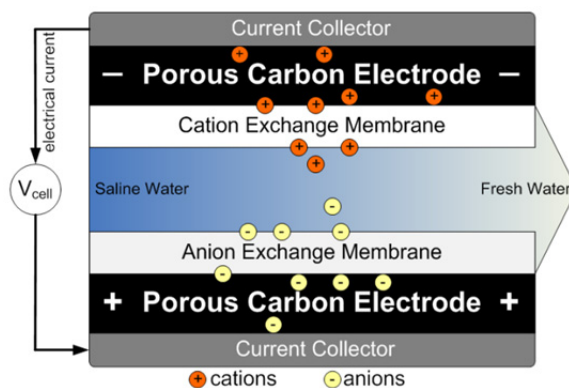
Fig. 1.4. Schematic design of a cell for Membrane Capacitive Deionization, MCDI, where in front of the cathode a cation-exchange membrane is placed, while an anion-exchange membrane is placed in front of the anode.[17]

1.5 Objectives

The objectives of the thesis are to understand the fundamental ion adsorption at equilibrium mechanism of the capacitive deionization technology, to compare the desalination performance between capacitive deionization and membrane capacitive deionization in terms of salt adsorption, charge efficiency, and energy consumption, and to optimize the operational mode in order to achieve the highest salt adsorption rate.

1.6 Aim and outline of thesis

The scope of this thesis covers many perspectives. Firstly it is aimed to investigate a way to probe the fundamental properties of porous carbon electrodes for salt adsorption in capacitive deionization (CDI) process. Why, how and where can the salt ions be adsorbed? Therefore, in **Chapter 2**, a modified Donnan model based on electrical double layer (EDL) theory is proposed, and theoretical results of salt adsorption and charge, etc. at equilibrium state are compared with experimental data. Through the comparison, the EDL properties, namely the Stern layer capacitance, and the micropore volume, can be identified. Those properties are afterwards integrated into a two-porosity (intraparticle micropores and interparticle macropores) transport model, which describes electrokinetics of ion transport during the ion-adsorption step when a voltage is applied between the electrodes, and also during the ion-release step when a short-circuiting condition (zero-volt) is applied.

What happens to the CDI performance when ion-exchange membranes (IEMs) are employed? Can the membrane improve the salt adsorption capacity? As a continuation of **Chapter 2**, **Chapter 3** provides answers to those questions by conducting an in-depth comparison between CDI and membrane capacitive deionization (MCDI), both experimentally and theoretically for a series of

adsorption electrical voltages. It is concluded that MCDI overwhelms CDI not only in salt adsorption capacity but also in charge efficiency. Also it is found that the fact MCDI adsorbs more salt ions than CDI is because the interparticle space (macropores) can also be utilized for salt storage during adsorption because of the presence of the IEMs.

Until now most experiments of either CDI or MCDI were conducted by applying a constant voltage difference between the electrodes during ion-adsorption. However, is it also possible to operate the system by applying a constant current? **Chapter 4** presents the way to operate (M)CDI by applying a constant electrical current. This constant current operation may be more suitable for commercial applications than constant voltage operation, due to its capability to produce an effluent with unchangeable and tuneable effluent concentration. In addition the energy consumption of MCDI and CDI for both operational modes was also compared, which demonstrates that MCDI is more energy-efficient than CDI.

To follow up, **Chapter 5** discusses how to optimize the operation of MCDI for both constant current and constant voltage operational modes in order to achieve highest salt adsorption in a given time period. This chapter can be used as a guideline for designing the most optimum MCDI operational mode for a particular application.

To conclude, **Chapter 6** summarizes and discusses all achievements of the research, discusses possible modifications, compares the energy consumption of MCDI with that of Reverse Osmosis, and recommends future research perspectives.

Chapter 2　Characterization of porous electrodes at equilibrium using the modified Donnan model

Capacitive deionization (CDI) is a novel desalination technology where ions are adsorbed from solution into the electrical double layers formed on the electrode/solution interface in the carbon micropores inside two face-to-face placed porous electrodes. A key property of the porous electrode is the charge efficiency of the electrical double layer Λ defined as the ratio of equilibrium salt adsorption over electrode charge for the 1:1 salt, such as NaCl. We present experimental data for Λ as a function of voltage and NaCl salt concentration and use this data set together with the modified Donnan model to characterize the double layer structure inside the electrode, and determine the microporosity for ion adsorption. In this research we give accurate experimental assessment of these two crucial properties for the NaCl solution, which enables more structured optimization of electrode materials for desalination purposes. In addition, we also present the use of modified Donnan model for more complicated conditions, e.g., $CaCl_2$ solution and NaCl/$CaCl_2$ mixtures.

2.1 Introduction

CDI [7, 19, 20, 24, 25, 27, 37, 39, 52, 62-89] is a technology where an electrical potential difference is applied between two oppositely placed porous electrodes (often activated carbon with internal surface area of the order of 1000 m^2/g). Ions in the aqueous solution flowing through the transport spacer channel, or "flow channel", in between the electrodes, are extracted. Cations are stored in the cathode (the electrode of negative electrical bias) and anions are stored in the anode, as a result, the effluent water will be desalinated to a certain degree. The assembly of electrodes and transport channel is called a "cell", see Fig. 2.1a. CDI is a technology similar to that of electrical double layer (EDL) supercapacitors [62, 74, 90-92], but focuses on salt removal, not on charge storage. In CDI, ions removed from the inflowing solution are stored in the EDLs within the micropores of the porous electrode, and when the ion storage capacity is reached (or a certain percentage thereof), the cell can be short-circuited and ions are again released into the solution leading to a product stream concentrated in ions. CDI is envisioned to be a very energy-efficient water desalination technology especially when the salinity is relatively low such as for brackish water. The lower limit of brackish water is of the order of 10 mM, in which case there is only one ion among 3000 water molecules. Specifically removing these few ions (based on their charge) has the potential to be more energy-efficient than the state-of-the-art technologies, such as distillation and reverse osmosis, which remove all the water molecules. Recently it has been discovered that it is possible to reverse this process ("reverse-CDI") and recoup electrical energy from the salinity difference between sea and river water, using the same experimental setup [93].
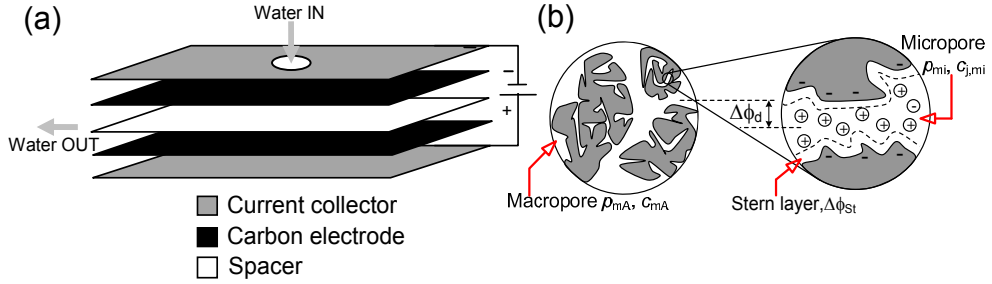
Fig. 2.1. (a) Schematic view of one CDI-cell, (b) graphical description of the modified Donnan model and the two types of porosities inside the porous carbon electrodes. p_{mi} is microporosity, $c_{j,mi}$ is concentration of a certain type of ions j in the micropores, p_{mA} is macroporosity, c_{mA} is concentration of salt in the macropores, $\Delta\phi_{st}$ is the potential drop over the Stern layer, and $\Delta\phi_d$ is the electrostatic potential difference between the micropores and macropores.

To understand the CDI process, the first step is to characterize the porous electrodes which are the core compartments of the cell. In this work we will show how we characterize the porous electrodes, in other words, derive the fundamental properties, e.g., charge efficiency (Λ), volumetric Stern Layer Capacitance ($C_{St,vol}$) and microporosity of the electrode (p_{mi}) by using the experimental equilibrium data of salt adsorption and charge as a function of cell voltage and salt concentration together with the 'modified Donnan model' which is a novel approach from the electrical double layers (EDLs) theory. Both theoretical and experimental results of salt adsorption and charge at equilibrium state will be given, not only for single symmetric (1:1) electrolyte, NaCl, but also the equilibrium adsorption for asymmetric electrolyte, for instance $CaCl_2$ (1:2 electrolyte), and mixtures of NaCl and $CaCl_2$ can be reproduced by the modified Donnan model.

2.2 Experimental section

Experimental data were obtained in a laboratory-scale CDI-stack with 8 cells. As shown in Fig. 2.1a, each cell consists of 2 graphite current collectors (Cixi

Sealing Spacer Material Factory, Ningbo City, China, thickness δ=250 μm, same in all chapters in this thesis), 2 porous carbon electrodes (PAC MM™ 203, Materials and Methods LLC, USA. Note that it is the standard and the only electrode material being used for all experiments in this thesis, of which the thickness δ_{elec}, the total mass m_{tot}, and the electrode density ρ_e vary between different batches in this work, see Appendix B), and a polymer spacer (Glass fibre prefilter, cat no. AP2029325, Millipore, Ireland, δ=250 μm, same in all chapters in this thesis) in between the two electrodes. The graphite current collectors are alternatingly positively or negatively biased. All materials are cut in pieces of 6x6 cm^2 dimension and assembled, after which the entire stack of all layers is firmly pressed together and placed in a Teflon (PTFE) housing. The photos of experimental stack and its compartments are shown in Fig. 2.2. An aqueous solution (NaCl, CaCl$_2$ or the mixtures of NaCl and CaCl$_2$) is continuously pumped through a small squared opening (1.5x1.5 cm^2) located in the exact middle of the stack, and goes radially outward through the spacer layers during the whole experiment period, see Fig. 2.1a (in reality the water flows in from opening "2" and flows out from opening "1", see Fig. 2.2a), or the solution is pumped from all sides of the stack inward through the spacer layers and flows out from the opening in the middle (in reality, the water flows in from opening "1" and flows out from opening "2"; in this chapter, only data from Fig. 2.5 were obtained with this flow direction). There is no difference between these two flow directions with regard to the equilibrium total salt adsorption and total charge transferred, which will be discussed later.
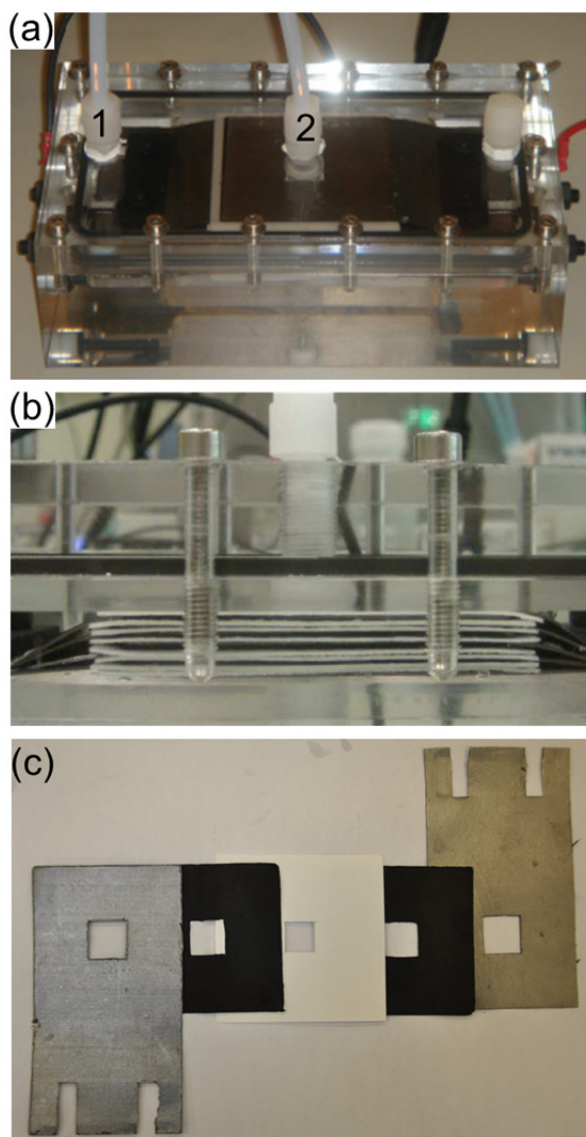
Fig. 2.2. (a) Photograph of the experimental CDI stack, (b) front view of cells stacked in the housing, (c) Sequenced components of one CDI, from left to right: graphite current collector, porous carbon electrode, glass fibre spacer, porous carbon electrode, and graphite current collector.

The experiments consist of two steps: ion-adsorption step and ion-release step. Together they are called one cycle. During the ion-adsorption step, a fixed electrical voltage is applied between the two electrodes. Because of the voltage difference across the cell, ions in the spacer channel are adsorbed into the electrodes. As a result, the effluent concentration c_{eff} decreases, reaches the lowest value, and then gradually increases, see Fig. 2.3a. At the same time, the electrical current decreases towards zero, see Fig. 2.3b. The voltage difference is applied sufficiently long (for single salts 0.5 hr to 2 hrs, for the mixtures up to 5 hrs) in order to assure that the current drops to zero (except for a leakage current) and the effluent salt concentration (ionic strength) returns to the inlet value, when the electrodes are saturated with ions. In this way we ascertain that the double layers everywhere within the electrodes are at equilibrium with the bulk salt solution, of which we know the salt concentration (ionic strength). During the ion-release step, a zero voltage is applied for the same time as the ion-adsorption step. In response, the ions adsorbed in the porous carbon electrode will be released into the spacer channel creating a temporary concentrated stream (Fig. 2.3a). After all adsorbed ions are released and because of the continuous replacement of the salt solution in the spacer channel by the influent, the concentration will drop again to its initial value, see Fig. 2.3a. It is also shown in Fig. 2.3b that the electrical current during the ion-release step will increase from a negative value towards zero.

The electrical voltage and current are applied and measured on-line using a potentiostat (Iviumstat standard, Ivium Technologies, The Netherlands). The measured current signal is integrated with time to obtain the electrode charge, Σ_F, see Fig. 2.3b. In all our experiments, a leakage current, observed as a constant small current (~ several mA) in both ion adsorption- and desorption-step is subtracted from the data. This procedure ensures that the total charge transferred in one direction during ion removal, equals the charge transferred in the opposite direction during ion-release, in other words, the "charge balance" is obtained.

There are two ways to measure the effluent salt (or ion) concentration. First, if the influent stream only contains a single salt, e.g., NaCl or $CaCl_2$, the conductivity of the effluent stream can be simply measured on-line, and be converted into salt concentration according to a calibration curve of salt concentration *vs*. conductivity. Effluent pH is also measured and used to correct the measured conductivity. This is because the total conductivity of a solution is a sum of individual conductivity of all ions present in the solution, according to the Nernst-Einstein equation

$$\Lambda_m^0 = \frac{F^2}{R \cdot T} \sum_j \left(z_j^2 \cdot D_j \cdot c_j \right)$$, where F is the Faraday constant, R is the ideal gas

constant, T is the thermodynamic temperature, z, D and c are the valence, diffusion coefficient and concentration of a specific ion j in the solution, respectively. When the pH is close to 7, the contribution from protons and hydroxyl-ions is rather small (since there concentrations are very low compared to the concentration of salts in the solution), thus can be safely omitted. However, the pH varies during our experiments, and sometimes it can reach very acidic (<4) or basic (>10) condition, then the presence of protons (H^+) or hydroxyl-ions (OH^-) will influence the total conductivity in the effluent solution strongly and cannot be ignored any more. Thus their contributions have to be subtracted (both H^+ and OH^- concentrations can be calculated from the measured pH value) from the measured conductivity of the solution, and afterwards, we can easily obtain the accurate concentration of the salt itself. For the NaCl/$CaCl_2$ mixtures, the concentration of each ion cannot be directly converted from the conductivity because the Na^+/Ca^{2+} ratio vary during the experiments for the multi-ion condition. Thus samples (~2 mL each) from the effluent stream were taken during the whole experiments with a time interval of several seconds, and then ion concentrations were measured by inductively coupled plasma optical emission spectrometry (ICP-OES). In the end, the concentrations of Na^+ and Ca^{2+} ions can also be plotted as a function of time, as is shown in Fig. 2.7. The salt adsorption Γ_{salt} can be calculated from integrating the difference between

the influent salt concentration and the effluent salt concentration (c_{in}-$c_{effluent}$) with time and multiplying with the solution flowrate Φ, see Fig. 2.3a. Obviously, the amount of salt adsorbed must equal the amount of salt released, a condition which we checked to hold during our experiments. We calculate Λ from the independent measurement of the equilibrium salt adsorption, Γ_{salt}, and equilibrium charge Σ ($=\Sigma_F/F$, F is Faraday constant).
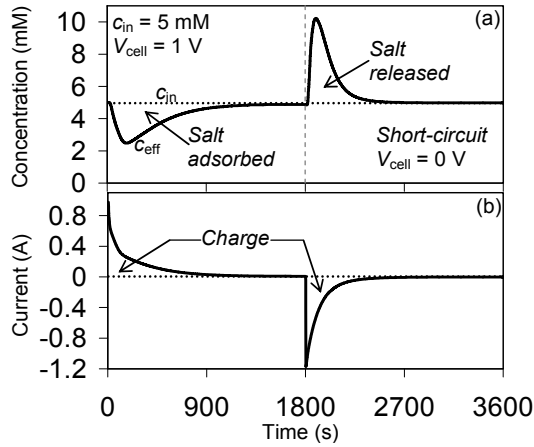
Fig. 2.3. Experimental results of (a) salt effluent concentration c_{eff} (solid line), salt influent concentration c_{in} (dots) and (b) electrical current as a function of time (solid line). Water flowrate Φ = 60 mL/min, influent NaCl concentration is 5 mM, cell voltage V_{cell} = 1 V is applied for half hour, and afterwards the cell is short-circuited (zero voltage is applied) for another half hour.

2.3 Theory of modified Donnan model

In this section we present a model for equilibrium ion adsorption and charge in the CDI cell. The ion adsorption capacity of the electrodes used in CDI is directly related to the volume of micropores. Therefore the electrodes typically are made of porous activated carbons with high porosity, which in our case are obtained via the fitting procedure by the modified Donnan model. Just as important is the nanoscale structure of the electrical double layers (EDLs) which form within

the micropores of the electrode. To understand ion adsorption within the EDLs, previously the classical Gouy-Chapman-Stern (GCS) model was used to describe equilibrium adsorption of salt and charge in porous electrodes as a function of cell voltage and ion strength [63, 64, 93-96]. The GCS-model assumes a diffuse layer (besides an inner, Stern layer) which has a typical extension into free solution of several times the Debye length (which is ~3 nm at 10 mM salt concentration). Note that the GCS model will be briefly explained in Appendix E. However, the micropores in porous activated carbon electrodes are small (less than 2 nm) and diffuse layers must be overlapping strongly [74, 75, 97]. This led us to use a novel approach which is called "modified Donnan (mD) model", see Fig. 2.1b. In the mD model, it is assumed that within the carbon particle the pore space has a constant electrostatic potential. This is a reasonable assumption because the Debye length is in most situations much larger than the micropore size. Compared to the classical Donnan approach used for charged gels, membranes, sedimentation of charged colloids [98], clays [99, 100] and porous electrodes [101], we make two modifications: firstly, we include the charge-free Stern layer in between the pore solution and the carbon matrix, and secondly we consider an additional attractive force for the ion to go from the macropores into the micropores, described by a chemical attraction of strength μ_{att}. In this way it will be possible to include in the model the fact that even at zero voltage, neutrally adsorbed salt already exist in the carbon material. This adjustment is also required because as shown in Fig. 2.4b (to be discussed further on) we measure a co-ion expulsion from the carbon particles, which cannot be explained in the absence of the chemical attraction (i.e., for $\mu_{att}=0$). In the present work we use for the cation and the anion the same value for μ_{att} to preserve symmetry between the two electrodes in the theory, but it is more likely that in reality the two numbers are different for each ion, and will also be different for different ions of the same sign [102].

Since we model a CDI cell consisting of two electrodes, firstly the voltage drop between the two electrodes across the cell, $V_{cell} = V_{anode} - V_{cathode}$, has to be explained. In this thesis the CDI cell, and the MCDI cell in later chapters are assumed to be perfectly symmetrical, which means equal values for electrode mass, porosities p, volumetric Stern capacity $C_{St,vol}$, and chemical attraction μ_{att} are taken for both electrodes. In addition, no pre-charge on the electrode exists. An overall equation to express the distribution of the cell voltage over all elements between in the cell is given by

$$V_{cell}/V_T = (\Delta\phi_d + \Delta\phi_{St})_{micropores,anode} + \Delta\phi_{elec,anode} + \Delta\phi_{sp} + \Delta\phi_{elec,cathode} - (\Delta\phi_d + \Delta\phi_{St})_{micropores,cathode} \quad (2.1)$$

where V_{cell} is the cell voltage, V_T is the thermal voltage ($=RT/F\sim25.7$ mV at room temperature), all $\Delta\phi$'s are dimensionless voltage drops for different elements in the sub-cell: $\Delta\phi_{sp}$ is the voltage drop across the spacer channel, $\Delta\phi_{elec}$ is the potential drop in the electrode, and $\Delta\phi_d$ and $\Delta\phi_{St}$ are Donnan potential and the Stern layer potential in the micropores, to be discussed further on. Note that under the equilibrium conditions, there is no current between the two electrodes, which means the voltage drop across the spacer channel ($\Delta\phi_{sp}$) and in the electrode ($\Delta\phi_{elec}$) vanishes. These terms, $\Delta\phi_{sp}$ and $\Delta\phi_{elec}$, will be elaborated later in the (M)CDI process model in Chapter 3, as they are changing variables in relation to current which are used to model the capacitive deionization process. Therefore Eq. 2.1 can be simplified to

$$V_{cell}/V_T = \left(\Delta\phi_d + \Delta\phi_{St}\right)_{micropores,anode} - \left(\Delta\phi_d + \Delta\phi_{St}\right)_{micropores,cathode} \quad (2.2)$$

Eq. 2.2 is a general equation which can be used for any combination of ions in the electrolyte. When only a simple 1:1 salt, NaCl, as the electrolyte is used, and equal masses of electrode are used without chemical pre-charge [88], the voltage drops in the micropores for anode and cathode can be assumed to be mirror images of one another (only the sign is different). Thus the voltage drop across the cell between two electrodes can be further simplified to

$$\tfrac{1}{2}V_{cell} \, / \, V_T = \left(\Delta\phi_d + \Delta\phi_{St} \right)_{micropores} \qquad\qquad (2.3)$$

Next, within the electrodes we assume that the porous carbon electrode consists of two types of porosities, macropores and micropores. The macropores, with porosity of p_{mA} (macropore volume per unit total electrode volume), are interparticle space, where the transport of ions across the electrode takes place. The micropores are where the counterions are preferentially stored, and where the electrical double layers (EDLs) form. The pore size of the micropores is typically a few nanometers.

In the macropores, the sum of the product of charge number and concentration of all ions $\displaystyle\sum_j z_j c_{j,mA}$ (j denotes a specific type of ions) is always zero. In the case of a single symmetric electrolyte, e.g., NaCl, $c_{cation,mA}$ has the same concentration as $c_{anion,mA}$, thus the salt concentration c_{salt} (per unit of macropore volume) is equal to the concentration of both cation and anion. In the equilibrium state (electrodes are saturated with ions for a given influent salt concentration in the spacer channel and a fixed cell voltage), the salt concentration in the macropores c_{mA} is the same as the influent salt concentration (bulk concentration). And thus, for modelling salt adsorption and charge at equilibrium state, the macropores can be omitted. Micropores are the pores inside the carbon particles, which have a porosity of p_{mi} (micropore volume per unit total electrode volume), in which the cation concentration, $c_{cation,mi}$ can differ from the anion concentration, $c_{anion,mi}$ (ion concentration per unit of micropore volume). As the size of the micropores is smaller than that of the Debye length (a length scale to characterize the thickness of the diffuse part of the double layer in the classical Gouy-Chapman-Stern theory for a single double layer), the EDLs will overlap strongly, which influences the ion distribution. This allows us to use the mD approach of assuming a constant electrostatic potential in the micropore space relative to that in the macropores, $\Delta\phi_d$,

and to relate the ion concentration in the micropores to that in the macropores, by assuming equal chemical potential of ions in micro- and macropores, according to

$$c_{j,mi} = c_{j,mA} \cdot \exp\left(-z_j \cdot \Delta\phi_d + \mu_{att}\right), \tag{2.4}$$

where $c_{j,mA}$ is the macropore concentration of a specific type of ions (for solution containing only symmetric salt, e.g., NaCl, $c_{j,mA}$ is equal to the salt concentration c_{mA} in the macropores), z_j is the charge number of ions, for example, $z_j = +1$ for Na$^+$, and $z_j = -1$ for Cl$^-$, and where μ_{att} is an attractive term which quantifies the chemical attraction between ions and the carbon material. In order to keep symmetry and simplicity in the present model, we will use the same value of μ_{att} for both the cation (Na$^+$) and the anion (Cl$^-$), though in a generalized model this assumption can be relaxed. In Eq. 2.4, $\Delta\phi_d$ is the Donnan potential difference between inside (micropores) and outside (macropores) of the porous carbon particle. The sum of the concentration of each ion multiplied by its charge number is defined as the 'charge concentration', which is negative in the anode, and positive in the cathode. At Eq. 2.5, this ionic charge is assumed to be homogenously distributed across the electrode without gradients, which is locally compensated by an equal amount of electronic charge in the carbon matrix (with opposite sign). In addition, as charge neutrality always holds in the micropores, the volumetric charge density can be defined as

$$c_{charge,mi} = \sum_j z_j c_{j,mi} \; . \tag{2.5}$$

According to the Donnan approach, the EDLs inside the micropores of the porous electrode are composed of the electrolyte-filled pore, where ions are accumulated, and a charge-free Stern layer being located on the surface of the micropores, where no ion is present. The electrical potential difference across the Stern layer $\Delta\phi_{st}$ is related to the charge concentration $c_{charge,mi}$, given by the Gauss equation,

$$c_{charge,mi} \cdot F = -V_T \cdot \Delta\phi_{St} C_{St,vol}, \tag{2.6}$$

where F is the Faraday constant (96485 C/mol), and $C_{st,vol}$ is the volumetric capacitance of the Stern layer. For $C_{St,vol}$, we use the empirical expression

$$C_{St,vol} = C_{St,vol,0} + \alpha \cdot c_{charge,mi}{}^2 , \tag{2.7}$$

where the second term makes $C_{St,vol}$ go up slightly with micropore charge, which can be explained by the higher attractive force that acts across the Stern layer at high charge [103, 104].

The set of equations above describes the ion distribution in the EDLs in the micropore of the electrodes at the equilibrium state, and thus predicts the total ion concentration in the micropores and the micropore charge density. These micropore concentrations can be converted to measurable properties, namely the charge Σ_F in C/g and in total ions adsorbed Γ_i (mol/g) by multiplying with the geometry factor, to be explained below. Note that in this thesis, charge is either described by Σ_F in C/g or by charge Σ expressed in mol/g. They are related according to $\Sigma_F = \Sigma \cdot F$ where F is Faraday's constant, F=96485 C/mol.

To get the ion adsorption Γ_j in a two electrode cell for one specific ion, we need to first add up its concentrations from both anode and cathode, and then multiply with the geometry factor $\dfrac{1}{2} p_{mi} \rho_e^{-1}$, where p_{mi} is the microporosity of the electrode, ρ_e is the overall mass density of the electrode, and 2 denotes an average property for the two electrodes), the adsorption of a specific ion is given by

$$\Gamma_j = \frac{1}{2} p_{mi} \rho_e^{-1} \cdot \left[\left(c_{j,mi} - c_{j,mi}^0 \right)_{anode} + \left(c_{j,mi} - c_{j,mi}^0 \right)_{cathode} \right] , \tag{2.8}$$

where the superscript '0' refers to the ion concentration at a cell voltage of V_{cell}=0. For 1:1 salts like NaCl, $\Gamma_{salt} = \Gamma_{Na} = \Gamma_{Cl}$. In case of symmetry, the concentration of adsorbed Na^+ at one electrode is equal to the amount of adsorbed Cl^- at the other electrode. For instance, $c_{Na,mi,anode} = c_{Cl,mi,cathode}$, and $c_{Na,mi,cathode} = c_{Cl,mi,anode}$. Thus

based on Eqs. 2.4 and 2.8, the salt adsorption can be further simplified to

$$\Gamma_{salt} = \frac{1}{2} p_{mi} \rho_e^{-1} \cdot \left(c_{counter,mi} - c_{counter,mi}^0 + c_{co,mi} - c_{co,mi}^0 \right),$$ (2.9)

Similarly for the equilibrium ionic charge, the general equation is given by

$$\Sigma = \frac{1}{2} p_{mi} \rho_e^{-1} \cdot c_{charge,mi} = \frac{1}{2} p_{mi} \rho_e^{-1} \cdot \sum_j z_j c_{j,mi} ,$$ (2.10)

and for the 1:1 salt, together with Eq. 2.4, Eq. 2.10 can be converted to

$$\Sigma = \frac{1}{2} p_{mi} \rho_e^{-1} \cdot \left(c_{counter,mi} - c_{co,mi} \right).$$ (2.11)

Being a ratio of salt adsorption to charge transferred onto the electrodes, the charge efficiency is defined as

$$\Lambda = \frac{\Gamma_{salt}}{\Sigma}.$$ (2.12)

Eqs. (2.9), (2.11), (2.12) present the way to obtain values for Γ_{salt}, Σ, and Λ by data analysis. Combing these equations with Eq. 2.4 defined in the EDL mD model, Eqs. (2.9) and (2.11) can also be expressed as

$$\Gamma_{salt} = p_{mi} \rho_e^{-1} \cdot c_{mA} \cdot \exp(\mu_{att}) \cdot (\cosh \Delta\phi_d - 1),$$ (2.13)

$$\Sigma = p_{mi} \rho_e^{-1} \cdot c_{mA} \cdot \exp(\mu_{att}) \cdot \sinh \Delta\phi_d .$$ (2.14)

Taking the ratio of Eq. 2.13 over Eq. 2.14, the charge efficiency is then calculated as

$$\Lambda = \tanh \frac{\Delta\phi_d}{2}.$$ (2.15)

2.4 Results and Discussion

2.4.1 Theoretical and experimental results for NaCl

Previous studies on porous electrode characterization focused on electrode charge (or, capacitance), often only at low cell voltages and for one, often high value of the ionic strength. Though from such a limited data set it is in principle possible to simultaneously derive the effective microporosity for ion storage, p_{mi}, and the Stern layer capacity, C_{St}, this is relatively inaccurate and has not been applied much. Therefore, questions like which part of the activated carbon is actually available for ion and charge storage, and do only pores in a certain size-range contribute to the adsorption process, are still a matter of debate. Related to that, available experimental data can hardly be used to accurately validate models for the EDL structure of porous materials. Obviously, the current situation hampers the design and effective optimization of (the structure of) electrode materials, for instance for desalination purposes.

In this section we analyse an alternative procedure that instead of only focusing on capacitance considers and combines data for charge Σ with data for the equilibrium salt adsorption from solution into the EDLs inside the electrode, Γ_{salt}. Importantly, Σ and Γ_{salt} are recorded simultaneously and independently. At first sight one may have the impression that measuring Γ_{salt} simultaneously with Σ will be superfluous. This idea may arise from the assumption that each electron charge will be fully charge-balanced by counterion adsorption. If so, this would imply indeed that the transfer of one electron from one electrode to the other is accompanied by the precise removal of one salt molecule out of the bulk solution. This is however not the case because simultaneously with counterion adsorption, co-ions are excluded from the double layer [24, 25, 63, 64, 69, 73, 93, 105]. The effect of co-ion exclusion reduces the ratio of Γ_{salt} over Σ, a ratio which we call the

charge efficiency, Λ. Theoretically, for very low potentials in the electrode micropores, counterion adsorption and co-ion desorption are actually of equal importance, i.e., for each electron transferred, there is half a cation adsorbed and half an anion desorbed and thus Λ will be close to zero, while for very high potentials the limit is approached that counterion adsorption fully compensates the electron charge and $\Lambda \rightarrow 1$. As we will show, data for Λ as a function of voltage and ionic strength are an excellent probe to test models for the structure of the double layer inside the porous electrode, without prior knowledge of the micropore porosity for ion adsorption. Actually, after having established that a certain double layer model accurately describes data for Λ, the micropore porosity p_{mi} can be directly determined from a simple fit to the full data sets of both Γ_{salt} and Σ. The use of Λ to determine double layer properties points to the fact that salt adsorption per volume is a basic characteristic of double layers, as much as electrode charge, independent of electrode porosity, weight or density.

Thus, the objective of the present chapter is to show that both p_{mi} and $C_{St,vol,0}$ (volumetric Stern layer capacitance at low charge limit) of porous electrodes can be accurately derived experimentally from two independently obtained data sets for equilibrium salt adsorption and electrode charge, both assessed as a function of ionic strength and cell voltage. These two parameters, in turn, are used as input parameters in an electrokinetic CDI process model in Chapter 3. Note that the theoretical parameter settings ($C_{St,vol,0}$, μ_{att}, α and p_{mi}) for data in Figs. 2.4, 2.5 and 2.6 are given in Appendix B.

Fig. 2.4a shows measured values for Λ based on data for equilibrium charge Σ and salt adsorption Γ_{salt}, as a function of cell voltage and ionic strength. These experimental findings confirm the behaviour of Λ predicted by Donnan theory in that Λ increases with increasing cell voltage, and, in addition, that at each cell voltage, Λ is higher when the ionic strength is lower. For the theoretical curves in

Fig. 2.4a, we use an optimized set of values of $C_{St,vol,0}$, μ_{att} and α (Appendix B), which results in a fairly good model fit for the charge efficiency. The micropore porosity p_{mi} now immediately follows from the model fitting to the full data sets of Σ_F (Fig. 2.4c) and Γ_{salt} (Fig. 2.4d), which are well described using a value of $p_{mi}{\sim}37\%$ of the total electrode volume, which is a very realistic number.
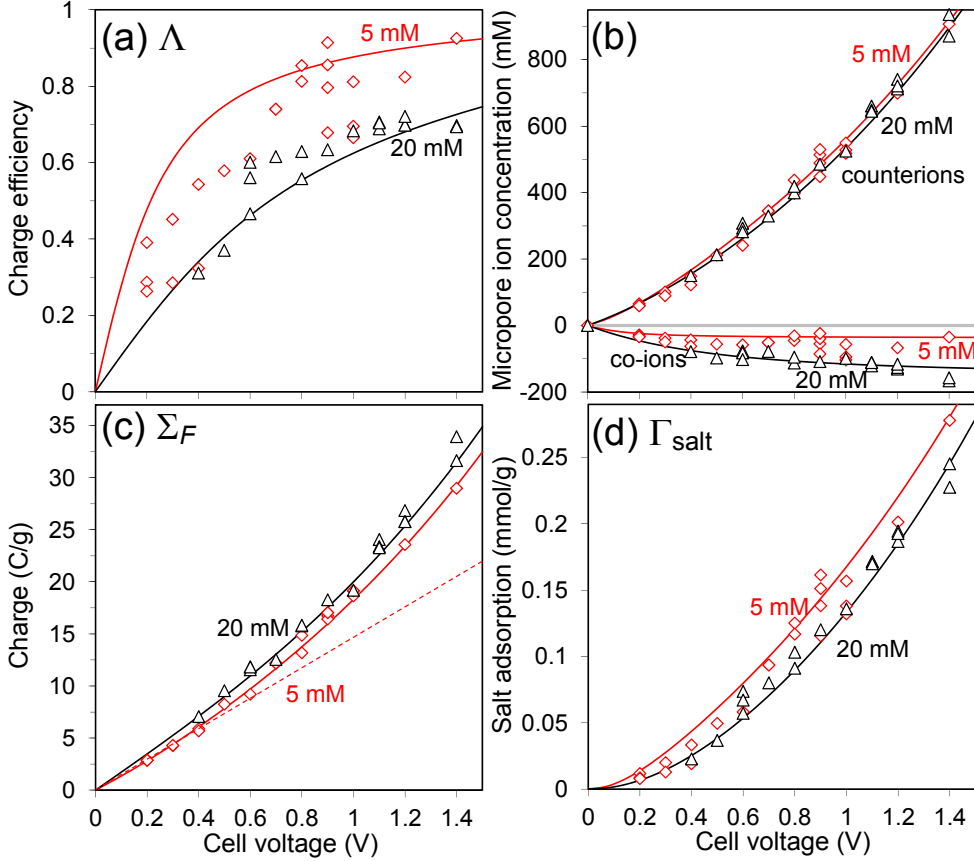
Fig. 2.4. (a) Charge efficiency as a function of cell voltage for 5 mM and 20 mM NaCl solution [106]. (b) Concentration of counterions and co-ions in porous carbon micropores [107]. (c) Equilibrium electrode charge as a function of cell voltage and ionic strength [106]. (d) Equilibrium salt adsorption as a function of cell voltage and ionic strength [106]. (diamonds: 5 mM; triangles: 20 mM; lines: theory curves). Theoretical curves are based on Eqs. 2.1-2.12. In panel (b) concentrations are given per unit micropore volume, relative to the adsorption at zero cell voltage.

The dashed line in Fig. 2.4c identifies the differential capacitance in the low-voltage limit, $C_{D,V \to 0}$ which is ~56 F/g when defined per single electrode mass and based on half the cell voltage, as usual in literature of electrodes for electrical double layer capacitors (EDLCs). This result is in the range of reported literature values [108, 109]. Furthermore, Fig. 2.4c shows that $C_{D,V \to 0}$ is an underestimate of C_D-values at higher voltages and that it is a function of ionic strength.

The data of Fig. 2.4c,d can be recalculated to obtain the volumetric ion concentration in the micropores of the electrode together with Eq. 2.9. In the case of 1:1 salt solution, combining Eqs. 2.9 and 2.11, the counterion and co-ion micropore concentrations can then be derived as

$$c_{\text{counter,mi}} - c^0_{\text{counter,mi}} = \left(\Gamma_{\text{salt}} + \Sigma \right) \cdot \rho_e / p_{\text{mi}} \quad , \quad c_{\text{co,mi}} - c^0_{\text{co,mi}} = \left(\Gamma_{\text{salt}} - \Sigma \right) \cdot \rho_e / p_{\text{mi}} \; . \qquad (2.13)$$

As a result, Fig. 2.4b shows micropore concentrations of counterions and co-ions. Note that in Fig. 2.4b micropore concentrations are given, relative to the ion concentrations at zero cell voltage, which at this condition are given by $c_{V\text{cell}=0}=c_\infty \cdot \exp(\mu_{\text{att}})$, i.e., $c_{V\text{cell}=0}=37$ mM and 148 mM for $c_\infty=5$ mM and 20 mM, respectively. The concentration of the counterions in the micropores increases as the cell voltage increases. For the co-ions we observe that the concentration (relative to zero voltage) is negative, which is as expected, because the co-ion is expelled from the EDLs. But, unexpectedly this co-ion concentration is in magnitude much larger (namely up to values of the order of 150 mM) than the expected pore concentration at zero voltage (which is equal to the concentration in the spacer channel in these equilibrium experiments, either 5 or 20 mM for the data in Fig. 2.4b). This is a very remarkable finding, which may prove to be an important piece of information in finding a proper EDL-model for porous electrodes in contact with aqueous solutions. We interpret these highly negative co-ion concentrations as being due to the fact that also without applying a cell voltage,

there is salt adsorption in the porous carbon particles due to a chemical affinity of the ions with the porous carbon. Upon applying the voltage, the co-ions of these chemically adsorbed salt molecules are expelled. This effect can only be found by using non-zero values of the attractive term μ_{att}. This assumption of a chemical attraction of ions into the micropores of activated carbon particles is supported by the fact that porous carbons are known to adsorb ions, also in the absence of an applied voltage [86].

In Fig. 2.4c and d, both data and theory show how for a given applied cell voltage, and when the ionic strength is reduced, we require less charge but still we adsorb more salt (i.e., Λ is higher at lower ionic strength). This conclusion seems to show that CDI is expected to be most promising for aqueous solutions of relatively low ionic strength. To exemplify, a much broader spectrum of NaCl salt concentration ranging from 0 to 100 mM was made both experimentally and theoretically, which suggests that the equilibrium charge goes up with the increase of salt concentration (Fig. 2.5). At the same time for salt, the salt adsorption only increases at the very beginning of the salt concentration spectrum (~ from 2.5 mM to 5 mM), and then it decreases in the salt concentration range of 5 mM to 40 mM, afterwards it levels off. The difference between theory and experimental data in Fig. 2.5 demonstrates that further modification is necessary, e.g. by making μ_{att} a function of $c_{j,mi}$ (see section 6.2.3).
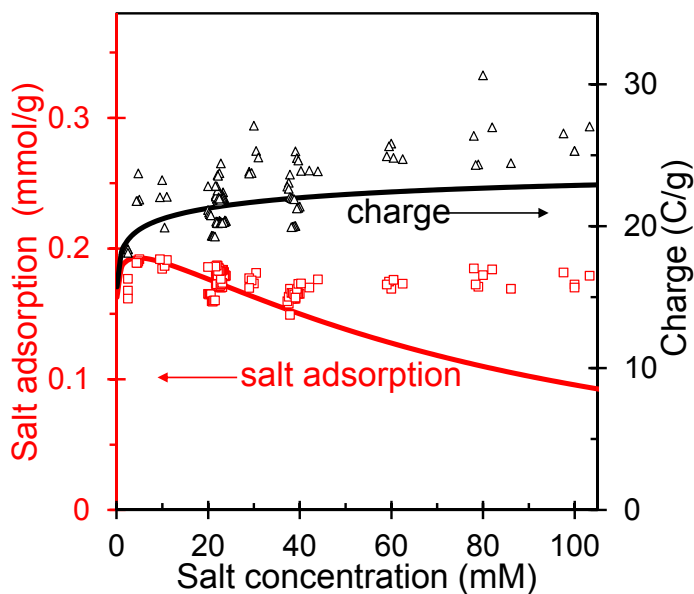
Fig. 2.5. Equilibrium data and theory for salt adsorption and charge (per gram of all electrodes) in CDI as a function of salt concentration (V_{cell}=1.2 V) [107].

2.4.2 Theoretical and experimental results for CaCl$_2$, and NaCl/CaCl$_2$ mixtures

Next, we will show that the mD model can also be used for asymmetric salt CaCl$_2$ and mixtures of NaCl and CaCl$_2$. Fig. 2.6a and b shows results for the equilibrium adsorption of CaCl$_2$ in porous electrode pairs. As expected, we find that salt adsorption and charge increase with cell voltage for the CaCl$_2$ salt concentrations of 5 mM and 20 mM. Fig. 2.6c shows the adsorption behaviour in mixtures of salts. Here we analyze the adsorption from a mixture of 5 mM NaCl and 1 mM CaCl$_2$ solution. Note that Fig. 2.6c shows adsorption data for the salt mixture for different durations of the adsorption step, namely 1 h and 5 h. For the 1 h experiment, the measured effluent ion concentration as a function of time is given in Fig. 2.7.

In Fig. 2.7, directly after applying the cell voltage, both the effluent concentration of Ca^{2+} and Na^{+} decrease rapidly. After this initial decrease in

effluent concentration, the electrodes start to saturate gradually, leading to increasing effluent concentrations, eventually converging back to their inlet values. Remarkably, all this time, up to the end of the adsorption step, the Ca^{2+}-concentration remains clearly below its inlet concentration of 1 mM, whereas the Na^+-concentration increases to beyond its inlet concentration of 5 mM and stays above it until the end of the adsorption step, a phenomenon also observed in ref. [110]. This behaviour is not witnessed in any of the single salt experiments, neither NaCl nor $CaCl_2$. This is a clear signature of a replacement process, in which the composition of the EDLs, initially predominantly containing Na^+, is slowly modified toward the final equilibrium composition which is dominated by Ca^{2+}.

The fact that in the end more Ca^{2+} is adsorbed than Na^+ is also evident from the effluent concentration profile during the desorption step, starting at 1 hr in Fig. 2.7, since the Ca^{2+}-peak during desorption is ~40% larger than the Na^+ release peak. Thus, the data in Fig. 2.7 show that Na^+ is first adsorbed into the EDLs in the electrodes but after ~10 min is being replaced again by Ca^{2+}, even though the cell voltage is still applied.

Contrary to the single-salt experiments described above, an experimental duration of 1 h turned out to be insufficient to reach equilibrium (both ions' concentrations did not converge to their initial values), so the adsorption was extended to 5 h, when the individual ion adsorptions reach values consistent with the fitted equilibrium theory, see Fig. 2.6c. Because the 5 h adsorption step is very long, the data were obtained by analysing the effluent samples during the desorption step. We assume that after 5 h, we have reached adsorption levels that are close to equilibrium. Fig. 2.6c shows that Ca^{2+} ions are preferably adsorbed by the electrodes than the Na^+ ions. This is because Ca^{2+} ion has a higher valence (+2) than the Na^+ ion (+1), although the influent concentration of Na^+ ions is five time that of the Ca^{2+} ions. Parameter settings of Fig. 2.6 are given in Appendix B. In Fig. 2.6, lines present results of the mD model, and as can be observed for mixtures we

can fit the data relatively well, using the same parameter settings that also describe data for pure $CaCl_2$-solutions, which suggests that the mD model is a useful tool to describe experimental data for the equilibrium structure of the EDL in porous electrodes in contact with mixtures of salts.
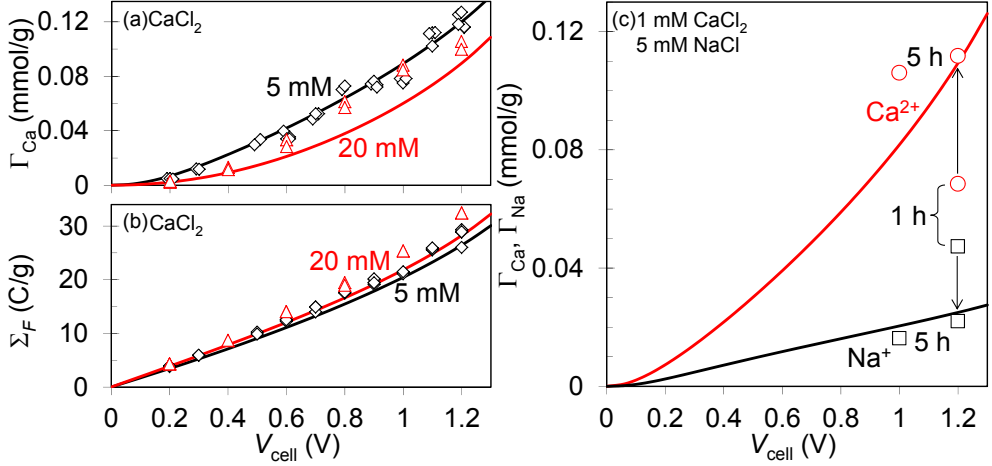
Fig. 2.6. (a,b). Equilibrium ion adsorption and charge as a function of cell voltage V_{cell} in $CaCl_2$ mixtures at two values of the $CaCl_2$-concentration (diamonds: 5 mM; triangles: 20 mM) [111]. (c). Individual excess cation adsorption by a pair of porous electrodes, as a function of V_{cell}, for one value of the $NaCl/CaCl_2$ mixing composition. Comparison of data (circles: Ca^{2+}, squares: Na^+) with modified-Donnan EDL-theory (lines) [111]. Parameter settings in the model are given in Appendix B.
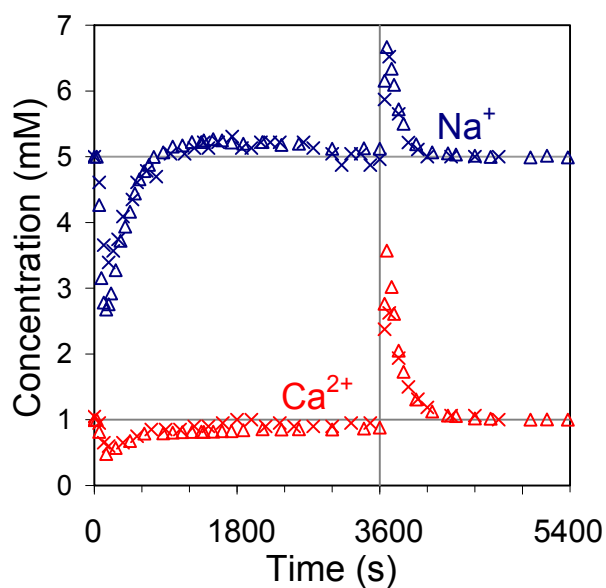
Fig. 2.7. Ion effluent concentration in a mixture of 5 mM NaCl and 1 mM CaCl$_2$ during adsorption at V_{cell}=1.2 V, and desorption after 1 hour at V_{cell} = 0 V [111]. Lines serve to guide the eyes. Crosses and triangles represent two separate experiments.

2.5 Conclusions

In conclusion, the charge efficiency Λ of a cell of two oppositely positioned porous electrodes can be determined from the total salt adsorption and electrode charge as reached at equilibrium without a-priori knowledge of the microporosity for ion storage. A data set for Λ as a function of cell voltage and ionic strength can be used to validate models of ion distribution within the electrical double layers which form inside micropores of the porous electrodes. We find that the modified Donnan model, in which the chemical attraction term μ_{att} and the Stern layer capacity $C_{St,vol}$ are freely adjustable parameters, describes our present data well. Based on the validated modified Donnan model, we can derive the microporosity of each employed carbon electrode. Our analysis points out that apart from the microporosity, the volumetric Stern layer capacity is an equally important parameter to characterize (and optimize) the capacity of porous electrode for salt storage. Furthermore, we have demonstrated that the mD model can also be used to describe equilibrium salt adsorption and charge data for more complex electrolyte conditions, such as $CaCl_2$ and mixtures of NaCl and $CaCl_2$.

Chapter 3   Transport theory of (Membrane) Capacitive Deionization

Membrane capacitive deionization (MCDI), a modified version of capacitive deionization, is a technology for water desalination based on applying an electrical field between two oppositely placed porous electrodes. Ions are removed from the water flowing through a channel in between the electrodes and are stored inside the electrodes. Ion-exchange membranes are placed in front of the electrodes allowing for counterion transfer from the channel into the electrode, while retaining the co-ions inside the electrode structure. We set up an extended theory for (M)CDI which includes the modified Donnan model (see Chapter 2) for describing the electrical double layers (EDLs) formed inside the porous carbon particles composing the porous electrodes, and the transport pathways in the electrode, i.e., the interparticle pore space. Because in MCDI the co-ions are inhibited from leaving the electrode region, the interparticle porosity becomes available as a reservoir to store salt, thereby increasing the total salt storage capacity of the porous electrode. Another advantage of MCDI is that during ion desorption (release) the voltage can be reversed. In that case the interparticle porosity can be depleted of counterions, thereby increasing the salt uptake capacity and rate in the next cycle. In this work, we compare both experimentally and theoretically adsorption/desorption cycles of MCDI for desorption at zero voltage as well as for desorption at reversed voltage, and compare with results for CDI.

3.1 Introduction

In the previous chapter, capacitive deionization (CDI) is discussed and the method to characterize porous carbon electrode properties by using the modified Donnan (mD) model is presented. In this chapter, we will introduce membrane capacitive deionization (MCDI), which is a modification of CDI by positioning ion-exchange membranes (IEMs) in front of the electrodes (cation-exchange membranes for the cathode, and anion-exchange membrane for the anode), see Fig. 3.1, and will incorporate the mD model in a transport process model in order to understand and predict the (M)CDI process.
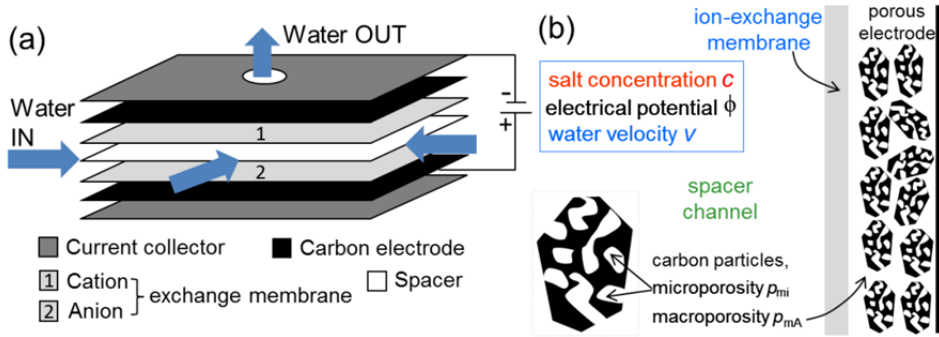
Fig. 3.1. Schematic view of (a) membrane capacitive deionization (MCDI), and (b) modelling approach for an electrode consisting of porous carbon particles. Governed by the cell voltage, cations present in the water flowing through the spacer channel migrate through the cation-exchange membrane and are stored inside the adjacent porous electrode; simultaneously, anions are stored in the opposite electrode. In CDI, the ion-exchange membranes are left out. [107]

Both CDI and MCDI are electro-capacitive processes, implying that electrochemistry does (ideally) not occur, with charge storage of a purely capacitive nature, and thus the process being repeatable without energetic losses. The size scale of our cells is typically of the order of 100-300 μm thickness for

each layer (which are spacers, membranes, electrodes, and current collectors), making a complete cell typically of the order of 1 mm thickness. Therefore, (M)CDI is an example of a "millifluidic" flow technology. In CDI, the electron current that goes from anode to cathode during ion adsorption is reversed during ion release, with ideally a perfect charge balance, as defined in Chapter 2. An external power source charges the CDI cell during the ion adsorption-step, i.e., energy is required to transfer electrons from the anode to the cathode, while during ion release (ion desorption) the electrons spontaneously flow in the reverse direction. During this stage, the electron current can be used to partially charge another CDI-cell during its ion adsorption step. In this way the overall energy consumption of a desalination stack consisting of multiple cells, can be reduced. It is the general aim to find operation schemes for CDI where the total energy use is as close as possible to the thermodynamic minimum energy input for desalination, which is for a 1:1 salt given by $\Delta G_{min} = 2RT\left(c_{in} - c_d\right) \cdot \left[\dfrac{\ln\alpha}{1-\alpha} - \dfrac{\ln\beta}{1-\beta}\right]$ per volume of dilute product (of salt concentration c_d, while the inflow has a salt concentration c_{in}, and the concentrate c_c), where $\alpha = c_{in}/c_d$ and $\beta = c_{in}/c_c$, an expression valid for ideal thermodynamic conditions [11, 63].

The only previous theoretical model for MCDI [94] considers that the ions are adsorbed in the EDLs which are formed inside the carbon particles where the electrolyte contacts the carbon matrix, without considering a possible salt storage in the interparticle pore space or transport pathways in the electrode (which we call macropores as in ref. [24], with the pores inside the carbon called the micropores [24, 99, 112]). However, co-ions expelled from the EDLs inside the particles will end up in these macropores. Because of charge neutrality there, more counterions can then be absorbed in the electrode as a whole. In the present work we will include the macropores in the theoretical model, and show that we are able to

describe experimental data for CDI and MCDI. Thus, the novel theoretical model is suitable for predictive purposes such as for system optimization.

The (M)CDI transport model describes how the ion current across the membrane into the electrode leads to a simultaneous electron current to keep charge balance in the electrode. The ion current is mainly due to counterion transport, but for non-ideal membranes also has a contribution from co-ions going in the reverse direction. Note that the counterions are the ions being attracted into the electrode during the ion adsorption-step (with opposite charge sign to that of the electrode surface), namely, cations are counterions in the cathode, and vice-versa anions in the anode. The co-ions are the ions being depleted during the ion release-step from the EDLs in the micropores. The electron current will be charge-balanced partially by counterion adsorption from the interparticle pore space (macropores, where the concentration of cations equals that of the anions) into the EDLs which are formed inside the micropores, and partially by the desorption of co-ions from the EDLs. After being expelled from the EDLs, these co-ions are largely retained by the membrane and thus accumulate in the interparticle pore space, increasing the concentration to values beyond that in the spacer channel. One may wonder how co-ions can be present behind the membrane (within the electrode structure) in the first place. The answer is that the membranes are slightly leaky to co-ions, and thus after several cycles, whatever the initial salt concentration behind the membrane is, a certain steady-state amount of co-ions can be found. In comparison, in CDI the co-ions are released from the electrodes, and end up in the spacer channel. This leads to a reduced charge efficiency of the system, i.e., per amount of transported charge, a lower number of salt molecules is removed from the water [63, 113]. In MCDI, because of charge neutrality in the macropores, this accumulation of co-ions also leads to an accumulation of counterions. Thus, effectively, part of the transported counterions (from the spacer channel through the membrane) is adsorbed in the EDLs in the micropores, and part is stored in the macropores.

Therefore, the macropores serve as an additional reservoir for ion storage, which play an important role in increasing the salt adsorption efficiency of MCDI, an effect which is absent in CDI because in CDI the salt concentration in the macropores is lower during ion-removal (not higher) while upon reaching equilibrium it becomes the same as the salt concentration outside the electrode, i.e., in the spacer channel, and thus the macropores have no salt storage capacity in CDI [95, 96].

A further advantage of MCDI is that it is possible to operate at reversed voltage during ion release. This is not possible in CDI (the technology without membranes) because then the ions that are released from the one electrode are quickly adsorbed in the other electrode, without releasing much salt into the effluent stream, i.e., the role of cathode and anode is simply reversed. In MCDI, the counterions are released from one electrode into the spacer channel, but cannot move into the other electrode because of the membrane. Thus both electrodes are depleted of their respective counterions. Not only are counterions removed to the point that the electrode is charge neutral again, but counterion desorption continues, first of all from the EDLs in the micropores, in which now the co-ions are attracted as counter charge, and secondly from the interparticle macropores, of which the salt concentration drops dramatically. Thus we have a very effective clean-up of the counterions from the electrode structure. Consequently, in the subsequent adsorption step of the next cycle, the counterion adsorption rate and capacity can be significantly increased [60, 94, 107].

In the next sections we will introduce the various theoretical elements of the MCDI-model which includes the above effects, list the various assumptions, present the mathematical framework to calculate desalination performance and electrical currents, and compare model predictions with experimental data for CDI and for MCDI in two operating modes: both for ion release at zero voltage ("0-MCDI"), and for ion release at reversed voltage ("r-MCDI").

3.2 General discussion of theory for CDI and MCDI

In this section we introduce the elements of the theoretical process model which can be used both for MCDI and CDI. We will describe the modifications relative to previous theories in the literature, and list the various assumptions that are made.

- As discussed in the previous section, the theory distinguishes between the interparticle pores (the macropores in between the carbon particles) where $c_{cation}=c_{anion}$, and the micropores inside the carbon particles, where the concentration of the cations and anions can be different, i.e., EDLs are formed [24, 99, 100, 112]. The pore volume inside the carbon particles (intraparticle porosity), we call the microporosity, p_{mi}, while the pores outside, i.e., in between, the carbon particles is the interparticle, or macro-porosity, p_{mA}. Formally, micropores and macropores are defined as those pores with sizes <2nm and >50 nm, respectively, but we follow literature on porous electrode transport theory [24] where microporosity is used for the pores inside the carbon particles, and macroporosity for the much larger, transport, pores, outside the carbon particle.

- Transport of ions through the ion-exchange membrane in front of the electrode will be described using the Nernst-Planck equation allowing for both types of ions to permeate the membrane [114, 115]. Thus, the membranes are not considered to be ideally permselective as in [94]. We will exclude transport of protons or hydroxyl-ions and also set a possible water flow through the membrane to zero.

- At the membrane-solution edges Donnan-equilibrium is assumed which relates the ion concentration difference across each of these edges to the voltage drop (Donnan potential).

- Transport in the spacer channel is described in the flow direction (y) by considering several ideal-stirred volumes placed in series. Each stirred-volume is defined by a single salt concentration, i.e., we neglect a salt concentration gradient in the direction of the membrane. This is different from the approach in ref. [94]

where we made use of the concept of an equilibrium Nernst layer (stagnant boundary layer, diffusion film, mass transfer layer, concentration-polarization layer), a thin theoretical layer envisioned in front of the membrane, separating the membrane from the spacer channel bulk volume, see refs. [94, 96, 116, 117]. Actually, this approach is problematic in MCDI because the spacer channel is already quite thin, and thus a theoretical separation of the channel into a bulk-phase and two diffusion films, is not well possible (actually, the spacer thickness is of the order of a typical thickness of such a diffusion film, about 200 µm). Furthermore, full calculations using the Nernst-Planck equation showed that because our spacer channel is thin, and because a significant part of the ion transport resistance is located within the electrode, concentration variations across the spacer channel (in *x*-direction) are not that significant. Note that this is different in electrodialysis where mass transfer resistances are mainly in the flow channel.[12] Thus, across the thickness of the spacer channel in *x*-direction we consider a constant salt concentration (which depends on time, and on *y*-position) and thus we arrive at an expression for the ion current *J* in *x*-direction which is proportional to the spacer salt concentration, c_{sp}.

- Within the porous electrode we do not use the full nonlinear porous electrode theory for desalination described in refs. [95] and [96], but use a simplified approach in which we average the concentrations across the electrode region (i.e., neglect salt concentration and potential gradients in the macropores), as in ref. [118], and describe the transport resistance empirically by considering an electrical resistance which is linearly dependent on the macropore salt concentration, c_{mA}, analogous to the description of the resistance in the spacer channel.

- Additionally, for the electrode region we include the possibility that there is a small convective leakage flow of solution through the electrodes, on the "wrong side" of the membrane, entering the electrode "head-on".

- To describe the EDL adsorption properties in the carbon particles, we use the modified Donnan model, explained in Chapter 2, and define the salt adsorption and charge as a concentration per unit volume of intraparticle pore space (i.e., based on the micropore volume within the carbon particles). Assuming perfect symmetry of the two electrodes, we can then derive the concentration of counterions and co-ions in the micropores (relative to that at zero applied cell voltage) from measured salt adsorption and charge in a CDI-cell, see Fig. 2.4b.

- In this thesis we assume perfect symmetry in the cell: the membranes are either in front of both electrodes, or in front of neither electrode (which is CDI). Both membranes are assumed to have the same ion mobility and to have the same membrane fixed charge density, X. Note that experimentally it is certainly possible to place an IEM only in front of one membrane, and have water desalination, as reported in ref. [60]. Furthermore we assume an equal mass of the anode and cathode, and a symmetrical structure of the EDL, i.e., the EDL-structure in the anode is completely similar to that in the cathode (except for the difference in charge sign). We take the same diffusion coefficient for both ions, both in solution (the spacer channel) and in the membrane.

- We do not consider a possible role of protons and hydroxyl ions in determining the structure of the EDL, e.g. by modifying the chemical surface charge of the carbon. We only consider a monovalent 1:1 salt solution of ions that are fully dissociated, like NaCl. We neglect possible Faradaic, electrochemical, reactions in the electrodes.

3.3 Mathematical description of theory

In this section we present the mathematical model for the MCDI and CDI process, based on the elements and assumptions explained in the previous section. We start with discussing ion transport in the spacer, then the membrane, and finally describe

ion storage in the porous electrode as a whole, as well as in the EDLs within the porous particles. Fig. 3.2 schematically illustrates the MCDI transport model which will be elaborated in detail in this section.
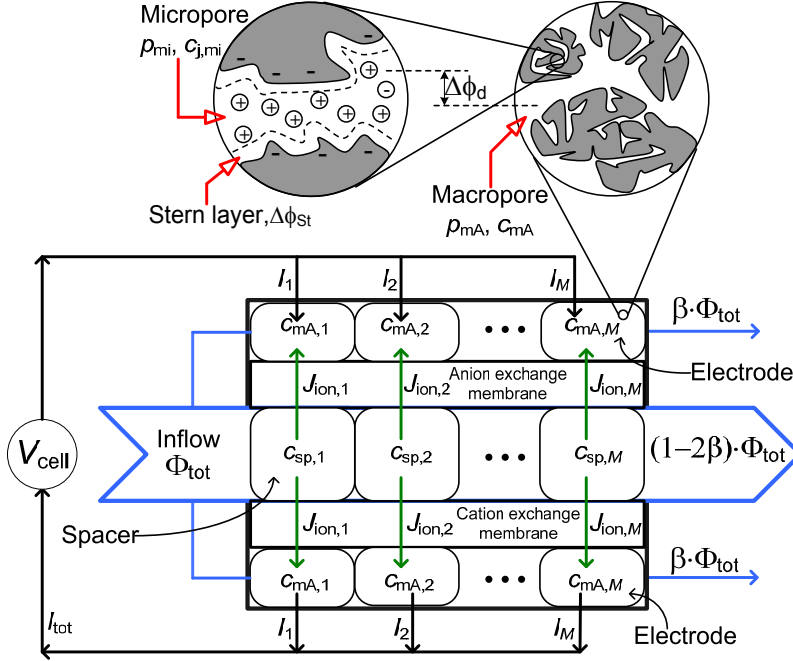
Fig. 3.2. Schematic view of MCDI model for ion transport and storage. Φ_{tot} is the total water flowrate through the cell. The fraction of that which runs inadvertently through each of the electrodes is β. $J_{ion,i}$ is the ion flux from spacer channel into the electrode for each of the i=1..*M* mathematical sub-cells that are placed in series in the model. I_i (i=1..M) is the electrical current density for each sub-cell, and I_{tot} is the total average ion current density. V_{cell} is the applied voltage difference across the cell between two electrodes. In the electrode, macropores and micropores co-exist. In the macropores cations and anions have the same concentration c_{mA}, while in the micropores the difference between cation and anion number is balanced by the electrical charge present in the carbon matrix. [119]

3.3.1 Transport in the spacer and membrane

For the spacer channel we set up a salt mass balance in which the accumulation of salt is determined by diffusion and migration in the *x*-direction into the

membrane (or for CDI directly into the electrode), and by convective flow in the axial, or y-, direction through the spacer channel, given by

$$\frac{\partial c_{sp}(y)}{\partial t} = -\frac{J_{ion}(y)}{\delta_{sp}} - v_{sp}\frac{\partial c_{sp}(y)}{\partial y}$$ (3.1)

where c_{sp} is the spacer salt concentration in mol/m^3 (mM), t is time, J_{ion} the ion flux in x-direction at one interface directed into the membrane or electrode (in a perfectly symmetric cell J_{ion} is the same in magnitude on each interface, and thus equal to the salt flux from the transport channel; note that we consider a 1:1 salt thus two ions constitute one salt molecule), v_{sp} the spacer water velocity, and y the coordinate along the length of the channel from y=0 at the entrance to y=L at the exit of the channel.

In using Eq. 3.1, we make several assumptions: 1. we neglect axial diffusion, or dispersion in the y-direction, and 2. we consider concentration gradients in the x-direction to be small. Both these assumption become the more valid the more the cell length L exceeds the channel width, δ_{sp}, a condition typically well met in an (M)CDI flow-cell (e.g. 5 cm for L vs. 200 μm for δ_{sp}). The velocity, v_{sp}, is given by v_{sp}=$\Phi_{sp}\cdot L/V_{sp}$, where Φ_{sp} is the water flowrate through the spacer channel (volume/time), is the length (in y-direction) of the channel and V_{sp} is the spacer channel volume.

The ion current density I in x-direction (flux of cations minus flux of anions) is invariant with x (also constant across the solution/membrane interfaces, and across the membrane; but it does depend on y). In the spacer channel, assuming absence of concentration gradients in x-direction, and for equal ion diffusion coefficients, the current I depends on the electrical potential difference across the spacer channel half-space (from midplane to edge), $\Delta\phi_{sp,half}$, according to ref. [12]

$$I(y) = -2D\cdot c_{sp}(y)\cdot\frac{\Delta\phi_{sp,half}(y)}{h},$$ (3.2)

where ϕ is nondimensional and can be multiplied by the thermal voltage, $V_T=RT/F$ ($\sim$25.7 mV), to arrive at a voltage with dimension Volt, and where $h=\delta_{sp}/2$. Current I has dimension of moles/area/time, and can be multiplied by Faraday's number, F, and integrated over the membrane area A to obtain a total cell current with dimension Ampère. The diffusion coefficient D is taken as the average of that of the anion and the cation [12].

At the two membrane/solution interfaces we have Donnan equilibrium, both at the edge of the membrane with the spacer channel, and at the edge of the membrane with the electrode. These two Donnan potentials are given by [120, 121],

$$\Delta\phi_{donnan} = \sinh^{-1}\frac{\omega X}{2c_{salt}}, \tag{3.3}$$

where c_{salt} is the salt concentration just outside the membrane (being either c_{sp}, or the macropore salt concentration in the electrode, c_{mA}), X is the membrane 'ion exchange capacity', i.e., the magnitude of the membrane fixed charge density, and ω is the sign of the membrane charge (e.g., $\omega=+1$ for an anion-exchange membrane).

Inside the membrane, charge balance is given by $c_{cation}-c_{anion}+\omega X=0$ which can be combined with the Nernst-Planck (NP) equation for each ion, and the resulting set of equations can be solved exactly [12, 115]. However, because full calculations showed that the concentration and potential profiles across the membrane are close to linear in a highly charged membrane, we linearize the NP-equations leading for current I to

$$I(y) = -\frac{D_{mem}}{\delta_{mem}}\left\langle c_{T,mem}(y)\right\rangle\Delta\phi_{mem}(y), \tag{3.4}$$

where subscript "mem" is used for properties within the membrane, where $c_{T,mem}$ is the total ion concentration in the membrane, given by $c_{T,mem}=c_{cation,mem}+c_{anion,mem}$, where $<..>$ denotes an average property, where Δ is the difference across the

membrane, and where δ_{mem} is the membrane thickness. At both solution/membrane

$c_{T,mem} = 2 \cdot c_{salt} \cdot \cosh(\Delta\phi_{donnan}) = \sqrt{X^2 + (2 \cdot c_{salt})^2}$ edges, the total ion concentration in

the membrane, $c_{T,mem}$, is given by , with c_{salt} as for Eq. 3.3 either c_{sp} or c_{mA}. The

average concentration $<c_{T,mem}>$ required in Eq. 3.4 is calculated as the average of

these two boundary values for $c_{T,mem}$. Likewise, the linearized total ion flux through

the membrane, $J_{ion,mem}$, is given by

$$J_{ion,mem}(y) = -\frac{D_{mem}}{\delta_{mem}}\left(\Delta c_{T,mem}(y) - \omega X \Delta\phi_{mem}(y)\right). \tag{3.5}$$

In this linearized membrane-model we assume that the ion flux is constant across the membrane and there is no accumulation of salt in the membrane. Full calculations, however, based on the full NP-equation for the membrane, implemented in a differential mass balance, show that this is not exactly true, and that there can be differences in $J_{ion,mem}$ across the membrane (especially upon voltage reversal in r-MCDI), leading to salt storage or depletion of the membrane itself. This model extension, however, is not further considered in the present work.

For the linearized model, the ion flux through the membrane $J_{ion,mem}$, is equal to the ion fluxes in solution at the two solution/membrane edges. On the side of the spacer channel, $J_{ion,mem}$ goes directly into Eq. 3.1, while on the side of the electrode, it enters in the electrode ion balance, Eq. 3.10. The current density in the membrane, I, given by Eq. 3.4, equals the current density in the spacer channel, given by Eq. 3.2, and is equal to the current that runs into the micropores within the electrode, see Eq. 3.9. These are the boundary conditions which apply in the x-direction. In the axial y-direction, we only have to prescribe the inflowing concentration $c_{sp}(y=0)=c_{in}$.

We solve Eq. 3.1 by discretization into M ideally-stirred volumes placed in series, like in ref. [94]. In that case, Eq. 3.1 can be simplified to:

$$\frac{\mathrm{d}c_{\mathrm{sp,i}}}{\mathrm{d}t} = -\frac{J_{\mathrm{ion,i}}}{\delta_{\mathrm{sp}}} - \frac{M}{\tau_{\mathrm{sp}}}\left(c_{\mathrm{sp,i}} - c_{\mathrm{sp,i-1}}\right). \tag{3.6}$$

where i is a counter running from 1 for the first volume to M, the last, and τ is the spacer channel residence time (spacer channel volume $V_{\mathrm{sp}}=A\cdot\delta_{\mathrm{sp}}$, divided by the water flowrate Φ_{sp}). The inflow salt concentration into the cell is $c_{\mathrm{in}}=c_{\mathrm{sp,0}}$ and the effluent or outflow salt concentration is $c_{\mathrm{eff}}=c_{\mathrm{sp,M}}$. All of the following equations in this section are solved for each stirred volume ($1<i<M$) separately.

Finally, we consider the voltage across the cell which is given by the sum of the potential drop over each spacer channel half-space (from 0 to h), $\Delta\phi_{\mathrm{sp,half}}$, the Donnan potential, $\Delta\phi_{\mathrm{donnan}}$, at the membrane/spacer edge, the potential across the membrane, $\Delta\phi_{\mathrm{mem}}$, minus $\Delta\phi_{\mathrm{donnan}}$ at the membrane/electrode edge, the potential drop in the electrode, $\Delta\phi_{\mathrm{elec}}$, and the Donnan potential and the Stern layer potential in the micropores, $\Delta\phi_{\mathrm{d}}+\Delta\phi_{\mathrm{St}}$. Those contributions together sum up to half of $V_{\mathrm{cell}}/V_{\mathrm{T}}$, where V_{cell} is the cell voltage, i.e. the voltage applied between the two electrodes, $V_{\mathrm{cell}}=V_{\mathrm{anode}}-V_{\mathrm{cathode}}$. This can be summarized as

$$\tfrac{1}{2}V_{\mathrm{cell}}/V_{\mathrm{T}} = \Delta\phi_{\mathrm{sp,half}} + \Delta\phi_{\mathrm{donnan,membrane/spacer}} + \Delta\phi_{\mathrm{mem}}$$
$$-\Delta\phi_{\mathrm{donnan,membrane/electrode}} + \Delta\phi_{\mathrm{elec}} + \left(\Delta\phi_{\mathrm{d}} + \Delta\phi_{\mathrm{St}}\right)_{\mathrm{micropores}} \tag{3.7}$$

where the electrode potential drop, $\Delta\phi_{\mathrm{elec}}$ relates to current density I according to

$$\Delta\phi_{\mathrm{elec}}\cdot V_{\mathrm{T}} = -I\cdot F\cdot R_{\mathrm{elec}}/c_{\mathrm{mA}} \tag{3.8}$$

with R_{elec} an electrode specific resistance with dimension Ω.mol/m.

The above model can be used both for MCDI and for CDI. For CDI, the membrane is absent, which can be modelled simply by setting the membrane thickness δ_{mem} and the membrane charge X to zero. In CDI this means that the concentration in the spacer channel at the edge with the (now vanished) membrane becomes equal to the concentration in the electrode macropores, c_{mA}. Moreover, exclusively for experiments in Fig. 3.4, the water is pumped from opening "2" (Fig.

2.2) into the stack, and is collected from opening "1" (Fig. 2.2), which causes mixing of desalinated water and water in the "dead volume" of the stack. To simulate this phenomena, the effluent salt concentration at opening "1", c_{eff}, can be related to the water flowrate per stack Φ, the dead volume V_{dead}, and the concentration at the M sub-cell $c_{sp,M}$, according to $\dfrac{d}{dt} c_{eff} = \dfrac{\Phi}{V_{dead}} (c_{sp,M} - c_{eff})$. This modification is not necessary for any of the other experiments discussed in this thesis, where the flow direction is towards opening "2" (Fig. 2.2).

3.3.2 Electrodes and electrical double layers

Within the electrodes, we do not consider in the x-direction any gradients in potential, ϕ, and concentration, c, but take an average value for ϕ and c. Detailed theory to describe ion migration and diffusion across a porous electrode, and thus the resulting gradients in ϕ and c, is given in refs [95, 96, 122]. In the electrode, there are two different porous (electrolyte-filled) phases. First of all, there are the macropores, where we assume $c_{cation}=c_{anion}$, which equals the macropore salt concentration, given by c_{mA}. This is the volume in between the carbon particles, and has porosity p_{mA}. Secondly, we consider the micropores with porosity p_{mi}, in which the cat- and anion concentrations, $c_{i,mi}$, can be different from one another, which we can determine using the modified Donnan model as is explained in Chapter 2. The porosities p_{mA} and p_{mi} are defined as pore volumes per unit total electrode volume, with the macropore salt concentration c_{mA} defined per unit macropore volume, and the ion concentrations in the micropores, $c_{i,mi}$, defined per unit of micropore volume.

The first electrode balance describes how the "charge concentration" in the micropores, $c_{charge,mi}=c_{cation,mi}-c_{anion,mi}$, relates to the current density I (defined on the projected area of the electrode, A) according to

$$\frac{\mathrm{d}}{\mathrm{d}t}\left(p_{mi} \cdot c_{charge,mi,i}\right) = \frac{I_i}{\delta_{elec}} , \tag{3.9}$$

where δ_{elec} is the electrode thickness.

The second electrode balance relates the membrane ion flux, J_{ion}, to the total ion concentration in the electrode,

$$\frac{\mathrm{d}}{\mathrm{d}t}\left(2 \cdot p_{mA} \cdot c_{mA,i} + p_{mi} \cdot \left(c_{cation,mi,i} + c_{anion,mi,i}\right)\right) = \frac{J_{ion,i}}{\delta_{elec}} + \frac{M}{\tau_{elec}}\left(c_{mA,i} - c_{mA,i-1}\right) , \tag{3.10}$$

where τ_{elec} is the superficial residence time in the electrode due to convective flow of solution through the electrode. The residence time τ_{elec} is given by the total electrode volume V_{elec} divided by the electrode flowrate Φ_{elec}. This leakage flow of water is calculated as follows. The total water flowrate per cell is Φ_{tot}, and the fraction of that which runs through an electrode is $\Phi_{elec}=\beta \cdot \Phi_{tot}$, and thus the flow directed through the spacer channel is $\Phi_{sp}=(1-2\beta) \cdot \Phi_{tot}$. The flows through the spacer channel and through the two electrodes are combined into the effluent which leaves the cell, and of this mixture the salt concentration, c_{eff}, is given theoretically by $c_{eff}=(1-2\beta) \cdot c_{sp,M}+2\beta \cdot c_{mA,M}$, see Fig. 3.2.

To model the structure of the EDLs in the electrodes, we employ the "modified Donnan model", as described in Chapter 2. The concentration of a specific ion $c_{j,mi}$ in the micropore volume related to the macropore salt concentration c_{mA} is given by Eq. 2.4 in Chapter 2. Moreover, micropore charge concentration $c_{charge,mi}$ relates to the Stern layer potential drop $\Delta\phi_{st}$, according to Eq. 2.6. This finalizes the cell model as will be used both for CDI and MCDI, both with ion release at zero voltage (0-MCDI) and for ion release at reversed voltage (r-MCDI).

3.4 Experimental setup and parameter settings for transport modelling of (M)CDI

Experimental details of our CDI test stack have been described in Chapter 2 (also see Fig. 2.2). To construct an MCDI stack, the modification we implement is inserting a cation-exchange membrane between the cathode and the spacer channel and an anion-exchange membrane between the anode and the spacer channel. In brief, N=8 cells as depicted in Fig. 3.1 are assembled from current collectors, electrodes, ion-exchange membranes and spacers. Each current collector is used in two adjacent cells (one above, and one below). Therefore, for MCDI it is important to reverse the sequence of ion-exchange membranes from cell to cell because the cathode and anode positions are also reversed. The salt solution flows from outside the stack on all four sides into the square 6x6 cm^2 spacer channel of each of the N cells, and leaves from a hole in the middle of each cell (area 1.5x1.5 cm^2), or the reverse (only for experiments in Fig. 3.4). These are the dimensions of all layers. Thus, the projected area A per electrode (membrane) is given by A=33.8 cm^2. Materials used are graphite current collectors as described in section 2.2, porous carbon electrodes (the electrode properties are given in Appendix B). Besides, we use anion and cation-exchange membranes (Neosepta AMX, δ_{mem}=140 μm, and Neosepta CMX, δ_{mem}=170 μm, Tokuyama, Japan), and a polymer spacer (Glass fibre prefilter, Millipore, Ireland, δ_{sp}=250 μm), see Fig. 3.3. After assembly, the entire stack of all layers is firmly pressed together and placed in a Teflon (PTFE) housing.
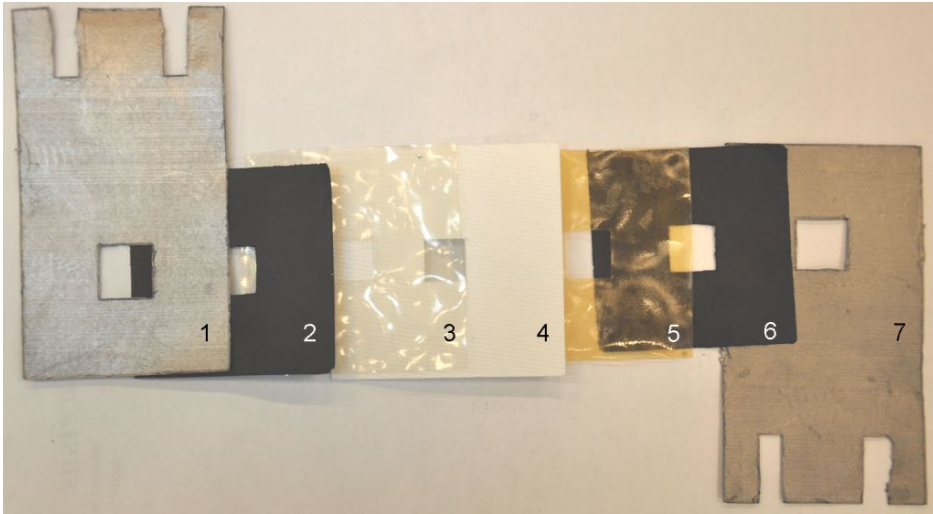
Fig. 3.3. Photograph of the sequenced components of one MCDI cell, from left to right: (1) graphite current collector, (2) porous carbon electrode, (3) anion exchange membrane, (4) glass fibre spacer, (5) cation exchange membrane, (6) porous carbon electrode, and (7) graphite current collector.

As described in Chapter 2 already, the conductivity of the effluent salt concentration of the stack, in this chapter only NaCl, and the effluent pH are measured on-line, and together are converted into the net salt concentration according to a calibration curve. For all experiments in section 3.5.2, the water flowrate per stack Φ is fixed at 60 mL/sec. Since we have 8 cells in one stack, per cell the water flowrate Φ_{tot} is equal to 0.125 mL/sec. The cell voltage is applied using a potentiostat which measures the current between cathode and anode after applying a step change in cell voltage. To get the total charge with dimension Coulomb in Fig. 3.5, the current is integrated for the duration of the ion adsorption step, given that the total charge transferred is equal (within measurement error and for a small leakage current) to the charge released again in the ion-release step. The effluent salt concentration is calculated from the measured conductivity, and the salt removal per total electrode mass, Γ_{salt}, is derived from the first equality in Eq. 3.11 below. To calculate salt removal in the theoretical model, we use two

methods: 1. Integration over time of the difference between the effluent concentration c_{eff} and the inflowing concentration c_{in}, times the total water flowrate, Φ_{tot}, like we do for the analysis of the data, or 2. Taking the difference in total salt storage in the cells between time t_1 and t_2, mathematically, these two methods are expressed as:

$$
\begin{aligned}
\Gamma_{salt} &= \frac{N\Phi_{sp}}{m_{tot}} \int_{t_1}^{t_2} \left(c_{eff} - c_{in} \right) dt \\
&= \frac{NA}{m_{tot}M} \left[\sum_{i=1}^{M} \left(\delta_{sp} c_{sp,i} + 2\delta_{elec} \left(p_{mA} c_{mA} + \tfrac{1}{2} p_{mi} \left(c_{cation,mi} + c_{anion,mi} \right) \right) \right) \right]_{t_1}^{t_2}
\end{aligned}
\tag{3.11}
$$

where t_1 denotes the moment that the cell voltage undergoes a step change, t_2 denotes the end of the step starting from t_1.

In section 3.5.2, when the applied desorption time is not long enough for all the ions adsorbed in the porous electrode during the ion adsorption step to be released again, the ions retained in the electrode region will reduce the salt adsorption capacity in the next ion adsorption step. Therefore, we have to run several (M)CDI cycles in a row, both experimentally and theoretically, in order to reach the 'dynamic equilibrium' (DE), where the measured salt adsorption during one phase of the cycle is equal to the salt desorption in the other phase of the cycle (salt balance is maintained). Likewise, the total charge transferred in one direction (from cathode to anode) during the salt adsorption step, is close to the charge transfer directed in the opposite direction during the salt release-step. Note that all results shown in this chapter are obtained under the DE condition.

To calculate the voltage drop across the spacer channel we take the average of the diffusion coefficients [12] of Na$^+$ and Cl$^-$, resulting in $1.68 \cdot 10^{-9}$ m^2/s. For the diffusion coefficient in the membrane we arbitrarily take 10% of the value of solution, thus $D_{mem}=1.68 \cdot 10^{-10}$ m^2/s. For the spacer and membrane thickness we take $\delta_{sp}=250$ μm and $\delta_{mem}=140$ μm, while we use a membrane fixed charge density

of X=8 M. In the calculation, the number of stirred volumes placed in series, M, is set to M=6. Values of input parameters for section 3.5.1 and 3.5.2 are summarized in Appendix B. For some parameters, values slightly differ between the two sections. This is because of different batches of electrode material used.

3.5 Results and discussion

3.5.1 Comparison of experimental results and theory for CDI

In this section, we present the reproduction of the CDI process by the theory. Fig. 3.4 compares calculations with experimental data for effluent salt concentration and electrical current. All calculations are based on a single set of input parameters listed in Appendix B, both for ion adsorption and for ion release. To begin with, we fix the water flowrate at 60 mL/min, and the influent salt concentration at 5 mM, and vary the applied cell voltage. Panels a and c show experimentally the effluent salt concentration and the electrical current as a function of time, indicating that a higher cell voltage leads to higher salt adsorption per cycle and also higher charge transferred. Panels b and d are theoretical results which reproduce the experimental ones very well. Since the equilibrium is reached (the effluent salt concentration is at its initial value at the end of the adsorption/desorption step, and the electrical current converges to zero), charge efficiency Λ can be derived by taking the ratio of salt adsorption to total charge. The results of total salt adsorption, total charge and charge efficiency are shown in Fig. 2.4, Chapter 2. In Fig. 3.4, panels e and f are experimental and theoretical results for different water flowrates, while the influent salt concentration and the cell voltage are fixed. By varying the water flowrate, although at lower water flowrate, 'fresher' water can be produced (the effluent salt concentration is lower), the total salt adsorption remains the same. This is because when calculating the total salt adsorption, not only we have to

integrate the effluent salt concentration relative to the influent concentration (c_{eff}-c_{in}) over time, the water flowrate also need to be taken into account, see Eq. 3.11. In the end, we show the effluent salt concentration as a function of time for three influent salt concentrations (5, 10 and 20 mM) both experimentally (panel g) and theoretically (panel h). The total salt adsorption for those concentrations can also be derived based on the method given by Eq. 3.11, and the results can be found in Fig. 2.4, Chapter 2. To conclude, CDI process without ion-exchange membrane can be extrapolated by our (M)CDI process model on the basis of certain reasonable assumptions made in the model (X=0, δ_{mem}=0).
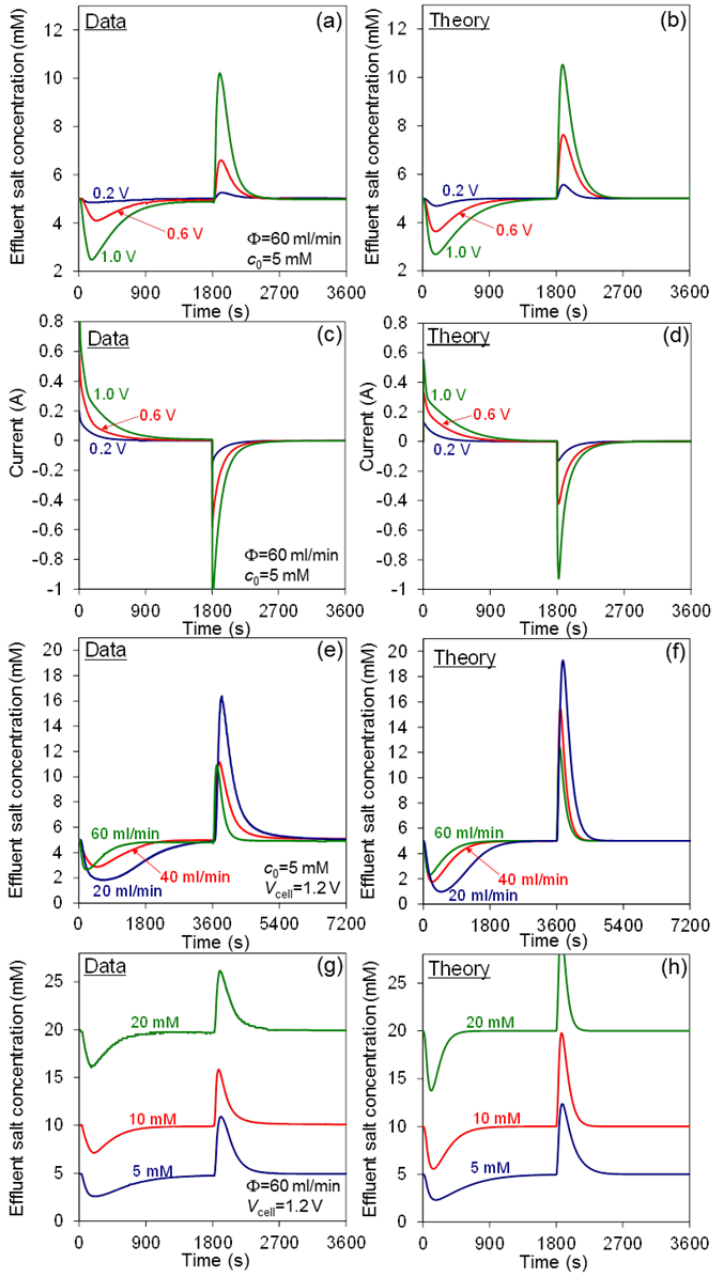
Fig. 3.4. CDI process data (left column) and theory (right column) as a function of cell voltage V_{cell} (a-d), flowrate Φ (e-f) and ionic strength of inlet solution c_0 (g-h). At time zero a positive cell voltage is applied, which is reduced to zero halfway the cycle. [106]

3.5.2 Comparison of theory with experiments for salt adsorption and charge in CDI
and MCDI as a function of cycle time

   In this section we discuss data where we accurately compare CDI with 0-MCDI
(MCDI with ion release at zero cell voltage) and with r-MCDI (where ion release
occurs at reversed voltage). Experimentally, CDI and 0-MCDI were previously
compared by Kim and Choi, in ref. [60] for V_{cell}=1.2 V and c_{salt}=3.5 mM, in ref.
[123] for V_{cell}=1.5 V and c_{salt}=3.5 mM, and in ref. [124] for V_{cell}=1.2-1.6 V and
c_{salt}=17 mM. In all cases the half-cycle time to be defined below, was HCT=180 s.
In refs. [60] and [123] only a cation-exchange membrane was placed in front of the
cathode (without a membrane placed in front of the anode), while in ref. [124] both
cation-exchange and anion-exchange membranes were used, in front of cathode
and anode, respectively (just as in the present work). When going from CDI to 0-
MCDI, the reported increase in salt removal per cycle was about 30% in ref.[60],
about 20% in ref. [123], but was much higher in ref. [124] where the salt
adsorption per cycle was reported to increase by at least 100% (see Fig. 2 of ref.
[124]). This large increase may be related to the low current efficiency reported for
CDI there (i.e., CDI-performance may not have been optimal in these experiments).

   Theoretically, 0-MCDI and r-MCDI were previously only briefly compared in ref.
[94] (Fig. 5, V_{cell}=1.4 V, c_{NaCl}=36 mM) showing a predicted ~20% increase in salt
removal for r-MCDI compared to 0-MCDI. In the present work, we compare CDI
with 0-MCDI and r-MCDI, both experimentally and theoretically. This will be
done on the basis of data for $c_{NaCl,in}$=20 mM at a cell voltage of V_{cell}=1.2 V and a
flowrate of Φ_{tot}=0.125 mL/s per cell. The data are presented as a function of the
'half-cycle time', HCT, i.e., the duration of an ion adsorption-step, which is set
equal to the duration of the subsequent ion-release step. Thus, the full cycle time is
twice the HCT. For application of (M)CDI in practice, it is important that HCT is
optimized to maximize the average salt removal rate, see Chapter 5.

Fig. 3.5 shows first experimental data where CDI is compared with 0-MCDI and r-MCDI as a function of HCT, showing that for long HCT the salt adsorption and charge level off, while for low HCT both tend to zero. Going from CDI to 0-MCDI and to r-MCDI, we see that the salt removal increases in two about equal steps of ~20%, making r-MCDI about 40% more effective than CDI. For both MCDI-options we observe that the salt adsorption decreases again at long HCTs, but not for CDI. For charge we observe that the plateau values are the same for CDI and 0-MCDI with a 20% increase in charge observed for r-MCDI.
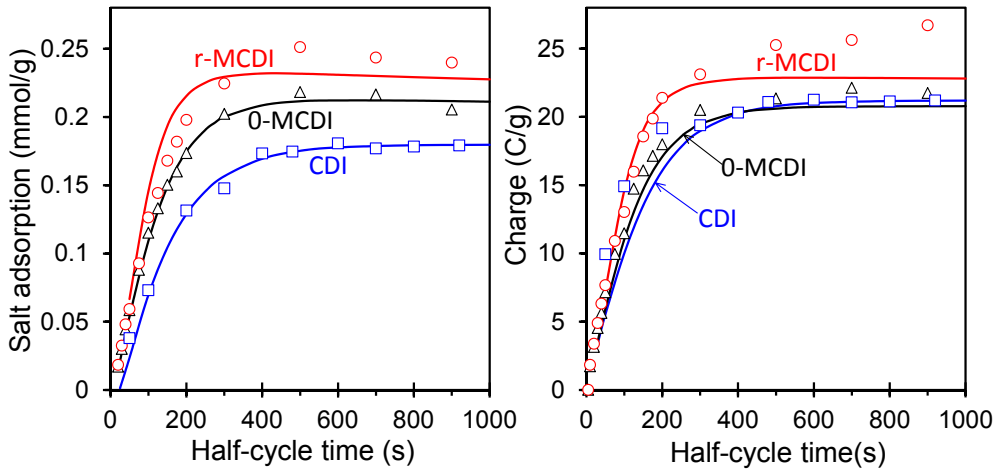
Fig. 3.5. Salt adsorption and charge in CDI (squares), 0-MCDI (triangles), and r-MCDI (circles) as a function of half-cycle time ($c_{salt,in}$=20 mM, V_{cell}=1.2 V). Lines are theoretical results. [107]

Comparing theory with data, we find a very good agreement: first of all, we observe that the value of the plateaus at high HCT is well predicted, both for salt adsorption and for charge, and for each of the three process modes. We also find that in MCDI the predicted plateau-value in salt adsorption decreases slightly with HCT, which is also observed in the data, though more evidently. In our model this decrease is due to the water flow behind the membrane (i.e., that $\beta \neq 0$) and the membrane not being 100% ideally permselective. Because of these two effects, slowly the salt which is stored in the macropores leaks away (i.e., c_{mA} goes down in

time). The decline in salt adsorption and charge when HCT goes to zero is also well reproduced for all three process options.

Fig. 3.6 shows experimental data and theoretical predictions for the effluent concentration as a function of time, for one value of the half-cycle time, namely HCT=300 s. As can be observed the predicted curves are quite similar to the experimental ones, certainly for CDI and 0-MCDI. For r-MCDI the minimum in effluent salt concentration occurs later in theory than in the experiment, and is deeper, while the maximum (upon voltage reversal) is much higher, and the decline in c_{eff} is more rapid than experimentally.
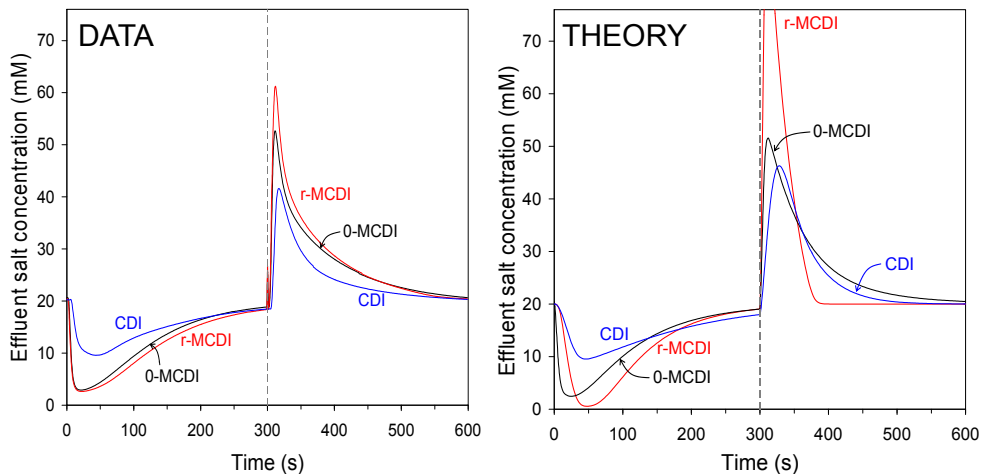
Fig. 3.6. Comparison of experimental data and theoretical model for CDI, 0-MCDI, and r-MCDI, for a half-cycle time of 300 sec ($c_{salt,in}$=20 mM, V_{cell}=1.2 V). [107]

Finally, Fig. 3.7 shows the predicted development of the macropore concentration, c_{mA}, as a function of time, showing the very marked differences between CDI, 0-MCDI and r-MCDI. For both MCDI-options, the macropore concentration, c_{mA}, goes up during ion adsorption while it goes down for CDI, explaining the higher ion adsorption capacity for MCDI vs CDI.

In conclusion, in this work we have made significant progress in setting up a comprehensive model which can describe both CDI and MCDI, with ion release at

zero voltage as well as at reversed voltage. Important is consideration of the macropore volume, where the cation concentration equals that of the anions, as well as the use of the modified Donnan model for charge and salt storage in the micropores within the carbon particles.
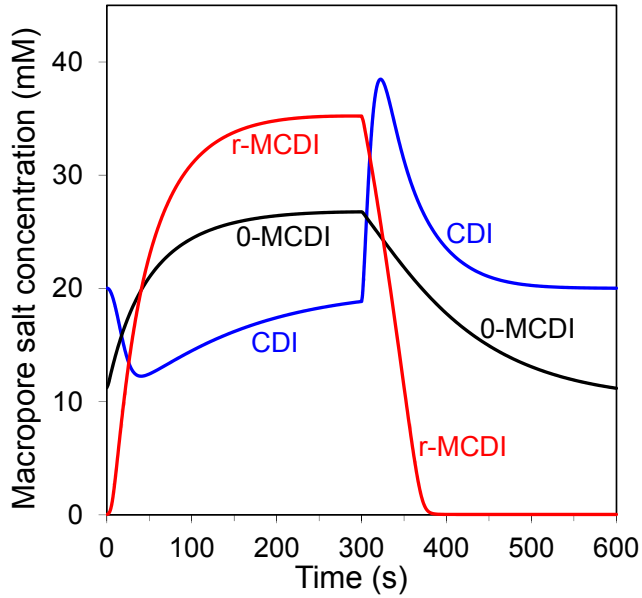
Fig. 3.7. Theoretical prediction for macropore salt concentration for CDI, 0-MCDI, and r-MCDI (4th sub-cell out of the total of *M*=6), for conditions as in Fig. 3.6. [107]

3.5 Conclusions

We have set up a comprehensive model which describes both capacitive deionization (CDI) and membrane capacitive deionization (MCDI). For MCDI two operation modes are considered, either "0-MCDI" where ions are release at zero cell voltage, and "r-MCDI" where the ions are release at reversed voltage. Experiments and modelling agree that 0-MCDI removes around 20% more salt than CDI, and r-MCDI again 20% more. The model includes several novel elements, such as including the fact that also co-ions can pass the ion-exchange membrane, while for the electrode, a distinction is made between the transport pathways, or macropores, where the concentration of both ions is the same, and the micropores inside carbon particles where charge is stored and thus the ion concentrations can be different. For the micropores a modified Donnan model is implemented to describe equilibrium data for salt adsorption and charge. An ion transport resistance in the electrode was included by considering a resistance which is inversely proportional to the macropore salt concentration. Major trends in salt adsorption and charge as a function of the duration of the (M)CDI-cycle are well reproduced by the theory, as well as the profiles of effluent concentration vs. time. The validated MCDI process model can be used for design and process optimization studies.

Chapter 4   Energy Consumption and Constant Current Operation in Membrane Capacitive Deionization

M embrane capacitive deionization (MCDI) is a water desalination technology based on applying a cell voltage between two oppositely placed porous electrodes sandwiching a spacer channel that transports the water to be desalinated. The classical operational mode of MCDI at a constant cell voltage results in an effluent stream of desalinated water of which the salt concentration varies with time. In this chapter, we propose a different operational mode for MCDI, whereby desalination is driven by a constant electrical current, which leads to a constant salt concentration in the desalinated stream over extended periods of time. Furthermore, we show how the salt concentration of the desalinated stream can be accurately adjusted to a certain set point, by either varying the electrical current level and/or the water flowrate. Finally, we present an extensive data set for the energy requirements of MCDI, both for operation at constant voltage, and at constant current, and in both cases also for the related technology in which membranes are not included (CDI). We find consistently that in MCDI the energy consumption per mole of salt removed is lower than in CDI. Within the range 10-200 mM ionic strength of the water to be treated, we find for MCDI a constant energy consumption of ~22 kT per ion removed. Results in this chapter are an essential tool to evaluate the economic viability of MCDI for the treatment of brackish water.

4.1 Introduction

A Membrane Capacitive Deionization (MCDI) cell is a modification of a conventional CDI cell, which in addition contains anion and cation-exchange membranes which are positioned between the spacer channel and the anode, and between the spacer channel and the cathode, respectively [52, 58, 60, 107, 110, 124-127], see Fig. 3.1 in Chapter 3. It is also possible to use only one membrane, in front of only one electrode [57, 60]. Because of the use of ion exchange membranes MCDI has two major advantages over conventional CDI, which are discussed in Chapter 3.

At present, it is common practice to control the desalination cycles of (M)CDI by applying a constant cell voltage (the electrical potential difference between the two porous electrodes) during charging (ion adsorption) as well as during discharging (ion desorption) of the electrodes. For example, during ion adsorption, a typical value of V_{cell}=1.2 V is applied to adsorb ions and produce fresh water, while during discharge, the two electrodes can be short-circuited, i.e., the cell voltage is reduced to 0 V. However, operation at a constant cell voltage has as a disadvantage that the effluent salt concentration changes in time, i.e., the ion concentration in the desalinated water stream (fresh water) changes during the ion removal step. This is because at the start of the adsorption step, the EDLs are still mainly uncharged, and thus the driving force over the channel is at a maximum (no loss of cell voltage in the EDLs). Consequently, there is a large ion flux directed into the electrodes. As ion adsorption in the EDLs progresses, the EDL voltage gradually increases and the remaining voltage across the spacer channel steadily decreases in time. The overall effect is that the effluent salt concentration will first decrease, go through a minimum, and then gradually increase again. This gradual change of effluent concentration over time may not be desired in practical applications; instead, it may be more advantageous if water is produced of a constant desalination level.

To obtain fresh water with a constant reduced salt concentration, we propose a different mode to carry out the MCDI desalination cycles, namely by applying a constant current (CC) running between the two electrodes, instead of using a constant cell voltage (CV). The externally applied constant electron current, *I*, translates into an equally large ionic current in the cell, which has contributions from the ionic flux of positive ions (such as Na^+) and negative ions (such as Cl^-). As we will show, in MCDI, operation with constant current results in an effluent salt concentration which is constant in time, both during the ion adsorption step and during the ion desorption-step. Another advantage of operation using constant current is that the effluent concentration can be easily and accurately controlled at a certain required value by varying the current level. This may be advantageous from the viewpoint of the consumer who desires a supply of fresh water with constant and tunable salt concentration.

Furthermore, we present an extensive data set for the energy requirement of MCDI versus CDI, not only for the novel operational mode of CC, but also for the classical CV-mode of operation. These data can be used to assess the economic viability of the technology, as well as to validate process models; models which are an essential tool for the design and optimization of CDI and MCDI. We show that the energy requirement is closely linked to the dynamic charge efficiency, an important operational parameter both in CDI and MCDI.

4.2 Experimental Section

4.2.1 Experimental setup

The experimental setup of our MCDI stack is described in Chapter 3, see Appendix B for details. The salt adsorption and charge in an MCDI-cycle can be

derived from the data of salt effluent (outflow) concentration versus time, and electric current versus time. For salt adsorption, the difference between inflow salt concentration and outflow concentration is integrated with time, and multiplied with the water flow rate, while for charge, the current is integrated with time. All data shown in this chapter are obtained under the dynamic equilibrium (DE), where both salt and charge balance are maintained, as explained in Chapter 3. In the standard experiment we apply ±1 A to the full stack of N=8 cells, which translates to an average current density (per unit cell area) of ±37 A/m^2.

4.2.2 Energy requirements

To calculate the energy requirement for the removal of one ion, as presented in Fig. 4.3, we take the ratio of energy consumption over desalination, both calculated strictly based on the duration of the ion adsorption step. In the present work, the adsorption step is defined to start and end at the exact moments that voltage or current signals are changed, not by the moments that the effluent salt concentrations drops below, or increases to beyond, the inlet salt concentration (which is 20 mM in Figs. 4.1 and 4.2). For a discussion on alternative methods, see section 6.3. Desalination is calculated from integration over time, during the ion adsorption step, of the difference c_{in}-$c_{effluent}$, and multiplying by water flow rate Φ, and by the factor 2. The factor 2 is because we present data for the energy to remove an ion, not to remove a salt molecule. The energy is calculated as cell voltage V_{cell} times current I, integrated again over the duration of the ion adsorption step. The ratio energy/desalination gives us the energy in J per mole of ions removed. Dividing this number by a factor RT (=2.48 kJ/mol at room temperature) results in the energy in units of "RT per mole of ions", which has the same numerical value as is expressed in "kT per ion" as in Fig 4.3a-c. We neglect energy recovery during the ion release-step, see section 6.3.

4.2.3 Dynamic charge efficiency

The dynamic charge efficiency, Λ_{dyn}, denotes the ratio of two properties: the total desalination during ion adsorption (in moles), as described above, divided by total charge transferred in the same period (charge with unit Coulomb must be divided by Faraday's constant, F, to obtain charge in moles). In the present work, the parameter Λ_{dyn} is obtained during relatively short cycles in which the EDLs are not allowed to come to equilibrium with the salt concentration in the spacer and inlet flow. Thus, formally, we have not measured (nor do we theoretically model), the equilibrium charge efficiency, Λ, as defined in Chapter 2, which requires that the system becomes equilibrated at set values of the cell voltage with the salt concentration in the macropores the same as in the inlet stream. Thus, to describe the measured ratio of desalination and charge, in the present work we use the modified term, "dynamic charge efficiency."

4.3 Theory

The theoretical model used to describe ion transport and storage in MCDI and CDI is described in detail in Chapter 3. All calculations presented in Figs. 4.1-4.3 are based on a single set of parameter values, given in Appendix B. Note that in most of the experiments presented here we do not apply a constant voltage, but we apply a total current to the whole cell. In the model, this total (average) ion current density, I_{tot}, distributes self-consistently over the M sub-cells, thus $I_{tot} = \frac{1}{M}\sum_{i=1}^{M} I_i$ is solved for all M sub-cells simultaneously. In all sub-cells, the cell voltage is at each moment in time the same throughout the electrode. In order to avoid numerical problems for the CC operation, when applying a step change in current to the MCDI cell, a small external capacitance was added in the circuit model, see in Appendix C. Beyond this modification of the externally applied current-voltage

characteristic, there is for the ions no fundamental difference between CV- or CC-operation, in the sense that the forces acting on an ion to move into the pores and to be stored there are fundamentally unchanged.

4.4 Results and Discussion

In this section we show results of MCDI operation using different operational modes, focusing on the difference between constant voltage (CV) and constant current (CC) operation. Results are presented of two modes of CC operation. For these three modes in total, to be discussed below in detail, we show in Fig. 4.1 experimental and theoretical results for three main operational characteristics: effluent concentration, cell voltage, and current, all as a function of time. In all cases (also for Figs. 4.2 and 4.3), results are shown of a steady-state cycle, i.e., not the first or second cycle from a new series, but a cycle which repeats itself almost unchanged for a prolonged period. In all nine panels, data are presented as dashed red lines, and predictions of the theoretical model of Chapter 3 are shown by solid blue curves.
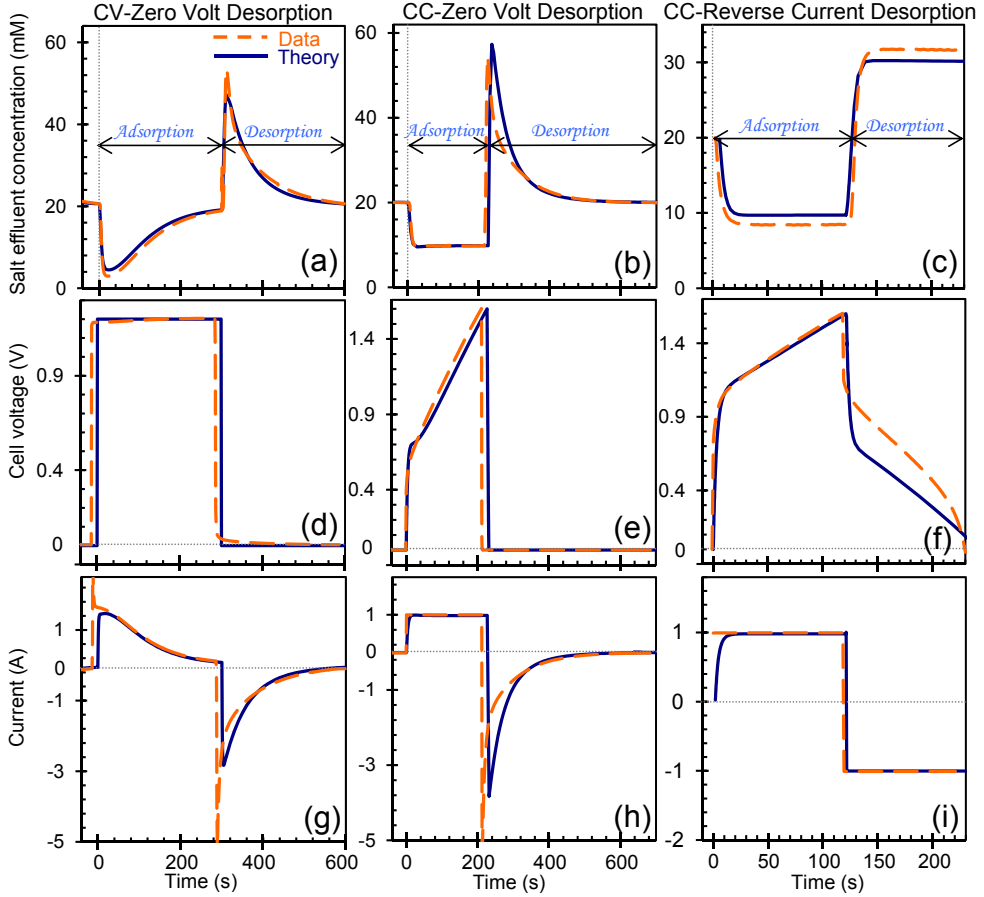
Fig. 4.1. Comparison of three operational modes of MCDI: constant voltage (CV, left column); constant current during adsorption (CC) with zero voltage during desorption (ZVD, middle column); and CC with reverse current during desorption (RCD, right column). Shown are results for effluent salt concentration (top row), cell voltage (middle row), and current (bottom row), as a function of time, for one cycle. Inlet salt concentration: $c_{salt,in}$=20 mM. In the CV-mode we have adsorption at V_{cell}=1.2 V and desorption at V_{cell}=0 V (both steps have a duration of 300 s); in CC-ZVD we have salt adsorption at +1 A until V_{cell}=1.6 V, while during desorption V_{cell}=0 V for 500 s; in CC-RCD desorption is controlled by a current of −1 A until the voltage is back at 0 V. Solid blue lines: theoretical simulations, dashed red lines: experimental data.

The three characteristics presented in Fig. 4.1 are: on the top row, first of all the effluent concentration (the concentration of the fresh water during the first period, denoted "adsorption" in panels a-c, and the concentration of the high-salinity stream in the desorption step); second the cell voltage (middle row; either applied or measured); and finally the electrical current (bottom row; either applied or measured). The first vertical column shows results of classical operation at constant voltage, as used in practically all previous work in the literature of CDI and MCDI. In this case, operation is first for a predetermined duration (here 300 s) at a pre-set value of the cell voltage, namely V_{cell}=1.2 V (see panel d) to desalinate the water, followed by a stage of the same duration at zero cell voltage. The current (panel g) is high at the start of each step and then decays back to zero. The salt effluent concentration (panel a) shows the minimum during ion adsorption as discussed previously, while during desorption we have a short peak in salt concentration before the concentration slowly decays back to the inlet value.

In the second column we show results of applying constant current (CC) conditions, but in this case CC is only applied during ion adsorption, while the ion desorption step is still defined by applying a zero voltage (now for 500 s; CC-ZVD mode). The CC-condition is applied until a pre-set upper voltage limit of V_{cell}=1.6 V is reached. At that moment we switch to the desorption step. Because of operation at CC during ion adsorption, the cell voltage steadily increases, after an initial rapid increase due to Ohmic resistances (panel e). Most importantly, we see in panel b that the freshwater salt effluent concentration is now at a stable value during the ion adsorption step (after a brief initial transition period), here around $c_{freshwater}$=10 mM.

In the third, right, column we show results of CC operation where also during desorption a constant current is applied, of equal magnitude but opposite in sign compared to adsorption (see panel i; CC-RCD mode). Both steps are now defined by limiting values of the cell voltage, being 1.6 V during adsorption and 0 V during

desorption. The cell voltage increases relatively linear for most of the time except for brief transition periods where it rapidly changes because of the Ohmic resistances, which we attribute in the theory to ion transport resistances in the spacer channel and in the electrode. Panel c shows the main result, namely that using CC operation in both steps of the cycle leads to very stable effluent ion concentrations, unvarying in time. Brief initial transition periods are due to the relatively large mixing volume in and after the stack in our small laboratory setup.

Fig. 4.1 has introduced the two novel modes of CC-operation, and shows how using CC-operation we can achieve a stable effluent freshwater salt concentration. Next we show how we can tune this effluent concentration by varying the current I, or the water flow rate Φ. As these are easily adjustable parameters during operation, these are suitable control variables to be adjusted when the setpoint of the system is to be changed, such as the salinity of the produced fresh water, or when we must correct for any gradual losses of performance over prolonged use. Results of these experiments are shown in Fig. 4.2, where we demonstrate the stable effluent concentration in the two steps of the cycle (first part with low effluent concentration is the ion adsorption step; the second part is for ion desorption) as a function of current (panel a), and water flow rate (panel c). The duration of the adsorption step is set to 120 s, while the desorption step ends when the cell voltage has returned to $V_{cell}=0$ V. It can be seen in panels a and c that upon increasing the current or upon decreasing the flowrate (in both cases following the direction of the arrows), the effluent salinity of the fresh water decreases. This is depicted in more detail in panels b and d where we show quantitatively the levels of the effluent concentration during adsorption and desorption, as a function of current I and flowrate Φ. Fig. 4.2b shows how the effluent concentration depends linearly on current, while Fig. 4.2d indicates that varying the water inlet flowrate Φ by a factor of ~3 allows us to change the effluent freshwater salinity also by a factor of ~3.

This makes sense because by reducing the water flow rate by a factor x, the total charge per unit water volume treated in a cycle increases by x and thus, for the same charge efficiency (see below), this will lead to x times more desalination per unit water volume. Fig. 4.2 shows, both experimentally and theoretically, how we can tune the effluent salt concentration to a desired setpoint, with the expected dependency that higher currents and lower water flow rates both lead to more desalination.
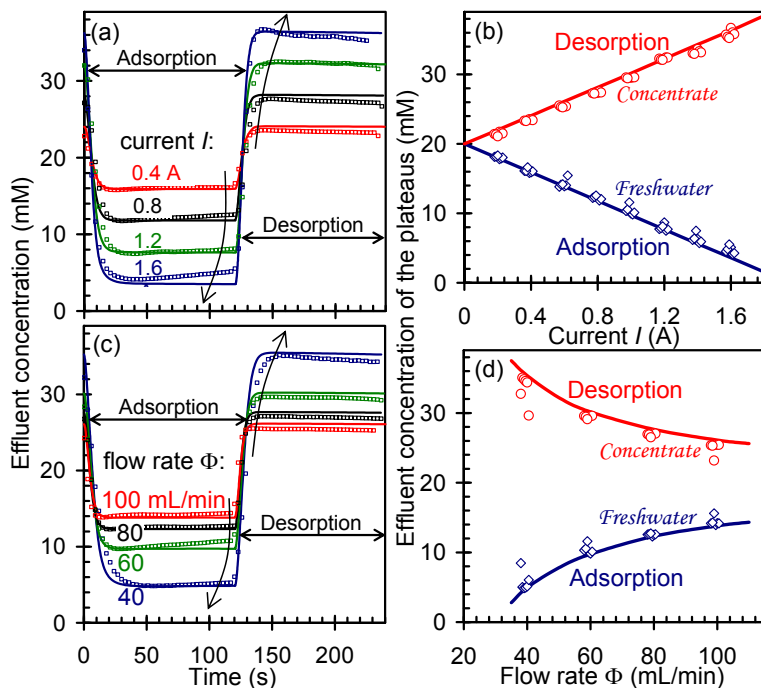
Fig. 4.2. Control of effluent concentration of fresh water and concentrate in MCDI-CC-RCD mode, using as control variable: (a) Electrical current, I, and (c) Water flow rate, Φ. The same magnitude of the current is used during ion adsorption (first 120 s), as during ion desorption (second period of ~120 s). Inlet salt concentration $c_{salt,in}$=20 mM. In (a,b) water flow rate Φ=60 mL/min; in (c,d) current ±1 A. Lines are based on theory, and data are shown as symbols. Arrows point in direction of higher desalination degree.

Finally, we show in Fig. 4.3 a large data set for the energy consumption in CDI and in MCDI, for the three operational modes discussed previously in Fig. 4.1, as a function of operational mode, system layout (with/out membranes), and inflow salt concentration, $c_{salt,in}$. To be able to compare MCDI with CDI, we add here data for CDI. Fig. 4.3 shows results both of experiments, and of the (M)CDI model. Note that energy recovery during the ion desorption step, possible in the CC-RCD mode of operation, is not included in this calculation, but it is discussed in section 6.3. For the experiments reported in Fig. 4.3, operational conditions are the same as in Fig. 4.1, except for the duration of each step in CV, which now is 500 s, and for the fact that now we vary $c_{salt,in}$. We observe that for MCDI a lower limit in energy consumption is found of around 22 kT/ion removed. Beyond $c_{salt,in}$=10 mM, this value is quite independent of $c_{salt,in}$ for CC operation, while the energy consumption increases moderately with $c_{salt,in}$ for CV-operation. For CDI, energy consumption is higher than for MCDI, and more dependent on $c_{salt,in}$, especially for CC-operation. Fig. 4.3 shows in general somewhat lower energy consumption for CC-operation than for CV-operation, but not as dramatic as a simple argument would suggest based on the fact that in CC-operation the average cell voltage is lower; neither is the energy-consumption in CC-operation higher than for CV-operation, which may be inferred in first approximation when considering that with the voltage increasing during the cycle, the energetic penalty for an extra ion to adsorb (for each electron to be transferred against the growing cell voltage) will increase steadily. Instead we find more subtle differences between the energy requirement in CC- and CV-operation, differences which will depend on the durations of the adsorption- and desorption steps, salt concentration, and chosen voltage and current levels.
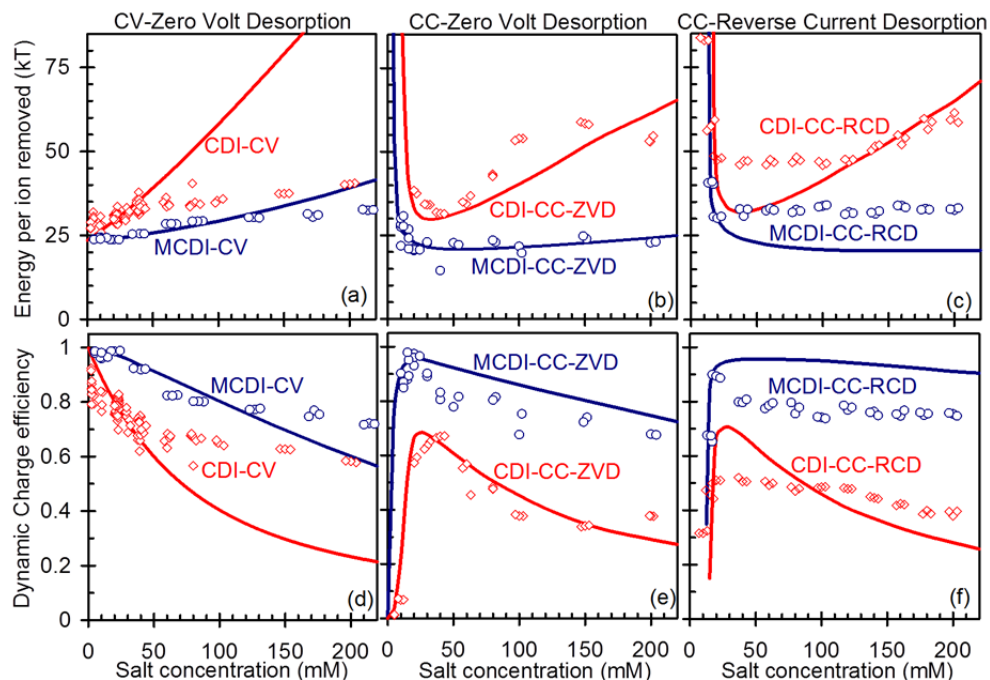
Fig. 4.3. Energy consumption and dynamic charge efficiency in CDI and MCDI. Comparison of same three operational modes as in Fig. 4.1, but now as a function of the inlet salt concentration, $c_{salt,in}$. For other parameter settings, see main text and Fig. 4.1. Panels a-c show the energy requirement per ion removed, and panels d-f show the dynamic charge efficiency, Λ_{dyn}, being the ratio of the salt adsorption vs charge. In all panels, lines are theory and points are data.

To explain, at least partly, the influence of the various variables on energy consumption, we evaluate in the second row of Fig. 4.3 the dynamic charge efficiency, Λ_{dyn}. This parameter denotes the ratio of two properties: the total desalination during ion adsorption, divided by total charge transferred in that same period. For technical details of this calculation, see the Experimental Section. Making use of the data points in Fig. 4.3, we plot energy per ion removed *vs.* dynamic charge efficiency for both CDI and MCDI in Fig. 4.4. MCDI data points aggregate in the right bottom region of Fig. 4.4, corresponding to higher dynamic charge efficiency Λ_{dyn} and lower energy per ion removed, while most CDI data are

with lower Λ_{dyn} and higher energy per ion removed. Taking all data points into consideration, it is observed that the energy per ion removed is strongly correlated with Λ_{dyn} and that the energy decreases in a non-linear pattern as the Λ_{dyn} increases.
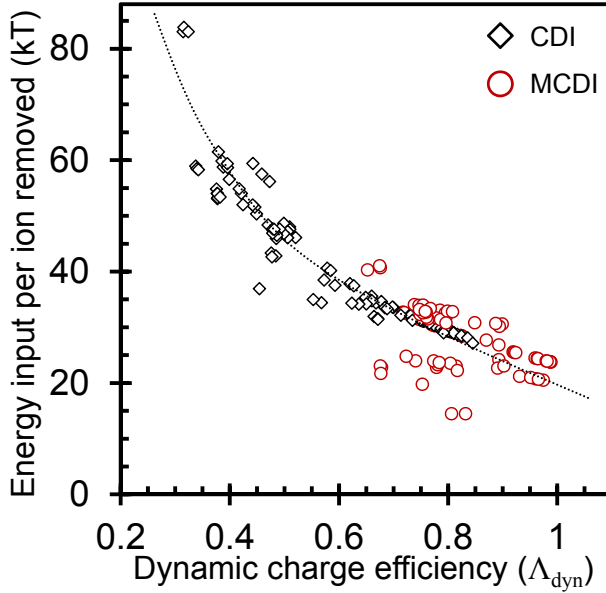
Fig. 4.4. Energy input per ion removed as a function of dynamic charge efficiency for CDI and MCDI. Diamonds are CDI data; Circles are MCDI data. The dotted line is for guiding the eyes.

Fig. 4.3, quite surprisingly, shows that the energy consumption does not decrease steadily with increasing salt concentration, which in first approximation would be expected because the ionic resistance in the spacer channel and macropores will decrease with increasing salinity. Instead, we find that for MCDI the energy consumption is fairly independent of salt concentration, while for CDI it even increases with c_{salt}. Though these experimental observations are well reproduced by the theory, a simple argument to rationalize these counterintuitive results is not so easily found.

4.5 Conclusions

In conclusion, we have demonstrated that the use of constant electrical current operation in membrane capacitive deionization (MCDI) results in a stable produced freshwater concentration, not strongly varying in time. By tuning the level of the electrical current, or the water flowrate, the freshwater salinity can be accurately adjusted. We present an extensive data set for the energy requirements of water desalination, both for CDI and for MCDI, and both for the constant current (CC) and constant voltage (CV) mode of operation. According to both the data and the theoretical model, in all situations considered, MCDI has lower energy requirements than CDI, and this difference is larger for CC-operation than for CV-operation. This difference correlates with higher dynamic charge efficiency (the ratio of salt adsorption over charge) for MCDI relative to CDI. The theoretical model reproduces most experimental data for MCDI well, though deviations remain, especially for CDI at high ionic strength in CV-operational mode. Nevertheless, the theoretical model is an essential tool to design and optimize the MCDI system, and for the evaluation of the economic viability of this technology.

Chapter 5　Optimization of Salt Adsorption Rate in Membrane Capacitive Deionization

Membrane capacitive deionization (MCDI) is a water desalination technique based on applying a cell voltage between two oppositely placed porous electrodes sandwiching a spacer channel that transports the water to be desalinated. In MCDI, ion-exchange membranes are positioned in front of each porous electrode to prevent co-ions from leaving the electrode region during ion adsorption, thereby enhancing the salt adsorption capacity. MCDI can be operated at constant cell voltage (CV), or at a constant electrical current (CC). In this chapter, we present both experimental and theoretical results for desalination capacity and rate in MCDI (both in the CV- and the CC-mode) as a function of adsorption/desorption time, salt feed concentration, electrical current, and cell voltage. We demonstrate how by varying each parameter individually, it is possible to systematically optimize the parameter settings of a given system to achieve the highest average salt adsorption rate and water recovery.

5.1 Introduction

Chapter 4 demonstrates operational modes of CDI and MCDI. The first operational mode is also the most frequently used one in the literature, which is applying a constant cell voltage (CV) between the electrodes during the adsorption step, followed by short-circuiting of the electrodes, or reversing the voltage, during the desorption step. Also it has been demonstrated that in MCDI charging and discharging the electrodes at constant current (CC) can have several major advantages in comparison with CV, such as a constant (i.e., not varying in time) and adjustable effluent concentration (Chapter 4).

For all desalination technologies, it is essential to maximize the desalination performance, i.e., the extent of desalination per unit time, besides optimizing the water recovery (WR), which is the ratio of the flow of fresh water relative to the flow of feed water. In the present manuscript, we focus exclusively on MCDI and analyse the influence of several process parameters such as adsorption time, water flowrate, and adsorption current on two key performance indicators in MCDI, namely the average salt adsorption rate (ASAR) and water recovery, WR. We discuss both the CC operational mode, as well as CV operation. The aim of this chapter is to demonstrate how the average salt adsorption rate and the water recovery can be systematically optimized for a given MCDI system.

5.2 Materials and Methods

Experimental details of the MCDI stack design used in this work have been outlined in Chapter 3, and the MCDI transport model described in Chapter 3 is again used in this chapter to compare experimental data with theoretical predictions. Employed electrode property values and theoretical parameter settings can be found in Appendix B. In this chapter, experimental and theoretical work of MCDI is reported as a function of several input parameters. In the experiments, we vary each of them in turn, while keeping the others at their reference settings, see Tables 5.1 and 5.2. For constant current operation (CC), the reference settings for the whole stack are defined as follows: during ion adsorption we apply an electrical current of 1 A to the entire stack, until the cell voltage reaches V_{cell}=1.6 V. At this moment we switch from the ion adsorption step to the ion desorption step by changing either the voltage or the current. Note that an electrical current of 1 A is equal to a current density of ~37 A per m^2 electrode area. During desorption, we either immediately switch off the cell voltage to V_{cell}=0 V for a fixed period of time (500 s) (as if short-circuiting the cell), which is the zero-volt desorption mode (ZVD), see Table 5.1, or we apply an electrical current of -1 A until the cell voltage drops back to 0 V, which is the reverse-current desorption mode (RCD), see Table 5.2. The ZVD and the RCD mode will be discussed in section 5.3.1. Note that in these experiments for CC-RCD operation of MCDI, only one input parameter, namely the desorption current, is varied in the range of -0.2 A and -2 A, while the other input parameters are unchanged, see Table 5.2 and Fig. 5.3. Note that in all cases, the duration of the adsorption step is a parameter that varies.

Table 5.1. Reference settings for MCDI-CC operation in ZVD mode.

Influent salt concentration (NaCl)	20 mM
Adsorption current (applied until the cell voltage reaches V_{cell}=1.6 V)	1 A (~37 A/m^2)
Water flowrate (stack)	60 mL/min
Desorption time	500 s

Table 5.2. Reference settings for MCDI-CC operation in RCD mode. Except for desorption current, all settings are fixed throughout section 5.3.1.2.

Influent salt concentration (NaCl)	20 mM
Adsorption current (applied until the cell voltage increases to V_{cell}=1.6 V)	1 A (~37 A/m^2)
Water flowrate (stack)	60 mL/min
Desorption current (applied until the cell voltage decreases to 0 V)	-0.2 to -2 A

For constant voltage operation (CV), we define the reference settings as follows: A cell voltage of V_{cell}=1.2 V is applied during ion adsorption for 500 s, and during ion desorption, we either immediately drop the cell voltage to V_{cell}=0 V for a fixed duration of 500 s, which is the zero-volt desorption mode (ZVD), or we apply a reversed voltage of -1.2 V, again for 500 s, which is the reverse-voltage desorption mode (RVD). These two reference settings for CV were defined in Chapter 3 as 0-MCDI and r-MCDI. A full cycle consist of an ion adsorption step followed by an ion desorption step. During both steps of the cycle, a 20 mM NaCl solution is continuously pumped into the stack at a constant water flowrate of 60 mL/min for the whole stack, which is equal to 7.5 mL/min per cell. The effluent is recycled back to the reservoir (solution residence time in reservoir ~3 hour).

The salt adsorption and charge in an MCDI-cycle can be derived from the data of the salt effluent (outflow) concentration versus time, and from the data for electrical current versus time, respectively, following the procedures as explained in previous Chapters. For salt adsorption, the difference in inflow salt

concentration and outflow concentration is integrated with regard to time, and multiplied with the water flowrate, while for charge, the current is integrated over time. All data shown in this chapter are obtained under the DE condition.

5.3 Results and discussion

In this section, we first discuss desalination cycles for CC operation of MCDI under the DE condition and show the influence on a series of performance indicators, such as salt adsorption, charge transferred, and especially the average salt adsorption rate (ASAR) and water recovery (WR), by varying the following input parameters, namely: inflow salt concentration, adsorption current, water flowrate, desorption time, and desorption current. We will show the results for each parameter independently by varying each one in turn. In the second part of this section we describe results of CV operation of an MCDI system, focusing on the influence of cycle duration and desorption voltage. In all cases we compare experimental results with theoretical model predictions. To describe the desalination performance of MCDI theoretically, we use the process model for the MCDI process as described in Chapter 3. Values of input parameters are summarized in Appendix B.

5.3.1 Constant current (CC) operation of MCDI

5.3.1.1 Desorption in "Zero Volt Desorption"-Mode

In section 5.3.1 we present results of CC operation of MCDI in two operational modes: zero-volt desorption (ZVD) and reverse-current desorption (RCD).

Fig. 5.1 presents results for MCDI-CC-operation in ZVD mode, where the variation in effluent salt concentration during a single desalination cycle is shown. Both experimental and theoretical results are presented, and as can be observed all experiments can be well reproduced by the model. First of all, Fig. 5.1a shows that

the duration of the desalination cycles depends on the influent salt concentration. For instance, when the influent salt concentration is decreased from 20 mM to 5 mM, the adsorption time drops from 200 s to only a couple of seconds. This can be explained by the fact that at lower influent concentrations we have a higher spacer resistance and quicker ion depletion. Therefore, at a fixed constant current of 1 A, the cell voltage reaches the set end voltage of 1.6 V much more rapidly.

MCDI constant current operation with zero-volt desorption (ZVD)
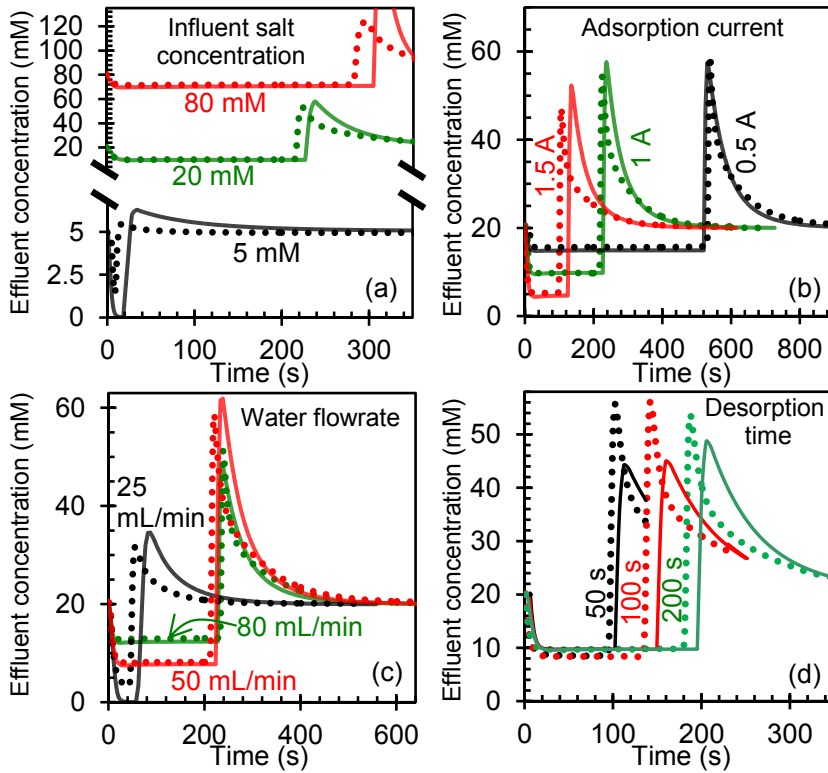
Fig. 5.1. Effluent salt concentration during a dynamic equilibrium cycle for CC-MCDI in ZVD-mode as a function of experimental parameters varied around the reference settings, see Table 5.1: (a) influent salt concentration, (b) adsorption current, (c) water flowrate, and (d) desorption time. The dotted lines are experiments, and the solid lines are theory.

In Fig. 5.1b and c it is shown that a lower effluent salt concentration can be achieved by increasing the electrical current during the adsorption step, as well as by decreasing the water flowrate. Fig. 5.1d shows that when we decrease the desorption time, the adsorption capacity per cycle decreases and consequently the adsorption time also becomes shorter. This is because a decrease in the desorption time leads to incomplete release of counterions from the electrodes and consequently leads to a lower ion removal in the next adsorption step.

It can be observed in Fig. 5.1b and c that by varying the current during ion adsorption and/or by varying the water flowrate, the salt concentration in the effluent can either be increased or decreased, and therefore in the CC mode it is possible to fine-tune the salt concentration in the effluent water stream to a desired level, see Chapter 4.

Data such as obtained for the experiments shown in Fig. 5.1 are presented in aggregate form in Fig. 5.2 with each panel (a-d) in Fig. 5.1 corresponding to one column (I-IV) in Fig. 5.2. In Fig. 5.2 row A we present the total cycle time (t_{cycle}) and the water recovery (WR) as a function of influent salt concentration (column I), adsorption current (column II), water flowrate (column III), and desorption time (IV). *WR* indicates the fraction of the salt stream which is reclaimed as fresh water. WR can be calculated according to:

$$WR = \frac{\Phi \cdot t_{ads}}{\Phi \cdot t_{ads} + \Phi \cdot t_{des}} = \frac{t_{ads}}{t_{cycle}} \tag{5.1}$$

where Φ is the water flowrate, t_{ads} the adsorption time, t_{des} the desorption time, and t_{cycle} is the sum of t_{ads} and t_{des}. As in our examples Φ is always the same for the adsorption and desorption step, we can use a simplified expression for WR ($=t_{ads}/t_{cycle}$).
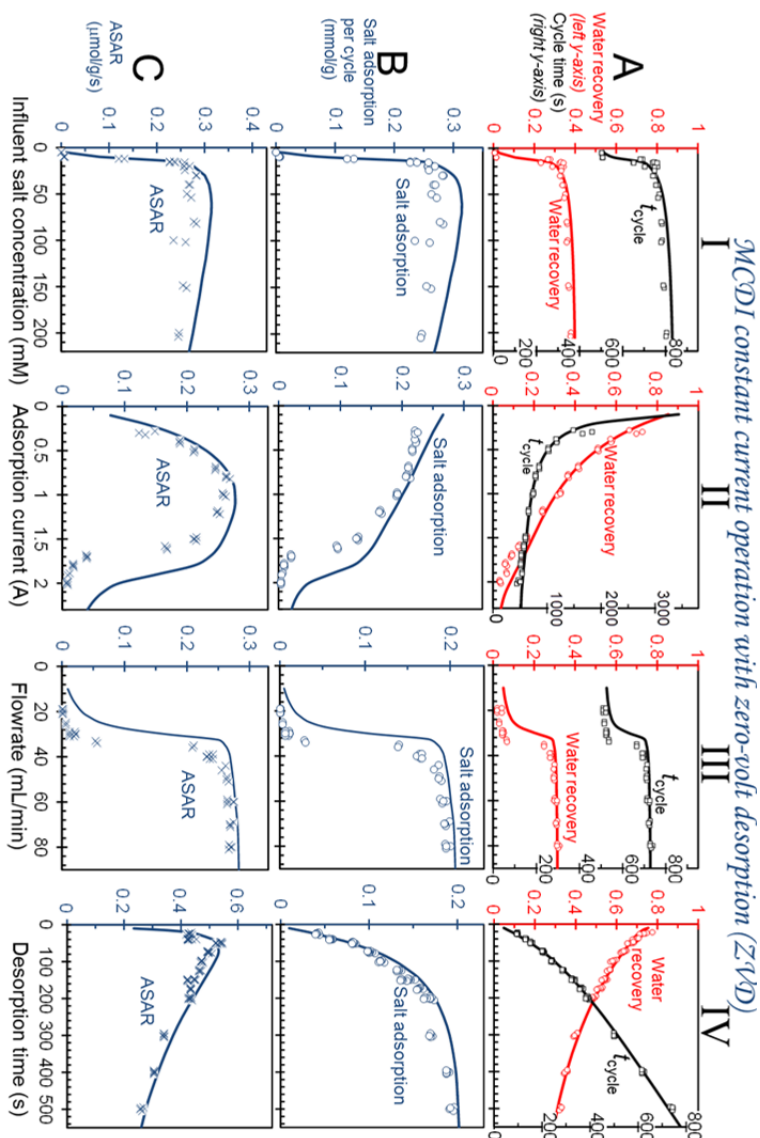
Fig. 5.2. Experimental and theoretical results for operation of MCDI-CC in ZVD-mode. Water recovery and total cycle time (t_{cycle}) (row A), salt adsorption per cycle, per gram of total electrode mass (row B), and average salt adsorption rate (ASAR) (row C). Each column describes the results based on varying one input parameter at a time: column I influent salt concentration, column II adsorption current, column III water flowrate, and column IV desorption time. Symbols are experimental data, and lines are theory. Reference settings are given in Table 5.1.

Results of salt adsorption are given in row B, both experimentally and theoretically, as a function of the same four parameters (column I-IV). Fig. 5.2-B-I shows that when the influent salt concentration is increased from close to zero to around 20 mM, the salt adsorption rapidly increases, but after that the salt adsorption again slightly decreases. Fig. 5.2-B-II shows that when the electrical current during adsorption is increased, the salt adsorption decreases and when the electrical current is above 1.5 A, the decrease is even faster. Fig. 5.2-B-III shows the existence of two regions, one of low salt adsorption at a low flow rate $\Phi<35$ mL/min, and one of high salt adsorption for $\Phi>35$ mL/min. All the experimental data can be reproduced very well with our theoretical model. However, some phenomena, for instance the rapid increase of salt adsorption when the influent salt concentration increases from zero to ~20 mM, or when the flowrate is increased beyond ~35 mL/min, do not have a single and easy explanation and must be due to the interplay of various process parameters.

For commercial use of an MCDI system it is important to have maximum salt removal within a given period of time. Therefore, in order to evaluate how quickly salt can be adsorbed, we introduce a new performance indicator, namely the average salt adsorption rate (ASAR) (see Fig. 5.2 row C), which is the salt adsorption per cycle, per gram of total electrode mass (Fig. 5.2-row B), divided by the cycle time (Fig. 5.2-row A). Thus, ASAR is a measure of the average 'speed', or rate, of salt adsorption. The data in Fig. 5.2-row C demonstrate that when we vary each input parameter in turn, optimal values for ASAR are obtained in some cases. Beyond 20 mM, ASAR is fairly independent of salinity (Fig. 5.2-C-I), and independent of flowrate when flowrate is higher than 40 mL/min (Fig. 5.2-C-III). However, a maximum ASAR is achieved at around ~1 A (Fig. 5.2-C-II), and at a desorption time of 50 s (Fig. 5.2-C-IV). Note that these optimized input parameters depend on the specific device, its operational mode, and values for other

parameters. A general conclusion that can, however, be drawn is that the input parameter settings that lead to the highest salt adsorption per cycle do not always lead to the highest ASAR.

In addition, closer inspection of the results in Fig. 5.2 shows that for column III, the trends in WR and ASAR are nearly the same. However, in column II when the adsorption current is higher than 1 A, and in column IV when the desorption time is higher than 50 s, the ASARs have the same declining trend as the water recovery. Only in column I when the influent salt concentration is beyond 20 mM, the water recovery increases slightly, while the ASAR levels off.

In brief, we have demonstrated that in the CC-ZVD mode, variation of input parameters has a great impact on WR and on ASAR, which are the two most important indicators to evaluate the performance of an MCDI system.

5.3.1.2 Desorption in "Reverse Current Desorption"-Mode

In a different operational mode, we apply a reversed current during desorption until V_{cell} becomes zero again (RCD mode).

Fig. 5.3a shows that by applying a less negative current during the desorption step, we extend the period of desorption and consequently also extend the duration of the adsorption step. This leads to more salt removal per cycle, see Fig. 5.3c. However, Fig. 5.3b shows that less negative desorption currents decrease the WR and increase the total cycle time. Combination of these effects is shown in Fig. 5.3d, where we show that as the desorption current becomes more negative, ASAR first increases and then decreases again. Thus, for this system, it is found that the highest ASAR is at a desorption current between -0.8 and -1.8 A, while WR is highest at a desorption current of -2 A.

MCDI constant current operation with reverse-current desorption (RCD)
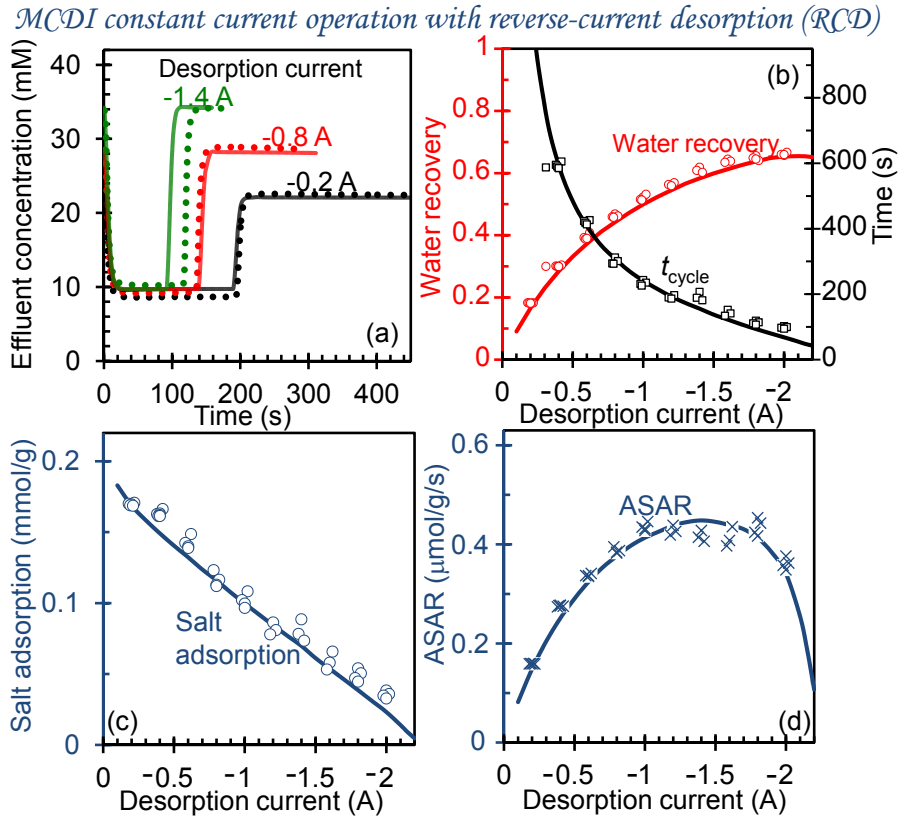
Fig. 5.3. Experimental and theoretical results for MCDI-CC operation in RCD mode. (a) Effluent salt concentration as a function of time during one cycle. Dotted lines: experiments, solid lines: theory. (b) Water recovery and total cycle time. (c) Salt adsorption and charge per cycle per gram total electrode mass. (d) Average salt adsorption rate (ASAR). For panels (b), (c) and (d) symbols are experimental data and lines are theory. See Table 5.2 for reference settings.

5.3.2 Constant voltage (CV) operation of MCDI

5.3.2.1 Desorption in "Zero Volt Desorption"-Mode and in "Reverse Voltage Desorption"-Mode

Next, we discuss CV operation of MCDI, which implies that during the adsorption step a constant voltage is applied, instead of a constant current. Constant Voltage (CV) is the classical operational mode of CDI and MCDI. CV operation can be done in the ZVD and the RVD mode, the difference to be discussed below. For all CV experiments, during salt adsorption a cell voltage of V_{cell}=1.2 V is applied for a fixed period of time. During desorption in ZVD-mode we short-circuit the cell (i.e., apply V_{cell}=0 V) for the same period. For the RVD-mode, we apply V_{cell}=-1.2 V (which is the reverse of the adsorption voltage) during desorption, also for the same period as adsorption. In both operational modes, because the water flowrate is the same in a complete cycle (60 mL/min for the full stack of N=8 cells), and we set the adsorption time equal to the desorption time (both are half of the cycle time, which is varied in Fig. 5.4), the water recovery is always 50%. In Fig. 5.4 data for MCDI operation in CV-ZVD and CV-RVD mode are presented as a function of cycle time. In Fig. 5.4a, salt adsorption per cycle per gram of total electrode mass is shown both experimentally and theoretically, and the CV-RVD mode leads to higher salt adsorption per cycle than the CV-ZVD mode. As Fig. 5.4a shows, when the cycle time exceeds 500 s, for both the operational modes, salt adsorption levels off. However, ASAR peaks in both modes at a much shorter cycle time, around 200 s, indicating that in the present setup such a low cycle time of 200 s is the optimum value to achieve the highest ASAR (Fig. 5.4b). Note that the highest ASAR is also obtained by using the CV-RVD mode.

MCDI constant voltage (CV) operation
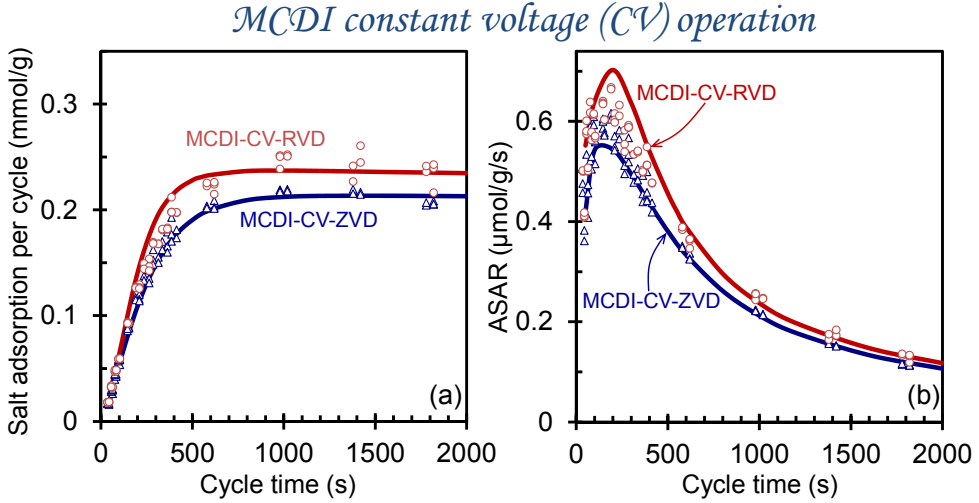
Fig. 5.4. Experimental and theoretical results for MCDI-CV operation for ZVD and RVD mode. (a) Salt adsorption per cycle. (b) Average salt adsorption rate (ASAR). For each experiment, the influent salt concentration is 20 mM, during adsorption V_{cell}=1.2 V, and during desorption V_{cell}=0 V for ZVD and V_{cell}=-1.2 V for RVD. Periods of adsorption and desorption are the same, and the cycle time is the sum of these two. Lines: theory; symbols: experimental data (circles: RVD, triangles: ZVD).

5.3.2.2 MCDI-CV operation with varying desorption voltage

As can be inferred from Fig. 5.4a, by applying a negative cell voltage during desorption, it is possible to achieve about 15% more salt adsorption per cycle than simply by short-circuiting the cell during the desorption step, which is the classical operational mode of CDI and MCDI.

In order to find the optimal desorption voltage to achieve the maximum in ASAR, we performed a further series of CV experiments, where we vary the desorption voltage. An adsorption voltage of +1.2 V was applied for 500 s, and during desorption, the cell voltage was varied between 0 V and -2 V, also for a

duration of 500 s. As the total cycle time for each experiment is 1000 s, ASAR follows the same trend as the salt adsorption per cycle shown in Fig. 5.5 and consequently is not shown. Both experimental data and results of theoretical calculations of salt adsorption and charge are presented in Fig. 5.5. It is observed that salt adsorption and charge increase slightly with desorption voltage, with for instance at a value of -1.4 V, approximately 15% more salt adsorption than for desorption at 0 V. However, at voltages more negative than -1.0 V, the charge per cycle increases strongly, which is not predicted by the model. For CDI, a similar observation was made when increasing the cell voltage during adsorption [128]. We believe the effect is due to Faradaic reactions, e.g. water splitting, at high desorption voltages. As a result, MCDI operated at very negative desorption cell voltages utilizes more charge, resulting in a less energy-efficient salt adsorption process, and is therefore not recommended.
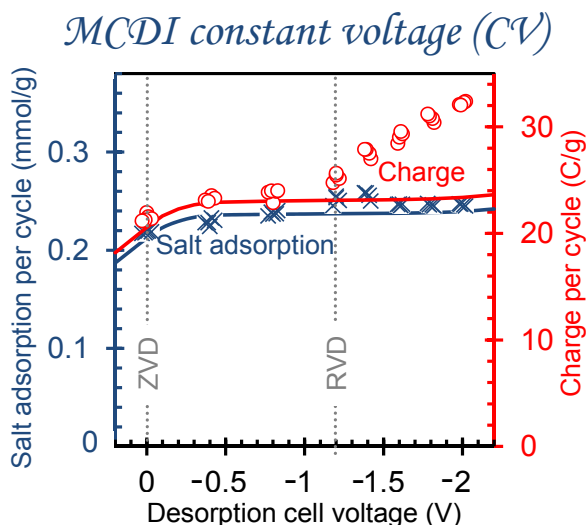
Fig. 5.5. Salt adsorption and charge per gram of total electrode mass per cycle in MCDI-CV as a function of negative desorption voltage (0 to -2 V). Influent salt concentration $c_{salt,in}$=20 mM, durations of the adsorption and desorption step each 500 s, and voltage during adsorption V_{cell}=1.2 V. Symbols: data; lines: theory. Symbols intersected by the dashed vertical lines correspond to the CV-ZVD and CV-RVD data at cycle time of 1000 s in Fig.5.4.

5.3.3 Discussion

The interesting question is what can exactly be inferred from the data. Starting at Fig. 5.2, a comprehensive data set for MCDI-CC operation in the ZVD-mode is presented, focusing on the two key performance indicators for MCDI, namely water recovery (WR) and average salt adsorption rate (ASAR). As can be observed, varying influent salt concentration (column I), water flowrate (III), or desorption time (IV), in all cases leads to a similar trend in WR and in ASAR, both either going up or down with a change in one of the parameter settings. A deviation is found in the dependence of ASAR and WR on the adsorption current (II), where

the former has a maximum at an adsorption current around 1 A, while to achieve the highest WR, the adsorption current must be minimized.

Next, Fig. 5.3 summarizes data for MCDI-CC in the RCD-mode of operation. In this case we also find that ASAR and WR have a different dependency on the input parameter that is varied, being in this case the adsorption current, with ASAR being at a maximum for a fairly large range of values for the desorption currents (between -0.8 and -1.8 A), while WR steadily increases with less negative desorption currents. The results for MCDI-CV (Figs. 5.4 and 5.5) demonstrate that optimum cycle times (to have the highest ASAR) are much shorter than typically required for the carbon electrodes to get saturated in this thesis (often beyond 10 min, approaching one hour); here we find a maximum ASAR at a cycle time of only 200 s, much shorter than previously used values. All of these results show that the complete optimization of an MCDI system, considering also energy costs and material properties, is a complicated task requiring multidimensional optimization.

In general, Figs. 5.1-5.5 show that our two-porosity modified-Donnan model well describes the data when we fit the CV-data and CC-data separately, using as freely adjustable parameters the membrane charge density X, the ion diffusion coefficient in the membrane D_{mem}, the fraction of the total water flow going through one electrode, β, as well as the specific electrode resistance, R_{elec}. However, as may be observed from Appendix B, to fit these two large data sets (one for CV- and the other for CC-operation), we need to use different numbers for X, D_{mem} and β. This is not an optimal situation and indicates that our model is not yet fundamentally rigorous, because ideally one set of model parameters describes data both for CC and CV operation at the same time. Several model improvements can be made to help us achieve this aim, as summarized next: first of all, full porous electrode theory has not yet been implemented, but instead we have assumed that in each sub-cell we have equalized properties across the electrode, with the ionic

resistance empirically described by a single parameter R_{elec}. An improved model makes use of porous electrode theory and does not need this parameter R_{elec}. Secondly, for the membrane we have assumed equal ion diffusion coefficients for the counterion and the co-ion. However, as known from membrane open-circuit voltage diffusion potential measurement [129], the co-ion can have a different mobility (diffusion coefficient) from the counterion in the membrane. This effect can be included in an improved model. Furthermore, the spacer channel is modelled as a series of stirred tanks, and the exact concentration profile of ions across the channel (in the direction from membrane to membrane) is not yet considered. Finally, our model assumes perfect symmetry of anode and cathode, which is not true in reality because the cation and anion have different diffusion coefficients (both in the open space, and in the membranes), and because the anion-exchange membrane and the cation-exchange membrane have a different charge density. When all of these effects are included in a full-scale model, it is hopefully possible to fit all presented data sets in Chapters 3-5 by one and the same model, with one set of input parameters. Such a model can be confidently used for process optimization studies.

5.4 Conclusions

In Chapter 5 we have presented experimental and theoretical results for CC and CV operation in the membrane capacitive deionization (MCDI) process. We have systematically varied the following input parameters, namely influent salt concentration, water flowrate, adsorption and desorption current, desorption voltage, and adsorption and desorption times, and presented their effect on salt adsorption per cycle, total charge, and water recovery (WR). We define the average salt adsorption rate (ASAR) to evaluate the rate of desalination, and demonstrate a systematic procedure to optimize the input parameters in order to reach the highest ASAR. A theoretical MCDI process model is validated by comparison with experimental data, with the outcome that in most cases the theory describes the experimental results very well, though the need for parameter settings that differ between CC and CV operation makes it clear that the model must be significantly improved. In the future, an exact optimization of parameter settings can be realized based on a validated MCDI process model, in order to obtain the highest ASAR and WR for the operation of a particular MCDI system.

Chapter 6   Discussions and Conclusions

6.1 Introduction

This thesis deals with capacitive deionization and membrane capacitive deionization from various perspectives. In Chapter 2, we illustrate the electrical double layer structure inside the micropores of carbon electrode based on the modified Donnan model. Combining the equilibrium model with a transport model, we have demonstrated the simulation of the (membrane) capacitive deionization process (Chapter 3). Then we discussed an alternative operational mode for MCDI, which is more advantageous than the classical constant voltage operational mode (Chapter 4). Finally, we discussed how to optimize the salt adsorption for the MCDI process with respect to the maximum salt adsorption rate (Chapter 5). Generally speaking, we provided a way to understand the (M)CDI process from the very fundamental side of ion adsorption and analysed the performance of (M)CDI systematically, and our findings can be of contribution to design an (M)CDI system. In this chapter we will discuss various issues with regard to what can be further modified or improved in our future work, and I will provide the reader with a comparison of energy consumption between MCDI and reverse osmosis, which can be used as an indicator to reveal the market prospect of a MCDI, followed by a general conclusion.

6.2 Measurable properties of porous carbon electrodes and ion-exchange membranes

In the theoretical work of this thesis, values of some properties are determined by fitting theory to data. However, those parameters can be measured independently with carefully designed experiments, which in the future can lead to improvement on the modelling part of work. In this section, we will discuss those measureable properties and possible ways to measure them.

6.2.1 Two porosities of porous carbon electrode

In this thesis, a two-porosity assumption was made to distinguish the electrode pores into two different categories: micropores (*i.e.*, intraparticle porosity) and macropores (*i.e.*, interparticle porosity). The microporosity "p_{mi}" is obtained by fitting theory to data in the equilibrium model, and the macroporosity "p_{mA}" is estimated. However in reality, these two porosities can actually be measured, if the content of carbon and polymer binder of the electrode is known. According to Ref. [130], they can be calculated via the following equations,

$$p_{mA} = \frac{\delta_{elec} A - \left(m_{elec} w_{carbon} / \rho_{carbon} + m_{elec} w_{polymer} / \rho_{polymer} + V_{mi} \right)}{\delta_{elec} A} \tag{6.1}$$

$$p_{mi} = \frac{\delta_{elec} A - \left(m_{elec} w_{carbon} / \rho_{carbon} + m_{elec} w_{polymer} / \rho_{polymer} + V_{mA} \right)}{\delta_{elec} A} \tag{6.2}$$

where δ_{elec} and A stand for the thickness and exchange area of the electrode, m_{elec}, w_{carbon}, and $w_{polymer}$ are electrode mass, weight fractions of the carbons, and polymer material (*i.e.*, polymer binder added for mechanical stability). For the weight fractions, together $w_{carbon} + w_{polymer} = 1$, if no other additives, e.g., carbon black, are present in the electrode. Next, ρ_{carbon} is the solid density of the carbon, which most of the time is assumed to be around 1.95 g/cm^3 for all carbons investigated [130],

and $\rho_{polymer}$ is density of polymer. Finally V_{mi} is the volume of pores inside carbon (in transport theory called micropores), which can be measured by the nitrogen gas sorption at -196°C using, for instance, an Autosorb iQ MP (Quantachrome instruments, Germany), and V_{mA} is the volume of transport pathways outside the particles (called in transport theory macropores), which is equal to $p_{mA}\delta_{elec}A$.

6.2.2 Membrane charge density

In the thesis, the employed anion- and cation-exchange membranes are AMX and CMX (Neosepta, Tokuyama, Japan), respectively. Their membrane charge densities or ion-exchange capacities are assumed to be the same, either 3000 or 8000 mM per volume of water in the membrane, see Appendix B. In this thesis, those values are selected by fitting the MCDI transport model to the experimental data. However, the ion-exchange capacity can be measured by ion sorption experiments under equilibrium conditions [131], where for AMX it is about 4800 mM and for CMX 6000 mM, or by the existing titration method [132-134]. The measured numbers for AMX and CMX are somewhat different from each other, and are also different from our employed values. Currently in the MCDI transport model, we only consider half of the MCDI cell, and later on, the model can be extended for a full cell, which allows both membranes to be included independently.

6.2.3 Chemical attraction term for neutral salt adsorption at zero cell voltage

During the modelling work of the salt adsorption in micropores at the liquid/electrode interface we have used the modified Donnan model which incorporates a chemical attraction term, μ_{att}. However, the value of this term is not measured, but instead we used an empirical number which is derived from the

fitting procedure of experimental data, either μ_{att}=1.4 kT or 2 kT for Na$^+$ and Cl$^-$, and 2.5 for Ca^{2+}. In practice, this term can also be measured. Herewith we give two possible solutions. One method is to firstly immerse the carbon electrode into a solution with prior knowledge of its ion concentration c_0. After sufficient time, remove the carbon electrode from the solution, measure the concentration of ions in the solution c_{end} again. The difference of the ion concentration between the two steps c_0-c_{end} times the volume of the solution V_s gives the adsorbed amount of ions. Another method is the ion exchange method, mostly used in determining the ion-exchange capacity of the ion-exchange membranes. We can first immerse the porous carbon electrodes into a solution which contains a given ion species (e.g. Na$^+$) for sufficient time to let the adsorption take place, and then exchange the adsorbed ions with another species of ions (e.g. Mg^{2+}) by placing the carbon electrode in its highly concentrated solution. In the end, after the exchange, the concentration of initially adsorbed ions now in the concentrated solution can be measured analytically by either inductively coupled plasma optical emission spectrometry (ICP-OES) (for cations) or ion chromatography (IC) (for anions). The two methods can be repeated several times at different concentrations in order to explicitly derive the exact concentration of the adsorbed ions in the micropores as a function of the bulk concentration in the electro-neutral conditions. Afterwards, with the concentration of the adsorbed ions in the micropores and the concentration in the macropores, the attraction term can be derived according to a simplified version of the Eq. 2.4 at electro-neutral conditions without considering the cell voltage, $\mu_{att} = \ln \dfrac{c_{j,mi}}{c_{j,mA}}$. The procedure can be used for determining the chemical attraction term for different ions and its dependence on all parameters.

In the future, based on accurate measurement of all the above mentioned properties in section 6.2, the theoretical model can be further modified in such a

manner that embraces more physical evidence instead of using assumed values or values obtained from theory/data fitting.

6.3 Optimal data processing for maximum salt adsorption and energy consumption

The salt adsorption and charge in an (M)CDI-cycle can be derived from the data of salt concentration and electrical current versus time, following the procedure as explained in previous chapters. For salt adsorption, the concentration difference between the inflow and the outflow is integrated over time from the moment when charging starts till its end, and multiplied with the water flowrate. For charge, the current is integrated over time. In addition, energy consumption is also calculated based on integrating the power (product of cell voltage V_{cell} and applied current I) over the adsorption-step, which is already explained in Chapter 4. In the procedure, the beginning and the end of a cycle is the moment when a step change of current or voltage occurs. If the desorption time is not enough for complete ion release (less than ~500 s), after DE condition is reached, normally there will be a systematic delay of the salt adsorption/desorption as a function of time compared to the current/voltage change, to be discussed later. Because of the delay, the data analysis procedure can be further modified in order to reflect the "real" salt adsorption and energy consumption. To begin with, we will present the analysis of data under the dynamic equilibrium (DE) condition in detail for salt adsorption and energy consumption. Fig. 6.1 shows an example of cycles of (a) effluent salt concentration, (b) current, and (c) cell voltage obtained during the experiment, where the influent is 40 mM NaCl solution, and the total water flowrate is 30 mL/min for a stack consisting of 8 cells. During the adsorption-step, an electrical current (1 A) is applied for 100 s, and during the desorption-step, -1 A is applied

until the cell voltage drops to V_{cell}=0 V. Note here 1 A can translate to the current density of 37 A/m².
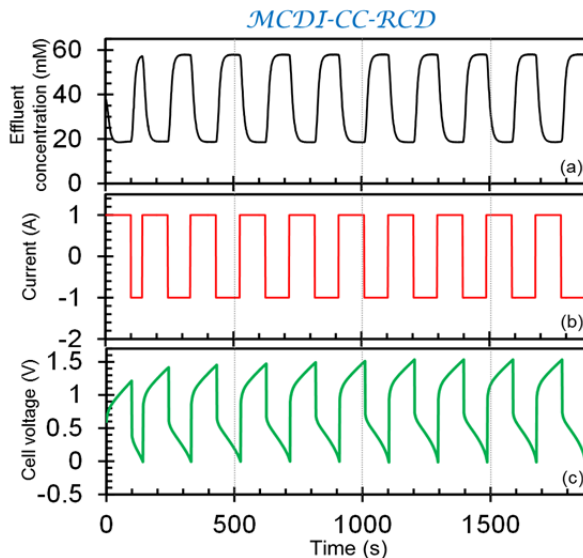
Fig. 6.1. Experimental results of (a) effluent concentration, (b) current and (c) cell voltage as a function of time for MCDI at constant current. Influent: 40 mM NaCl. During the adsorption-step an electrical current of 1 A was applied for 100 seconds, after that the current during the ion-release step was controlled at -1 A until the cell voltage dropped back to 0 V for each cycle. In total a number of 10 cycles is shown, and the DE was reached after the 3rd cycle. See Fig. 6.2 for detailed view.

Taking the 7th cycle that is under the DE condition in Fig. 6.1 as an example, see Fig. 6.2, once the electrical current is applied, the cycle starts. This is also the beginning of the salt adsorption with respect to the data analysis in previous chapters. Yet at this moment the effluent concentration is still higher than the influent concentration, in other words, the ions at this moment are still being released. It takes a few seconds for the effluent concentration to become lower than the influent concentration, only then the "real" adsorption-step starts. This "real" beginning of the adsorption step has a short systematic delay in comparison to the moment when the electrical current is applied, and this delay can be found in all cycles under the DE condition. Similarly, for desorption, when the current is

reversed from 1 to -1 A (adsorption ends, desorption starts), it takes the effluent concentration again a few seconds to rise above the influent concentration, and also when the discharging ends (current is reversed to 1 A again), the effluent concentration does not drop below the influent concentration immediately, but after several seconds. This systematic delay, as described above, is mainly caused by the continuous mixing of just produced fresh water with untreated water in the spacer channel and in the additional volume present in the stack (free space which is not filled with the MCDI cells), which occurs every time when the electrical current is changed. Hence to show the real salt adsorption, instead of integrating the concentration difference between influent and effluent from the point where the current is applied till the current is reversed, we integrate over the time period from point A (Fig. 6.2a), where the effluent concentration intersects the influent concentration, to the second intersection, point B (Fig. 6.2a). Similarly for the salt desorption, we integrate from point B to C, which is the third intersection of the influent concentration and the effluent concentration (Fig. 6.2a).
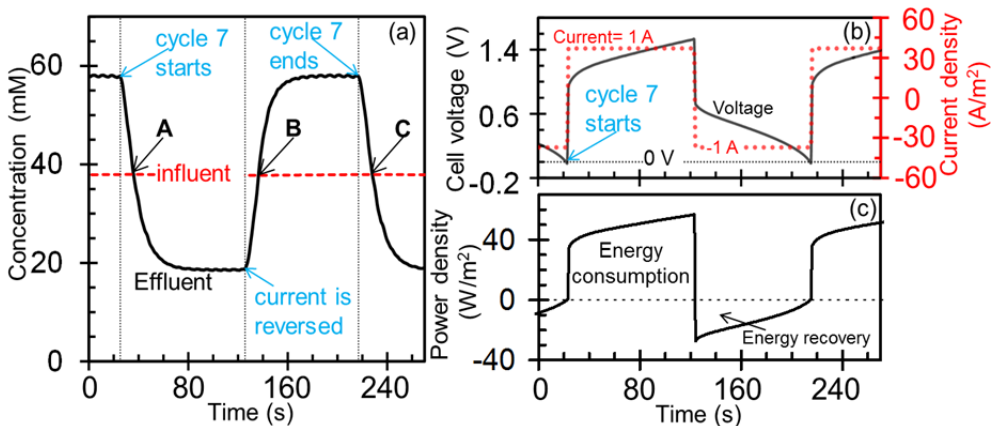
Fig. 6.2. Example data for MCDI operation at constant current (CC). (a) Influent/effluent concentration (mM) as a function of time. Dashed line: influent concentration; solid line: effluent concentration. (b) Cell voltage (V) and current density (A/m^2) as a function of time. Dashed line: current density; solid line: voltage. (c) Power density (W/m^2) that is the product of current and voltage as a function of time.

Fig. 6.2b shows the electrical current density and the cell voltage as a function of time, for the 7th cycle in the series presented in Fig. 6.1. To display the power (W) as a function of time as shown in Fig. 6.2c, the current (I) and the corresponding cell voltage at every moment in time are multiplied. The energy consumption can be computed via integrating the power over the time for the whole cycle. During the adsorption-step, the current (I) and the voltage (V) have the same sign (+), and thus the power (W) has always a positive value, implying ion adsorption costs energy. In Chapter 4, we only took the adsorption-step into account in the energy calculation. However, during the desorption-step, ions are released spontaneously thereby creating a negative current, and simultaneously the cell voltage is gradually declining to zero, which result in a negative power, meaning the system recover energy during the ion release-step, for example, by powering another (M)CDI system or a rechargeable battery. In the new approach, assuming all the released energy during the desorption-step can be recovered, we can integrate the power over the whole cycle, and thus the total energy consumption will be lower.

Using the new approach as an example, we re-analysed the data point at 200 mM (MCDI-CC-RCD) in Fig. 4.3, Chapter 4. Table 6.1 shows that with the new analysing method, we are able to "increase" the salt adsorption and the dynamic charge efficiency slightly, and "decrease" the energy consumption per ion removed significantly. Apparently, when presenting data of CDI performance, it is imperative to define the method of analysis.

Table 6.1. Comparison of salt adsorption, dynamic charge efficiency, and energy consumption per ion removed for the MCDI-CC-RCD data point at 200 mM in Fig. 4.3, Chapter 4, by two methods of analysis.

	Chapter 4	Chapter 6
salt adsorption (mmol/g)	0.108	0.112
dynamic charge efficiency	0.75	0.78
energy consumption per ion removed (kT)	33	24

6.4 Energy consumption for producing fresh water and comparison with reverse osmosis

It is indubitable that the thermodynamic minimal energy required for desalination is independent of the type of separation process [63]. However, because of fundamental differences between desalination technologies, the energy required to remove a given amount of salt can vary significantly. To testify if MCDI can be competitive in the desalination world, here, we compare its energy consumption per volume fresh water produced with the most prevalent technique, reverse osmosis (RO). For the energy consumption of RO, data are obtained from literature, see Appendix D; and for the comparison, a 13-cell MCDI unit is constructed consisting 26 electrodes (δ_e=383 μm, and m_{tot}=19.0 g). Apart from the electrode weight and thickness, for the other experimental settings, see Chapter 3.

A series of experiments are performed on the 13-cell MCDI stack, and in all cases we use NaCl as the influent salt solution. We flow solutions with the concentration ranging from 0.4 to 5.2 g/L TDS (20 to 90 mM NaCl, 1 g/L TDS=17.1 mM) into the stack, and desalinate them either to 0.5 g/L TDS (8.6 mM NaCl) or to 1 g/L TDS (17.2 mM NaCl), in both cases using the CC-RCD mode (I_{ads}=-I_{des}, desorption until V_{cell} back to zero), where the duration of both the adsorption and the desorption step is 120 s (water recovery WR=50%, the water flow rate is 30 mL/min per stack, and the required electrical adsorption current I_{ads} to achieve this aim is given in the Fig. 6.3b). The two freshwater concentration levels defined above represent palatable drinking water (with good taste), and the limit of drinking water, respectively [135]. As presented in Fig. 6.3a, the majority of energy consumption data for large scale RO system is below 2 kWh/m^3 within the whole concentration range. In the case of MCDI, if the product salinity is below 1 g/L TDS, (diamonds in Fig. 6.3a), when the influent salt content is below ~3 g/L, MCDI can be advantageous over RO. However if even purer water (~0.5 g/L TDS)

has to be produced, the energy consumption for each influent salt concentration is nearly doubled. As a result, MCDI becomes competitive only if the influent salt concentration is below 2 g/L TDS. Note that in this study the pumping energy of MCDI is not included. Unlike RO, MCDI does not need a high pressure to press water through the membrane, but instead, water is transported only in between the two ion-exchange membranes, which does not require a substantial pressure drop between the influent and the effluent of the stack. Since our system is not optimized for industrial objectives, the energy consumption can be further reduced by e.g. optimizing the system or reducing the electronic resistances. To conclude, MCDI has the potential to compete with RO to desalinate brackish water, and the future research on MCDI could focus on reducing the energy consumption, which is the most relevant issue to the application.
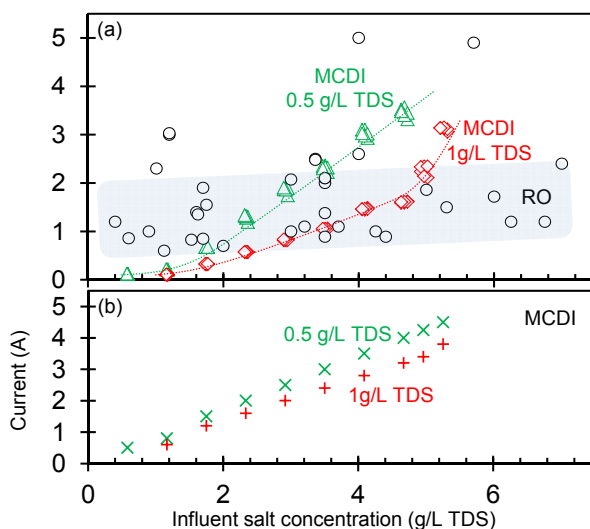
Fig. 6.3. (a) Comparison of energy consumption between MCDI and Reverse Osmosis. Triangles: energy consumption of MCDI to treat influent salt concentration to < 0.5 g/L TDS (palatable drinking water). Diamonds: energy consumption of MCDI to treat influent salt concentration to < 1 g/L TDS (limit drinking water). Circles: RO data. The data sources for RO are listed in Appendix D. Dashed lines are for guiding the eyes. (b) Electrical adsorption current (I_{ads}) applied to the MCDI stack in order to achieve the effluent salt concentration levels for the two different effluent salt concentrations.

6.5 General conclusions and perspectives

In this thesis, we have investigated many aspects of the capacitive deionization technologies, such as the fundamental electrical double layer properties of carbon electrodes under equilibrium conditions, advantages of the use of ion-exchange membranes, and operational modes for (M)CDI. We used the modified Donnan model combined with the transport model to further understand the adsorption and transport process of (M)CDI. Future research should focus on further optimization of the (M)CDI system in the following respects:

● Investigate the most suitable porous carbon electrodes, which have the optimal p_{mA}/p_{mi} ratio, and highest porosity.

● Improve the design of the system to reduce the ionic transport resistance thereby decreasing the energy consumption by e.g. adding carbon black to the carbon electrodes, coating membranes on the surface of the porous carbon electrodes, etc.

● Investigate the durability of the (M)CDI system, discover its resistance to scaling and biofouling, design proper pre- and post-treatment measures to meet requirements from different applications.

● Besides desalination, discover other possible applications by using the (M)CDI technology, e.g., recover valuable metals from waste streams with or without ion selective membranes.

To conclude, this thesis links the theory to the experimental results of (M)CDI. By fitting the modified Donnan model to the experimental equilibrium data, a series of theoretical properties has been discovered, thereby leading to better understanding of the CDI salt adsorption mechanism. By embedding the validated modified Donnan model into a transport model based on a few reasonable assumptions of electrode and ion-exchange membranes, we are able to reproduce changes of many

variables as a function of time, e.g. salt effluent concentration, electrical current, ion concentration in the macropores, for both CDI and MCDI processes. The constant current operational mode of MCDI was also proposed, in order to advance the feasibility of this technology. Moreover, MCDI was proved to be more energy-efficient than CDI, and in the end, we optimized the operational mode of MCDI by varying the experimental settings so as to reach a maximum salt adsorption rate.

Appendix A   Summary of CDI salt adsorption by using different electrode materials

In this appendix, we summarize reported data from the literature for the important CDI property of salt adsorption per gram of electrode material. Here, data are given as a function of salinity and cell voltage, per gram of both electrodes combined. The experiment in all cases is done in a symmetric cell with the two electrodes of the same mass and material. As can be read off from Table A, reported numbers vary in a large range between ~0.7 and ~15 mg adsorbed salt /g electrode mass.

In Table A, we distinguish the operational mode of CDI into two methods. One is called single-pass (SP)-method, where water is fed from a storage vessel and the salinity (conductivity) of the water leaving the cell is measured directly at the exit of the cell or stack, like what we used in the thesis, see Fig. Aa. In this case the measured effluent salinity will start to drop soon after applying the cell voltage. Later on, however, the effluent (measured) salinity rises again to the inlet value, because the electrodes have reached their adsorption capacity. The effluent water is either discarded or can be recycled to a reservoir container. This reservoir needs to be large to ensure that concentrations here only change very slightly within the adsorption half of the cycle, say less than 1%, to make sure that the influent concentration remains virtually constant during the cycle. In another common approach, called the batch-mode (BM) method, the recycling reservoir is much smaller, and it is in this container where the water conductivity is measured, which steadily drops during the ion adsorption step to reach a constant final value, see Fig. Ab.
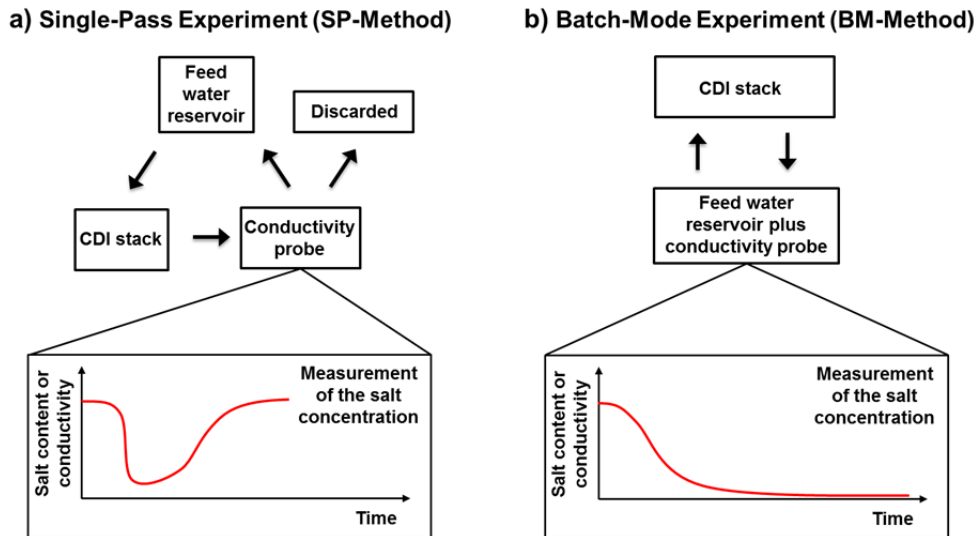
Fig. A. Schematic of two designs for CDI experiments. (a) Single-pass experiment (SP-method): The water conductivity is measured at the exit of the stack, or cell, and the outflow is discarded afterwards or recycled to a large container. (b) Batch-mode experiment (BM-method): The conductivity is measured in a (small) recycle beaker.

Table A. Overview of NaCl salt adsorption performance reported for different electrode materials applied for CDI.

Ref.	Carbon material	Experimental conditions				NaCl salt adsorption (mg/g)
		Initial salt concentration (mg/L)	Cell voltage (V)	Carbon content (%)	Operational mode	
[136]	ordered mesoporous carbon-carbon nanotube	~46	1.2	80	BM	0.63
[37]	ordered mesoporous carbon	~25	1.2	78	BM	0.68
[36]	ordered mesoporous carbon	~50	0.8	78	BM	0.93
[137]	MnO_2 activated carbon	~25	1.2	n/a	BM	1
[47]	graphene-like nanoflakes	~25	2	80	BM	1.3
[138]	graphene-carbon nanotube	~29	2	90	BM	1.4
[66]	carbon aerogel	~50	1.2	n/a	BM	1.4
		~500	1.2	n/a	BM	2.9
[139]	multi-walled carbon nanotubes	~3000	1.2	n/a	BM	1.7
[51]	graphene	~25	2	100	BM	1.8
[140]	reduced graphene oxide-activated carbon	~50	1.2	n/a	BM	2.9
[141]	reduced graphite oxidate-resol	~65	2	80	BM	3.2
[46]	carbon nanotubes-nanofibers	~110	1.2	100	BM	3.3
[123]	activated carbon	~200	1.5	n/a	SP	3.7
[33]	Ti-O activated carbon cloth	~5844	1	n/a	BM	4.3
[142]	carbon nanofiber webs	~95	1.6	100	BM	4.6
[143]	sulphonated graphite nanosheet	~250	2	72	BM	8.6
[55]	carbon aerogel monoliths	~2922	1.5	100	BM	9.6
[144]	single-walled carbon nanotubes	~23	2	70	BM	0.75
		~292	1.2	n/a	SP	10.5
This thesis	commercial activated carbon electrode	~292	1.2	n/a	SP	10.9
		~1170	1.4	n/a	SP	13
[39]	activated carbon (Norit DLC Super 50)	~292	1.2	85	SP	6.9
		~292	1.4	85	SP	8.4
		~292	1.2	85	SP	12.4
	carbide-derived carbon	~292	1.4	85	SP	14.9

Summary of CDI salt adsorption by using different electrode materials

Appendix B   Electrode property values and parameter settings for the modified Donnan model

In this appendix we present the values of electrode properties, namely total electrode weight m_{tot}, electrode thickness δ_{elec}, electrode density ρ_e, and parameter settings for CDI equilibrium model in Chapters 2 (Table B.1), and parameter settings for MCDI transport model in Chapters 3, 4, 5 (Table B.2).

Table B.1. Values of electrode properties and parameter settings for modified Donnan model for data in Figs. 2.4, 2.5 and 2.6 in Chapters 2. Numbers with symbol ‡ are for Na^+ and Cl^- ions, and † is for Ca^{2+} ion (Fig. 2.5).

Symbols	Description	Value			Dimension
		Fig. 2.4	Fig. 2.5	Fig. 2.6	
m_{tot}	total electrode weight	8.5	10.75	8	g
δ_{elec}	electrode thickness	270	362	270	μm
ρ_e	electrode density	0.58	0.55	0.55	g/mL
p_{mi}	porosity of micropores	0.37	0.33	0.37	
$C_{St,vol,0}$	volumetric Stern layer capacitance (low charge limit)	0.12	0.12	0.12	GF/m^3
α	parameter to describe the non-linear part of Stern capacity	17.3	17.3	35	F·m^3/mol^2
μ_{att}	chemical attraction term between ions and carbon	2	1.4	1.4‡ 2.5†	kT

Table B.2. Parameter settings for theoretical (M)CDI transport process model for Chapters 3, 4 and 5. Numbers with symbol † are for section 3.5.1 (Fig. 3.4), and ‡ for section 3.5.2 (Figs. 3.5-3.7) in Chapter 3. In Chapter 4, numbers with subscripts *cc* are for constant current operation (Figs. 5.1-5.3) and subscripts *cv* denote constant voltage operation (Figs. 5.4-5.5). 'n/a' denotes the parameters which are not applicable at certain cases.

Symbols	Description	Value Chapter 3	Value Chapter 4	Value Chapter 5	Dimension
m_{tot}	total electrode weight	8.5† 10.75‡	10.75	10.75	g
δ_{elec}	electrode thickness	270† 362‡	362	362	um
ρ_e	electrode density	0.58† 0.55‡	0.55	0.55	g/mL
p_{mi}	porosity of micropores	0.37† 0.30‡	0.3	0.3	
p_{mA}	porosity of macropores	0.3 0.3	0.3	0.3	
$C_{St,vol,0}$	volumetric Stern layer capacitance (low charge limit)	0.12 0.12	0.12	0.12	GF/m³
α	parameter to describe non-linear part of Stern capacity	17.3 17.3	17.3	17.3	F·m³/mol²
R_{elec}	specific electrode resistance	0.108	0.108	0.108cc 0.108cv	W·mol/m
X	fixed membrane charge density	n/a† 8000‡	3000	3000cc 8000cv	mol/m³
D	ion diffusion coefficient in the spacer channel	1.68	1.68	1.68	10^9 m²/s
D_{mem}	ion diffusion coefficient in the membrane	n/a† 0.168‡	1.12	1.12cc 0.168cv	10^9 m²/s
V_{sp}	total volume of one spacer channel	0.147	0.147	0.147	mL
V_{elec}	total volume of one electrode	0.114† 0.153‡	0.153	0.153	mL
V_{dead}	dead volume in the stack	50† n/a‡	n/a	n/a	mL
β	fraction of total flow going through one electrode	0%† 0.25 %‡	1%	1%cc 0.25%cv	
μ_{att}	chemical attraction term between ions and carbon	2† 1.4‡	1.4	1.4	kT
M	number of sub-cells in the model	6	6	6	
C_{cap}	capacitance in the external circuit	n/a	n/a	2cc n/acv	mF/m²

Appendix C   Modification on the MCDI electric circuit model by placing a small capacitance in Parallel

In this appendix we present a schematic diagram of the electric circuit analogue of the MCDI system, see Fig. D. In our numerical code, to avoid problems that occur when we apply a step change in current to the MCDI cell, we have placed a very small capacitance in the external circuit, C_{cap}=2 mF/m^2, parallel to the MCDI cell, so the applied electrical current, I_{max}, will first saturate the small capacitor and then charge the system with current I_{tot}, according to $\dfrac{\mathrm{d}V_{cell}}{\mathrm{d}t} = \dfrac{I_{max} - I_{tot}}{C_{cap}}$.

Initially, because of the spacer channel resistance, all the applied current, I_{max}, goes to the external capacitor, thus initially the current to the MCDI cell will be zero, I_{tot}=0. However, in time, when the external capacity saturates, I_{cap} becomes zero, and the average current into the MCDI cell, I_{tot}, will approach the value of I_{max}. Note that in the model I_{tot} distributes self-consistently over the M numerical sub-cells in one actual cell, see Fig. 3.2 in Chapter 3.

DC power source

I_{max}

I_{cap}

external capacitor, C_{cap}

I_{tot}
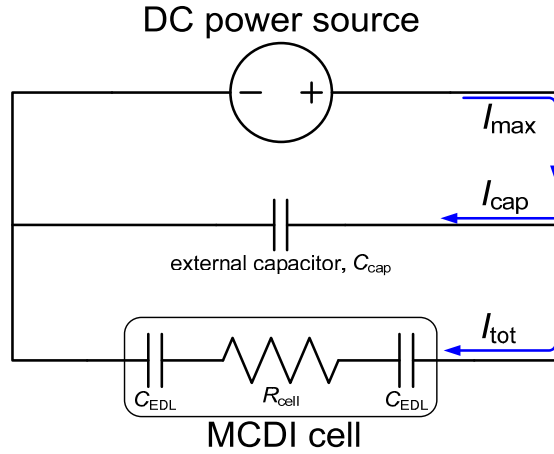
C_{EDL} R_{cell} C_{EDL}

MCDI cell

Fig. C. Electrical circuit analogue for MCDI cell combined with external capacity. Here, I_{max} is the constant applied electrical current, part of which, I_{cap}, will be used to charge the external capacitor, C_{cap}, which represents external wires and connections. I_{tot} depicts the electrical current going into the MCDI cell.

Appendix D   Summary of energy consumption of reverse osmosis plants

In this appendix, we present various data of Reverse Osmosis plants found in the literature [145-154] used for the comparison of energy consumption between MCDI and RO in Chapter 6.

Table D. Examples of configurations of reverse osmosis plants.

Location	Feed water concentration (g/L)	Capacity (m³/d)	Energy Consumption (kWh/m³)	Water cost (US$/m³)	Year of data access	Water Recovery	Reference
Elhamarawien, EG	3.5‡	53	0.89	11.6	1986	n/a	[145]
White Cliffs, AU	3.5‡	0.5	2	9	2003	n/a	[145]
Solar flow, AU	5‡	0.4	1.86	10~12	1982	n/a	[145]
Conception del Oro, MX	3‡	0.71	6.9	n/a	1982	n/a	[145]
Mesquite, US	3.5‡	1.5	1.38	3.6	2003	n/a	[145]
Denver, US	1.6‡	1.5	1.4	6.5	2003	n/a	[146]
Hassi-Khebi, DZ	3.5‡	0.85	2.1	10	1987	n/a	[146]
Pine Hill, AU	5.3‡	1.1	1.5	3.7	2008	n/a	[146]
Ksar Ghilene, TN	3.5‡	7	2.1	6.5	2005	n/a	[146]
Heelat Ar Rakah, OM	1.01‡	5	2.3	6.5	1999	n/a	[146]
Univ. of Almeria, ES	3.36‡	8.09	2.5	2.5	1988	n/a	[146]
Coite-Pedreiras, BR	1.2‡	6	3	12.8	2000	n/a	[146]
Seriwa, Perth, AU	5.7‡	0.55	4.9	9.6	1982	n/a	[146]
Lampedusa, IT	8‡	40	5.5	10.6	1990	n/a	[146]
VARI-RO, US	7‡	3.6	2.4	9	1999	n/a	[146]
Baja California Sur, MX	4‡	11.5	2.6	9.8	2005	n/a	[146]
Lipari, IT	8‡	13.7	6.5	10.6	1991	n/a	[146]
Univ. of Athens, GR	0.4‡	1000	7.7	2.8	2000	n/a	[146]
Cadarache, FR	2†	15	0.7	n/a	1978	n/a	[147]
El Hamrawein, EG	3†	216	1	n/a	1981	n/a	[148]
Maagan Michael, ES	4‡	6.8	5	3	1997	n/a	[149]
Caple, ES	6†	4000	1.72	0.29	2002	n/a	[150]
Vall D'Uixo, ES	1.125†	7500	0.6	0.14	1997	n/a	[150]
Nules, ES	1.529†	6000	0.83	0.17	2002	n/a	[150]
Cuevas de Almanzora, ES	6.75†	25000	1.2	0.246	2003	n/a	[150]
Drenajes, ES	6.25†	6000	1.2	0.3	1997	n/a	[150]
Terciario Alacanti Norte, ES	1.75†	5000	1.55	0.36	2010	n/a	[150]

Citrico del Andevalo, ES	0.6†	1200	0.86	0.14	2007	90%	[150]
Sidmed, ES	0.4†	750	1.2	0.22	1995	n/a	[150]
Xeresa Golf, ES	1.7†	5000	0.85	0.29	2003	n/a	[150]
Alicante University, ES	3.2†	450	1.1	0.22	1996	n/a	[150]
AENA, ES	0.9†	200	1	0.18	1999	n/a	[150]
San Vicente del Raspeig, ES	4.25†	100	1	0.25	1998	n/a	[150]
Gaza Strip area	1.625	60	1.35	n/a	1993	75%	[151]
Ceara, BR	1.2‡	6	3.03	n/a	2000	27%	[152]
Gran Canaria, ES	3.36‡	0.8	2.48	n/a	1988	26-64%	[152]
Algeria	3‡	22.4-26.4	2.075	n/a	1988	24-40.7%	[152]
Egypt	4.4‡	0.24	0.89	n/a	1986	51%	[152]
Jordan	1.7‡	0.22-1.27	1.9	n/a	2011	22%	[153]
Kerkennah Islands, TN	3.7	3300	1.1	n/a	2003	75%	[154]

In Table D, feed water concentrations presented with ‡ are converted from ppm, and with † are converted from conductivity measurement (μS/cm). During conversion 1 ppm is assumed to be equal to 1 mg/L, and 1μS/cm is assumed to be equal to 0.5 mg/L, according to Refs. [155, 156]. "n/a" denotes "not available".

Appendix E   Outline of Gouy-Chapman-Stern model

In this appendix, we will generally outline the Gouy-Chapman-Stern (GCS) model, which is the classical electrical double layer (EDL) theory, used for salt adsorption and charge transferred at equilibrium in Capacitive Deionization. The GCS model considers two layers at the surface of a plane electrode in the aqueous phase. The two layers are the Stern layer and the diffuse layer. The Stern layer is assumed to be the inner layer attaching the electrode surface, where ions are absent, and only solvent molecules (H_2O in our case) exist. The outside boundary of the Stern layer is also called Outer Helmholtz Plane (OHP), from which the diffuse layer extends outwards to the bulk solution. It is assumed that in the diffuse layer the ions obey a Boltzmann distribution law. Fig. E illustrates an analogy to the EDL disregarding any specific adsorption that we also ignore in our work. Normally the length of the diffuse layer is defined by the Debye length λ_D, for a 1:1 salt $\lambda_D = \left(8\pi \cdot c \cdot N_{av} \cdot \lambda_B\right)^{-\frac{1}{2}}$, where c is the salt concentration of the electrolyte, N_{av} is the Avogadro number, and λ_B is the Bjerrum length (=0.72 nm in water at room temperature). In a dilute electrolyte, e.g. 5~20 mM NaCl, λ_D is usually several nm, which is larger than the micropore diameter (~2 nm) of the porous carbon electrode. As a result, strong double layer overlap will occur, which is also the reason why we use the modified Donnan model to describe the EDL in the carbon micropores.
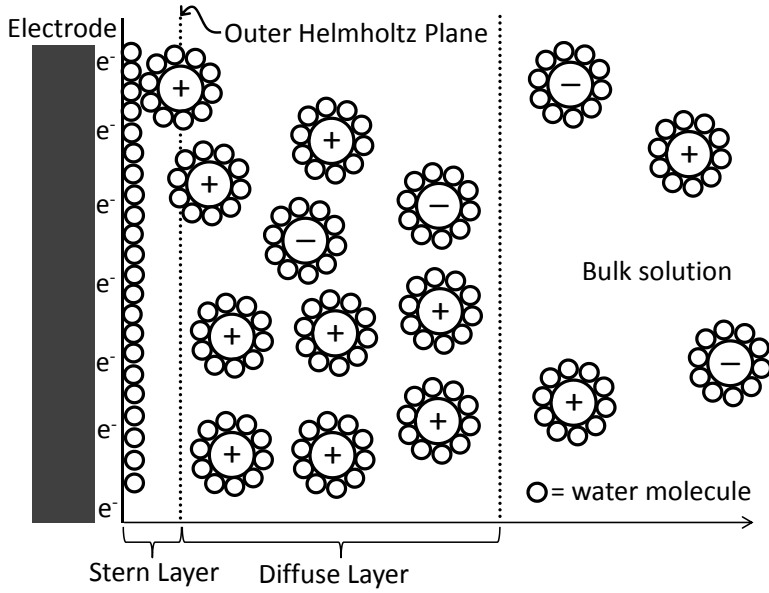
Fig. E. Schematic diagram of the electrical double layer in the absence of specific adsorption. "e⁻" represents electrons on the negatively charged electrode surface. From the Outer Helmholtz Plane, cations are absorbed until the diffuse layer vanishes. Anions are repelled away from the electrode surface. The x-axis presents the distance from the electrode surface.

In the GCS model, the surface charge density σ is given by

$$\sigma = \left(2RT\varepsilon\right)^{\frac{1}{2}} \left\{ \sum_j c_{j,0} \left[\exp(-z_j\Delta\phi_d) - 1\right]\right\}^{\frac{1}{2}}, \tag{E.1}$$

where ε is the dielectric permittivity of the electrolyte, R is the ideal gas constant, j denotes the ion species, $c_{j,0}$ is the ion concentration in the bulk solution, and z_j denotes the valence of the ion. Eq. E.1 can be applied for any combination of ions in a solution, such as NaCl, $CaCl_2$ or the mixture of them. For a z:z electrolyte, e.g. NaCl, or $MgSO_4$, Eq. E.1 becomes

$$\sigma = \left(8RT\varepsilon c_0\right)^{\frac{1}{2}} \sinh\left(\frac{1}{2}z\Delta\phi_d\right), \tag{E.2}$$

where c_0 is the salt concentration in the bulk solution, and z=z+=|z-|.

On the electrode surface the ion distribution obeys the Boltzmann distribution law, and thus the ion concentration at distance x from the OHP $c_j(x)$ can be related to the ion concentration in the bulk solution, $c_{j,0}$, given by

$$c_j(x) = c_{j,0} \exp(-z_j \phi_d(x)),$$ (E.3)

where $\phi(x)$ denotes the potential at distance x in the diffuse layer. Therefore, the excess number of ion j at any distance from the OHP is

$$c_j(x) - c_{j,0} = c_{j,0} \left[\exp(-z_j \phi_d(x)) - 1 \right].$$ (E.4)

By integrating Eq. E.4, the general equation for excess surface ion adsorption is

$$\Gamma_j = c_{j,0} \int_0^\infty \left[\exp(-z_j \phi_d(x)) - 1 \right] dx.$$ (E.5)

For 1:1 salt, Eq. E.5 can be integrated for both cation (Eq. E.6) and anion (Eq. E.7),

$$\Gamma_+ = 2\lambda_d c_0 \left(\exp\left(-\frac{1}{2} \Delta\phi_d \right) - 1 \right),$$ (E.6)

$$\Gamma_- = 2\lambda_d c_0 \left(\exp\left(\frac{1}{2} \Delta\phi_d \right) - 1 \right),$$ (E.7)

where Γ_+ is the excess surface cation adsorption, and Γ_- is the excess surface anion adsorption. Thus the total salt adsorption per surface area Γ_{salt} is the sum of the two, given by Eq. E.8:

$$\Gamma_{salt} = \Gamma_+ + \Gamma_- = 2\lambda_d c_0 \left(\exp\left(-\frac{\Delta\phi_d}{2} \right) + \exp\left(\frac{\Delta\phi_d}{2} \right) - 2 \right) = 4\lambda_d c_0 \left(\cosh\frac{\Delta\phi_d}{2} - 1 \right),$$ (E.8)

and the surface charge density is the difference of Γ_+ and Γ_-, multiplied by the Faraday constant, according to

$$\sigma = F(\Gamma_+ - \Gamma_-) = 2\lambda_d c_0 F \left(\exp\left(-\frac{\Delta\phi_d}{2} \right) - \exp\left(\frac{\Delta\phi_d}{2} \right) \right) = 4\lambda_d c_0 F \left(\sinh\frac{\Delta\phi_d}{2} \right),$$ (E.9)

By taking the ratio of surface salt adsorption to surface charge, the charge efficiency of the 1:1 salt can be derived,

$$\Lambda = \frac{\Gamma_{salt}}{\sigma/F} = \frac{\cosh\dfrac{\Delta\phi}{2} - 1}{\sinh\dfrac{\Delta\phi}{2}} = \tanh\frac{\Delta\phi_d}{4} \; . \tag{E.10}$$

For 1:2 salt, and for mixed electrolyte solutions, a numerical solution for salt adsorption is given in Ref. [157], however, it is also possible to derive the algebraic equation for those more complex conditions. For instance, we derived the equations for the mixture of NaCl and $CaCl_2$,

$$\Gamma_{Na} = \beta_2 \cdot \beta_1 \ln\frac{1 + 2\beta_1(u+1) + 2\sqrt{u\beta_1}\sqrt{(u+2)\beta_1 + 1}}{1 + 4\beta_1 + 2\sqrt{\beta_1(3\beta_1 + 1)}} \; , \tag{E.11}$$

$$\Gamma_{Ca} = \beta_2 \cdot (\sqrt{u}\sqrt{(u+2)\beta_1 + 1} - \sqrt{3\beta_1 + 1}) - \frac{1}{2}\Gamma_{Na} \; , \tag{E.12}$$

where $u = \exp(-\Delta\phi_d)$, the ratio of ion concentrations outside the EDL is given by $\beta_1 = c_{Ca,0}/c_{Na,0}$, and $\beta_2 = \sqrt{\varepsilon V_T c_{Na,0}/(2F)}$.

References

1. Cipollina, A., *Seawater desalination : conventional and renewable energy processes* 2009, Berlin: Springer.
2. Shiklomanov, I.A. *Appraisal and assessment of world water resources*. Water Int., 25, 11 (2000).
3. Buerkle, T. *Making every drop count*. 2007 [cited 2007 14 Feb.]; Available from: http://www.fao.org/newsroom/en/news/2007/1000494/index.html.
4. Shannon, M.A., P.W. Bohn, M. Elimelech, J.G. Georgiadis, B.J. Marinas, and A.M. Mayes. *Science and technology for water purification in the coming decades*. Nature, 452, 301 (2008).
5. Semiat, R. *Energy Issues in Desalination Processes*. Environmental Science & Technology, 42, 8193 (2008).
6. Schiermeier, Q. *Purification with a pinch of salt*. Nature, 452, 260 (2008).
7. Anderson, M.A., A.L. Cudero, and J. Palma. *Capacitive deionization as an electrochemical means of saving energy and delivering clean water. Comparison to present desalination practices: Will it compete?* Electrochimica Acta, 55, 3845 (2010).
8. Fritzmann, C., J. Löwenberg, T. Wintgens, and T. Melin. *State-of-the-art of reverse osmosis desalination*. Desalination, 216, 1 (2007).
9. Avlonitis, S.A., K. Kouroumbas, and N. Vlachakis. *Energy consumption and membrane replacement cost for seawater RO desalination plants*. Desalination, 157, 151 (2003).
10. Arras, W., N. Ghaffour, and A. Hamou. *Performance evaluation of BWRO desalination plant — A case study*. Desalination, 235, 170 (2009).
11. Wilson, J.R., *Demineralization by electrodialysis*. 1960: Butterworths Scientific Publications.
12. Sonin, A.A. and R.F. Probstein. *A hydrodynamic theory of desalination by electrodialysis*. Desalination, 5, 293 (1968).
13. Ortiz, J.M., E. Expósito, F. Gallud, V. García-García, V. Montiel, and A. Aldaz. *Desalination of underground brackish waters using an electrodialysis system powered directly by photovoltaic energy*. Solar Energy Materials and Solar Cells, 92, 1677 (2008).
14. Strathmann, H., *Electrodialysis* in *Membrane Separation System: Recent Developments and Future Directions*, R.W. Baker, Editor. 1991, Noyes Data Corporation: Park Ridge, NJ. p. 396.
15. Cath, T.Y., A.E. Childress, and M. Elimelech. *Forward osmosis: Principles, applications, and recent developments*. Journal of Membrane Science, 281, 70 (2006).
16. Sharma, P. and T.S. Bhatti. *A review on electrochemical double-layer capacitors*. Energy Conversion and Management, 51, 2901 (2010).
17. Porada, S., R. Zhao, A. van der Wal, V. Presser, and P.M. Biesheuvel. *Review on the Science and Technology of Water Desalination by Capacitive Deionization*. Progress in Materials Science, (2013).

18. Blair, J.W. and G.W. Murphy, *Electrochemical Demineralization of Water with Porous Electrodes of Large Surface Area*, in *SALINE WATER CONVERSION*. 1960, American Chemical Society. p. 206.

19. Arnold, B.B. and G.W. Murphy. *Studies on electrochemistry of carbon and chemically modified carbon surfaces*. Journal of Physical Chemistry, 65, 135 (1961).

20. Murphy, G.W. and D.D. Caudle. *Mathematical theory of electrochemical demineralization in flowing systems*. Electrochimica Acta, 12, 1655 (1967).

21. Murphy, G.W., J.L. Cooper, and J.A. Hunter, *Activated carbon used as Electrodes in Electrochemical Demineralization of Saline Water*. 1969, U.S. Dept. of the Interior: Washington.

22. Evans, S., M.A. Accomazzo, and J.E. Accomazzo. *Electrochemically Controlled Ion Exchange*. Journal of the Electrochemical Society, 116, 307 (1969).

23. Johnson, A.M., A.W. Venolia, R.G. Wilbourne, J. Newman, C.M. Wong, W.S. Gilliam, S. Johnson, and R.H. Horowitz, *The Electrosorb process for desalting water*. 1970, U.S. Dept. of the Interior: Washington.

24. Johnson, A.M. and J. Newman. *Desalting by Means of Porous Carbon Electrodes*. Journal of The Electrochemical Society, 118, 510 (1971).

25. Soffer, A. and M. Folman. *The electrical double layer of high surface porous carbon electrode*. Journal of Electroanalytical Chemistry and Interfacial Electrochemistry, 38, 25 (1972).

26. Oren, Y. and A. Soffer. *Electrochemical Parametric Pumping*. Journal of the Electrochemical Society, 125, 869 (1978).

27. Oren, Y. *Capacitive deionization (CDI) for desalination and water treatment - past, present and future (a review)*. Desalination, 228, 10 (2008).

28. Avraham, E., Y. Bouhadana, A. Soffer, and D. Aurbach. *Limitation of Charge Efficiency in Capacitive Deionization. I. On the Behavior of Single Activated Carbon.* Journal of the Electrochemical Society, 156, P95 (2009).

29. Avraham, E., M. Noked, Y. Bouhadana, A. Soffer, and D. Aurbach. *Limitations of Charge Efficiency in Capacitive Deionization. II. On the Behavior of CDI Cells Comprising Two Activated Carbon Electrodes.* Journal of the Electrochemical Society, 156, P157 (2009).

30. Farmer, J.C., D.V. Fix, G.V. Mack, R.W. Pekala, and J.F. Poco, *The Use of Capacitive Deionization with Carbon Aerogel Electrodes to Remove Inorganic Contaminants from Water*, in *Low Level Waste Conference*. 1995: Orlando.

31. Zou, L., G. Morris, and D. Qi. *Using activated carbon electrode in electrosorptive deionisation of brackish water*. Desalination, 225, 329 (2008).

32. Ryoo, M.W., J.H. Kim, and G. Seo. *Role of titania incorporated on activated carbon cloth for capacitive deionization of NaCl solution*. Journal of Colloid and Interface Science, 264, 414 (2003).

33. Ryoo, M.W. and G. Seo. *Improvement in capacitive deionization function of activated carbon cloth by titania modification*. Water Research, 37, 1527 (2003).

34. Cohen, I., E. Avraham, M. Noked, A. Soffer, and D. Aurbach. *Enhanced Charge Efficiency in Capacitive Deionization Achieved by Surface-Treated Electrodes and*

by Means of a Third Electrode. Journal of Physical Chemistry C, 115, 19856 (2011).

35. Oh, H.J., J.H. Lee, H.J. Ahn, Y. Jeong, Y.J. Kim, and C.S. Chi. *Nanoporous activated carbon cloth for capacitive deionization of aqueous solution*. Thin Solid Films, 515, 220 (2006).

36. Li, L., L. Zou, H. Song, and G. Morris. *Ordered mesoporous carbons synthesized by a modified sol–gel process for electrosorptive removal of sodium chloride*. Carbon, 47, 775 (2009).

37. Zou, L., L. Li, H. Song, and G. Morris. *Using mesoporous carbon electrodes for brackish water desalination*. Water Research, 42, 2340 (2008).

38. Presser, V., M. Heon, and Y. Gogotsi. *Carbide-Derived Carbons – From Porous Networks to Nanotubes and Graphene*. Advanced Functional Materials, 21, 810 (2011).

39. Porada, S., L. Weinstein, R. Dash, A. van der Wal, M. Bryjak, Y. Gogotsi, and P.M. Biesheuvel. *Water Desalination Using Capacitive Deionization with Microporous Carbon Electrodes*. ACS Applied Materials & Interfaces, 4, 1194 (2012).

40. Pekala, R.W., C.T. Alviso, F.M. Kong, and S.S. Hulsey. *Aerogels derived from multifunctional organic monomers*. Journal of Non-Crystalline Solids, 145, 90 (1992).

41. Yang, C.-M., W.-H. Choi, B.-K. Na, B.W. Cho, and W.I. Cho. *Capacitive deionization of NaCl solution with carbon aerogel-silicagel composite electrodes*. Desalination, 174, 125 (2005).

42. Gabelich, C.J., T.D. Tran, and I.H.M. Suffet. *Electrosorption of Inorganic Salts from Aqueous Solution Using Carbon Aerogels*. Environ Sci Technol, 36, 3010 (2002).

43. Farmer, J.C., D.V. Fix, G.V. Mack, R.W. Pekala, and J.F. Poco. *Capacitive Deionization of NaCl and NaNO[sub 3] Solutions with Carbon Aerogel Electrodes*. Journal of the Electrochemical Society, 143, 159 (1996).

44. Zhang, D., L. Shi, J. Fang, K. Dai, and X. Li. *Preparation and desalination performance of multiwall carbon nanotubes*. Materials Chemistry and Physics, 97, 415 (2006).

45. Zou, L., *Developing Nano-Structured Carbon Electrodes for Capacitive Brackish Water Desalination*, in *Expanding Issues in Desalination*, R.Y. Ning, Editor. 2011: INTECH.

46. Wang, X.Z., M.G. Li, Y.W. Chen, R.M. Cheng, S.M. Huang, L.K. Pan, and Z. Sun. *Electrosorption of NaCl Solutions with Carbon Nanotubes and Nanofibers Composite Film Electrodes*. Electrochemical and Solid-State Letters, 9, E23 (2006).

47. Li, H., L. Zou, L. Pan, and Z. Sun. *Novel Graphene-Like Electrodes for Capacitive Deionization*. Environmental Science & Technology, 44, 8692 (2010).

48. Peng, Z., D.S. Zhang, L.Y. Shi, T.T. Yan, S.A. Yuan, H.R. Li, R.H. Gao, and J.H. Fang. *Comparative Electroadsorption Study of Mesoporous Carbon Electrodes with Various Pore Structures*. Journal of Physical Chemistry C, 115, 17068 (2011).

49. Arulepp, M., J. Leis, M. Latt, F. Miller, K. Rumma, E. Lust, and A.F. Burke. *The advanced carbide-derived carbon based supercapacitor*. Journal of Power Sources, 162, 1460 (2006).

50. Li, J., X. Wang, Q. Huang, S. Gamboa, and P.J. Sebastian. *Studies on preparation and performances of carbon aerogel electrodes for the application of supercapacitor*. Journal of Power Sources, 158, 784 (2006).

51. Li, H.B., T. Lu, L.K. Pan, Y.P. Zhang, and Z. Sun. *Electrosorption behavior of graphene in NaCl solutions*. Journal of Materials Chemistry, 19, 6773 (2009).

52. Li, H., Y. Gao, L. Pan, Y. Zhang, Y. Chen, and Z. Sun. *Electrosorptive desalination by carbon nanotubes and nanofibres electrodes and ion-exchange membranes*. Water Research, 42, 4923 (2008).

53. Jung-Ae, L., P. Nam-Soo, P. Jin-Soo, and C. Jae-Hwan. *Fabrication and characterization of a porous carbon electrode for desalination of brackish water*. Desalination, 238, 37 (2009).

54. Farmer, J.C., S.M. Bahowick, J.E. Harrar, D.V. Fix, R.E. Martinelli, A.K. Vu, and K.L. Carroll. *Electrosorption of Chromium Ions on Carbon Aerogel Electrodes as a Means of Remediating Ground Water*. Energy & Fuels, 11, 337 (1997).

55. Suss, M.E., T.F. Baumann, W.L. Bourcier, C.M. Spadaccini, K.A. Rose, J.G. Santiago, and M. Stadermann. *Capacitive desalination with flow-through electrodes*. Energy & Environmental Science, 5, 9511 (2012).

56. Bourcier, W.L., R.D. Aines, J.J. Haslam, C.M. Schaldach, K.C. O'Brien, and E. Cussler, *Deionization and Desalination Using Electrostatic Ion Pumping*. 2011, Lawrence Livermore National Security, LLC, Livermore, CA: United States.

57. Porada, S., B.B. Sales, H.V.M. Hamelers, and P.M. Biesheuvel. *Water Desalination with Wires*. The Journal of Physical Chemistry Letters, 3, 1613 (2012).

58. Lee, J.-B., K.-K. Park, H.-M. Eum, and C.-W. Lee. *Desalination of a thermal power plant wastewater by membrane capacitive deionization*. Desalination, 196, 125 (2006).

59. Biesheuvel, P.M. and A. van der Wal. *Membrane capacitive deionization*. Journal of Membrane Science, 346, 256 (2009).

60. Kim, Y.-J. and J.-H. Choi. *Improvement of desalination efficiency in capacitive deionization using a carbon electrode coated with an ion-exchange polymer*. Water Research, 44, 990 (2010).

61. Li, H. and L. Zou. *Ion-exchange membrane capacitive deionization: A new strategy for brackish water desalination*. Desalination, 275, 62 (2011).

62. Biener, J., M. Stadermann, M. Suss, M.A. Worsley, M.M. Biener, K.A. Rose, and T.F. Baumann. *Advanced carbon aerogels for energy applications*. Energy & Environmental Science, 4, 656 (2011).

63. Biesheuvel, P.M. *Thermodynamic cycle analysis for capacitive deionization*. Journal of Colloid and Interface Science, 332, 258 (2009).

64. Biesheuvel, P.M., B. van Limpt, and A. van der Wal. *Dynamic Adsorption/Desorption Process Model for Capacitive Deionization*. Journal of Physical Chemistry C, 113, 5636 (2009).

65. Bouhadana, Y., E. Avraham, A. Soffer, and D. Aurbach. *Several basic and practical aspects related to electrochemical deionization of water*. AIChE Journal, 56, 779 (2010).

66. Farmer, J.C., D.V. Fix, G.V. Mack, R.W. Pekala, and J.F. Poco. *Capacitive Deionization of NaCl and NaNO3 Solutions with Carbon Aerogel Electrodes*. Journal of the Electrochemical Society, 143, 159 (1996).

67. Gabelich, C.J., T.D. Tran, and I.H.â.œ. Suffet. *Electrosorption of Inorganic Salts from Aqueous Solution Using Carbon Aerogels*. Environmental Science & Technology, 36, 3010 (2002).

68. Leonard, K.C., J.R. Genthe, J.L. Sanfilippo, W.A. Zeltner, and M.A. Anderson. *Synthesis and characterization of asymmetric electrochemical capacitive deionization materials using nanoporous silicon dioxide and magnesium doped aluminum oxide*. Electrochimica Acta, 54, 5286 (2009).

69. Oren, Y. and A. Soffer. *Water desalting by means of electrochemical parametric pumping*. J Appl Electrochem, 13, 473 (1983).

70. Seo, S.-J., H. Jeon, J.K. Lee, G.-Y. Kim, D. Park, H. Nojima, J. Lee, and S.-H. Moon. *Investigation on removal of hardness ions by capacitive deionization (CDI) for water softening applications*. Water Research, 44, 2267 (2010).

71. Welgemoed, T.J. and C.F. Schutte. *Capacitive Delonization Technology (TM) : An alternative desalination solution*. Desalination, 183, 327 (2005).

72. Xu, P., J.E. Drewes, D. Heil, and G. Wang. *Treatment of brackish produced water using carbon aerogel-based capacitive deionization technology*. Water Research, 42, 2605 (2008).

73. Avraham, E., Y. Bouhadana, A. Soffer, and D. Aurbach. *Limitation of Charge Efficiency in Capacitive Deionization I. On the Behavior of Single Activated Carbon*. Journal of the Electrochemical Society, 156, 95 (2009).

74. Hou, C.-H., P. Taboada-Serrano, S. Yiacoumi, and C. Tsouris. *Electrosorption selectivity of ions from mixtures of electrolytes inside nanopores*. The Journal of Chemical Physics, 129, 224703 (2008).

75. Yang, K.-L., T.-Y. Ying, S. Yiacoumi, C. Tsouris, and E.S. Vittoratos. *Electrosorption of Ions from Aqueous Solutions by Carbon Aerogel: An Electrical Double-Layer Model*. Langmuir, 17, 1961 (2001).

76. Bouhadana, Y., E. Avraham, M. Noked, M. Ben-Tzion, A. Soffer, and D. Aurbach. *Capacitive Deionization of NaCl Solutions at Non-Steady-State Conditions: Inversion Functionality of the Carbon Electrodes*. Journal of Physical Chemistry C, 115, 16567 (2011).

77. Broséus, R., J. Cigana, B. Barbeau, C. Daines-Martinez, and H. Suty. *Removal of total dissolved solids, nitrates and ammonium ions from drinking water using charge-barrier capacitive deionisation*. Desalination, 249, 217 (2009).

78. Huang, Z.-H., M. Wang, L. Wang, and F. Kang. *Relation between the Charge Efficiency of Activated Carbon Fiber and Its Desalination Performance*. Langmuir, (2012).

79. Jeon, B.G., H.C. No, and J.I. Lee. *Development of a two-dimensional coupled-implicit numerical tool for the optimal design of CDI electrodes*. Desalination, 274, 226 (2011).

80.   Lee, J.-H., W.-S. Bae, and J.-H. Choi. *Electrode reactions and adsorption/desorption performance related to the applied potential in a capacitive deionization process*. Desalination, 258, 159 (2010).

81.   Mayes, R.T., C. Tsouris, J.O. Kiggans Jr, S.M. Mahurin, D.W. DePaoli, and S. Dai. *Hierarchical ordered mesoporous carbon from phloroglucinol-glyoxal and its application in capacitive deionization of brackish water*. Journal of Materials Chemistry, 20, 8674 (2010).

82.   Nadakatti, S., M. Tendulkar, and M. Kadam. *Use of mesoporous conductive carbon black to enhance performance of activated carbon electrodes in capacitive deionization technology*. Desalination, 268, 182 (2010).

83.   Pan, L., X. Wang, Y. Gao, Y. Zhang, Y. Chen, and Z. Sun. *Electrosorption of anions with carbon nanotube and nanofibre composite film electrodes*. Desalination, 244, 139 (2009).

84.   Qi, D., L. Zou, and E. Hu. *Electrosorption: An alternative option for desalination*. Research Journal of Chemistry and Environment, 11, 92 (2007).

85.   Ryoo, M.-W. and G. Seo. *Improvement in capacitive deionization function of activated carbon cloth by titania modification*. Water Research, 37, 1527 (2003).

86.   Wang, M., Z.-H. Huang, L. Wang, M.-X. Wang, F. Kang, and H. Hou. *Electrospun ultrafine carbon fiber webs for electrochemical capacitive desalination*. New Journal of Chemistry, 34, 1843 (2010).

87.   Yang, J., L.D. Zou, H.H. Song, and Z.P. Hao. *Development of novel MnO(2)/nanoporous carbon composite electrodes in capacitive deionization technology*. Desalination, 276, 199 (2011).

88.   Porada, S., M. Bryjak, A. Van Der Wal, and P.M. Biesheuvel. *Effect of electrode thickness variation on operation of capacitive deionization*. Electrochimica Acta, 75, 148 (2012).

89.   Van Limpt, B., *Performance relations in Capacitive Deionization systems*, in *Sub-department of environmental science*. 2010, Wageningen University: Wagenigen. p. 182.

90.   Levi, M.D., G. Salitra, N. Levy, D. Aurbach, and J. Maier. *Application of a quartz-crystal microbalance to measure ionic fluxes in microporous carbons for energy storage*. Nature Materials, 8, 872 (2009).

91.   Simon, P. and Y. Gogotsi. *Materials for electrochemical capacitors*. Nature Materials, 7, 845 (2008).

92.   Kondrat, S., C.R. Perez, V. Presser, Y. Gogotsi, and A.A. Kornyshev. *Effect of pore size and its dispersity on the energy storage in nanoporous supercapacitors*. Energy & Environmental Science, 5, 6474 (2012).

93.   Brogioli, D., R. Zhao, and P.M. Biesheuvel. *A prototype cell for extracting energy from a water salinity difference by means of double layer expansion in nanoporous carbon electrodes*. Energy & Environmental Science, 4, 772 (2011).

94.   Biesheuvel, P.M. and A. Van der Wal. *Membrane capacitive deionization*. Journal of Membrane Science, 346, 256 (2010).

95.   Biesheuvel, P.M., Y. Fu, and M.Z. Bazant. *Diffuse charge and Faradaic reactions in porous electrodes*. Physical Review E, 83, 061507 (2011).

96.   Biesheuvel, P.M. and M.Z. Bazant. *Nonlinear dynamics of capacitive charging and desalination by porous electrodes*. Physical Review E, 81, 031502 (2010).

97.   Boon, N. and R. van Roij. *'Blue energy' from ion adsorption and electrode charging in sea and river water*. Molecular Physics, 109, 1229 (2011).

98.   Biesheuvel, P.M. *Evidence for charge regulation in the sedimentation of charged colloids*. Journal of Physics: Condensed Matter, 16, L499 (2004).

99.   Leroy, P., A. Revil, and D. Coelho. *Diffusion of ionic species in bentonite*. Journal of Colloid and Interface Science, 296, 248 (2006).

100. Murad, M. and C. Moyne. *A dual-porosity model for ionic solute transport in expansive clays*. Comput Geosci, 12, 47 (2008).

101. Müllier, M. and B. Kastening. *The double layer of activated carbon electrodes: Part 1. The contribution of ions in the pores*. Journal of Electroanalytical Chemistry, 374, 149 (1994).

102. Levi, M.D., S. Sigalov, G. Salitra, R. Elazari, and D. Aurbach. *Assessing the Solvation Numbers of Electrolytic Ions Confined in Carbon Nanopores under Dynamic Charging Conditions*. The Journal of Physical Chemistry Letters, 2, 120 (2011).

103. Bazant, M., K. Chu, and B. Bayly. *Current-Voltage Relations for Electrochemical Thin Films*. SIAM Journal on Applied Mathematics, 65, 1463 (2005).

104. Grahame, D.C. *The electrical double layer and the theory of electrocapillarity*. Chemical Reviews, 41, 441 (1947).

105. Bazant, M.Z., K. Thornton, and A. Ajdari. *Diffuse-charge dynamics in electrochemical systems*. Physical Review E, 70, 24 (2004).

106. Zhao, R., P.M. Biesheuvel, H. Miedema, H. Bruning, and A. van der Wal. *Charge Efficiency: A Functional Tool to Probe the Double-Layer Structure Inside of Porous Electrodes and Application in the Modeling of Capacitive Deionization*. The Journal of Physical Chemistry Letters, 1, 205 (2010).

107. Biesheuvel, P.M., R. Zhao, S. Porada, and A. van der Wal. *Theory of membrane capacitive deionization including the effect of the electrode pore space*. Journal of Colloid and Interface Science, 360, 239 (2011).

108. Chmiola, J., G. Yushin, Y. Gogotsi, C. Portet, P. Simon, and P.L. Taberna. *Anomalous Increase in Carbon Capacitance at Pore Sizes Less Than 1 Nanometer*. Science, 313, 1760 (2006).

109. Conway, B.E., *Electrochemical supercapacitors: scientific fundamentals and technological applications (POD)*. 1999, New York: Kluwer Academic/plenum.

110. Lee, J.-Y., S.-J. Seo, S.-H. Yun, and S.-H. Moon. *Preparation of ion exchanger layered electrodes for advanced membrane capacitive deionization (MCDI)*. Water Research, 45, 5375 (2011).

111. Zhao, R., M. van Soestbergen, H.H.M. Rijnaarts, A. van der Wal, M.Z. Bazant, and P.M. Biesheuvel. *Time-dependent ion selectivity in capacitive charging of porous electrodes*. Journal of Colloid and Interface Science, 384, 38 (2012).

112. Yaniv, B., A. Eran, S. Abraham, and A. Doron. *Several basic and practical aspects related to electrochemical deionization of water*. AIChE Journal, 56, 779 (2009).

113.   Sigalov, S., M.D. Levi, G. Salitra, D. Aurbach, and J. Maier. *EQCM as a unique tool for determination of ionic fluxes in microporous carbons as a function of surface charge distribution*. Electrochemistry Communications, 12, 1718 (2010).

114.   Szymczyk, A., H. Zhu, and B.a. Balannec. *Pressure-Driven Ionic Transport through Nanochannels with Inhomogenous Charge Distributions*. Langmuir, 26, 1214 (2009).

115.   Biesheuvel, P.M. *Two-fluid model for the simultaneous flow of colloids and fluids in porous media*. Journal of Colloid and Interface Science, 355, 389 (2011).

116.   Levich, V.G. and D.B. Spalding, *Physicochemical hydrodynamics*. Vol. 689. 1962: Prentice-Hall Englewood Cliffs, NJ.

117.   Mafé, S., J. Pellicer, and V. Aguilella. *Ionic transport and space charge density in electrolytic solutions as described by Nernst-Planck and Poisson equations*. The Journal of Physical Chemistry, 90, 6045 (1986).

118.   Sales, B., M. Saakes, J. Post, C. Buisman, P. Biesheuvel, and H. Hamelers. *Direct power production from a water salinity difference in a membrane-modified supercapacitor flow cell*. Environmental Science & Technology, 44, 5661 (2010).

119.   Zhao, R., O. Satpradit, H.H.M. Rijnaarts, P.M. Biesheuvel, and A. van der Wal. *Optimization of salt adsorption rate in membrane capacitive deionization*. Water Research, 47, 1941 (2013).

120.   Helfferich, F.G., *Ion Exchange*. 1962: Dover.

121.   Vetter, K.J., *Electrochemical Kinetics*. 1967: Academic Press.

122.   Biesheuvel, P.M., Y. Fu, and M.Z. Bazant. *Electrochemistry and capacitive charging of porous electrodes in asymmetric multicomponent electrolytes*. Russian Journal of Electrochemistry, 48, 580 (2012).

123.   Kim, Y.-J. and J.-H. Choi. *Enhanced desalination efficiency in capacitive deionization with an ion-selective membrane*. Separation and Purification Technology, 71, 70 (2010).

124.   Kim, Y.-J., J. Hur, W. Bae, and J.-H. Choi. *Desalination of brackish water containing oil compound by capacitive deionization process*. Desalination, 253, 119 (2010).

125.   Nie, C.Y., Y.K. Zhan, L.K. Pan, H.B. Li, and Z. Sun. *Electrosorption of different cations and anions with membrane capacitive deionization based on carbon nanotube/nanofiber electrodes and ion-exchange membranes*. Desalination and Water Treatment, 30, 266 (2011).

126.   Park, B.-H., Y.-J. Kim, J.-S. Park, and J. Choi. *Capacitive deionization using a carbon electrode prepared with water-soluble poly(vinyl alcohol) binder*. Journal of Industrial and Engineering Chemistry, 17, 717 (2011).

127.   Li, H.B. and L. Zou. *Ion-exchange membrane capacitive deionization: A new strategy for brackish water desalination*. Desalination, 275, 62 (2011).

128.   Bouhadana, Y., M. Ben-Tzion, A. Soffer, and D. Aurbach. *A control system for operating and investigating reactors: The demonstration of parasitic reactions in the water desalination by capacitive de-ionization*. Desalination, 268, 253 (2011).

129.   Barragán, V.M., J.P.G. Villaluenga, M.P. Godino, M.A. Izquierdo-Gil, C. Ruiz-Bauzá, and B. Seoane. *Experimental estimation of equilibrium and transport*

properties of sulfonated cation-exchange membranes with different morphologies. Journal of Colloid and Interface Science, 333, 497 (2009).

130. Porada, S., L. Borchardt, M. Oschatz, M. Bryjak, J.S. Atchison, K.J. Keesman, S. Kaskel, P.M. Biesheuvel, and V. Presser. *Direct prediction of the desalination performance of porous carbons for capacitive deionization*. submitted to Energy and Environmental Science, (2013).

131. Galama, A.H., J.W. Post, M.A.C. Stuart, and P.M. Biesheuvel. *Validity of the Boltzmann equation to describe Donnan equilibrium at the Membrane-Solution Interface*. Journal of membrane Science, submitted, (2013).

132. Wu, C., T. Xu, M. Gong, and W. Yang. *Synthesis and characterizations of new negatively charged organic–inorganic hybrid materials: Part II. Membrane preparation and characterizations*. Journal of Membrane Science, 247, 111 (2005).

133. Hwang, G.-J., H. Ohya, and T. Nagai. *Ion exchange membrane based on block copolymers. Part III: preparation of cation exchange membrane*. Journal of Membrane Science, 156, 61 (1999).

134. Komkova, E.N., D.F. Stamatialis, H. Strathmann, and M. Wessling. *Anion-exchange membranes containing diamines: preparation and stability in alkaline solution*. Journal of Membrane Science, 244, 25 (2004).

135. *Health implications of increased salinity of drinking water*. 2008; Available from: http://www.dh.sa.gov.au/pehs/PDF-files/ph-factsheet-water-salinity.pdf.

136. Peng, Z., D. Zhang, L. Shi, and T. Yan. *High performance ordered mesoporous carbon/carbon nanotube composite electrodes for capacitive deionization*. Journal of Materials Chemistry, 22, 6603 (2012).

137. Yang, J., L. Zou, H. Song, and Z. Hao. *Development of novel MnO_2/nanoporous carbon composite electrodes in capacitive deionization technology*. Desalination, 276, 199 (2011).

138. Zhang, D., T. Yan, L. Shi, Z. Peng, X. Wen, and J. Zhang. *Enhanced capacitive deionization performance of graphene/carbon nanotube composites*. Journal of Materials Chemistry, 22, 14696 (2012).

139. Dai, K., L. Shi, J. Fang, D. Zhang, and B. Yu. *NaCl adsorption in multi-walled carbon nanotubes*. Materials Letters, 59, 1989 (2005).

140. Li, H., L. Pan, C. Nie, Y. Liu, and Z. Sun. *Reduced graphene oxide and activated carbon composites for capacitive deionization*. Journal of Materials Chemistry, 22, 15556 (2012).

141. Wang, Z., B. Dou, L. Zheng, G. Zhang, Z. Liu, and Z. Hao. *Effective desalination by capacitive deionization with functional graphene nanocomposite as novel electrode material*. Desalination, 299, 96 (2012).

142. Wang, G., C. Pan, L. Wang, Q. Dong, C. Yu, Z. Zhao, and J. Qiu. *Activated carbon nanofiber webs made by electrospinning for capacitive deionization*. Electrochimica Acta, 69, 65 (2012).

143. Jia, B. and L. Zou. *Wettability and its influence on graphene nansoheets as electrode material for capacitive deionization*. Chemical Physics Letters, 548, 23 (2012).

144. Li, H., L. Pan, T. Lu, Y. Zhan, C. Nie, and Z. Sun. *A comparative study on electrosorptive behavior of carbon nanotubes and graphene for capacitive deionization*. Journal of Electroanalytical Chemistry, 653, 40 (2011).

145. Al-Karaghouli, A.A. and L.L. Kazmerski, *Renewable Energy Opportunities in Water Desalination*, in *Desalination, Trends and Technologies*, M. Schorr, Editor. 2011, InTech.

146. Ghermandi, A. and R. Messalem. *Solar-driven desalination with reverse osmosis: The state of the art*. Desalination and Water Treatment, 7, 285 (2009).

147. Maurel, A. *Dessalement et energies nouvelles*. Desalination, 31, 489 (1979).

148. Libert, J.J. and A. Maurel. *Desalination and renewable energies-a few recent developments*. Desalination, 39, 363 (1981).

149. Weiner, D., D. Fisher, E.J. Moses, B. Katz, and G. Meron. *Operation experience of a solar- and wind-powered desalination demonstration plant*. Desalination, 137, 7 (2001).

150. Martinesz, D.Z., C.G.G. Soto, and R.B. Candel. *Experiences on desalination of different brackish water*. in *IDA World Congress*. 2009. Atlantis, The Palm-Dubai, UAE.

151. Frenkel, V. and T. Gourgi. *Brackish water RO desalination plant in the Gaza Strip*. Desalination, 101, 47 (1995).

152. de Carvalho, P.C.M., D.B. Riffel, C. Freire, and F.F.D. Montenegro. *The Brazilian experience with a photovoltaic powered reverse osmosis plant*. Progress in Photovoltaics: Research and Applications, 12, 373 (2004).

153. Qiblawey, H., F. Banat, and Q. Al-Nasser. *Performance of reverse osmosis pilot plant powered by Photovoltaic in Jordan*. Renewable Energy, 36, 3452 (2011).

154. Fethi, K. *Optimization of energy consumption in the 3300 m3/d RO Kerkennah plant*. Desalination, 157, 145 (2003).

155. AppsLabrotaries. [cited 2013 Feb. 11]; Available from: http://appslabs.com.au/salinity.htm.

156. BroadsAuthority. [cited 2013 Feb. 11]; Available from: http://www.broads-authority.gov.uk/broads/live/managing/rivers-and-broads/broads-water-quality-partnership/Guide_to_the_relatioinship_between_salinity_measures.pdf.

157. Mohilner, D. *The electrical double layer*. Electroanalytical chemistry, 1, 331 (1966).

Summary

In Capacitive Deionization (CDI), the use of porous carbon electrodes adsorb charged ions from salt streams, thus producing fresh water, which has relatively low energy consumption than Reverse Osmosis for the desalination of brackish water. However, a major concern associated with the CDI is the salt adsorption mechanism. Previous studies based on the classic electrical double layer (EDL) theory relate the salt adsorption capacity to the effective surface area of the electrode. Thus selection and evaluation of carbon material for the CDI applications are basically based on the measured BET area. However, this method has its innate deficiency: In the classical Gouy-Chapman-Stern model, the thickness of the diffuse layer is normally larger than the size of the micropores of the porous carbon material, leading to a strong double layer overlap. This physical defect can be amended by assuming a uniform potential drop between anywhere in the micropores (regardless of the distance from the micropore surface to any location in the micropores) and the macropores (where the electrical neutrality holds) of the electrodes. Therefore in **Chapter 2**, a novel model based on the above mentioned assumption was set up, which is called modified Donnan (mD) model, in order to provide with a more realistic explanation of salt adsorption and charge distribution within the electrode structure.

Chapter 2 detailed the mD model and reproduced the equilibrium data of salt adsorption and charge. By fitting the theoretical results to the experimental ones, the structure of the EDLs can be further characterized: Stern layer capacitance, potential drops across the double layer, microporosity, and micropore charge can all be obtained via the fitting procedure. In **Chapter 2**, not only can the mD model be used for describing 1:1 salt (e.g. NaCl), but also it can be used for 1:2 salt (e.g. $CaCl_2$) and mixtures (e.g. $NaCl/CaCl_2$). The extensive use of the mD model on one

side proves its reliability, and on the other side validates the assumption of the two-porosity structure of the porous electrodes (microporosity and macroporosity).

Because (membrane) capacitive deionization is a transport process, only the equilibrium modeling work is not enough to understand the whole adsorption/desorption process. Thus, in **Chapter 3**, the mD model was embedded into a transport model, where the ion-exchange membrane properties were also included. With those efforts, it is possible to understand the salt adsorption/charging and the salt desorption/discharging processes, e.g. the concentration change in the macropores can be plotted as a function of time. Also this transport model helps us to understand the advantage of using ion-exchange membranes in CDI, e.g. during the adsorption step, the salt concentration in the macropores can increase above the salt concentration in the spacer channel, which in other words means macropores become another space for salt storage apart from the EDLs in the micropores. Except for the theoretical work, in **Chapter 3**, the salt adsorption capacities of CDI and MCDI are also compared, showing that MCDI can adsorb more than 20% salt than CDI in the "constant voltage mode". Moreover, during the desorption step, if the cell voltage is reversed, the salt adsorption can be further enhanced.

As a continuation of **Chapter 3**, **Chapter 4** focuses on operational modes. The classical operational mode of (M)CDI exists for decades, which is during the salt adsorption step applying a constant voltage across the CDI cell, and during the salt desorption step short-circuiting the cell or even reversing the electrical polarity. However, this way can not ensure a constant, unchangeable effluent during the salt adsorption phase. Therefore in **Chapter 4**, we introduced a novel operational mode for MCDI, which is named as "constant current mode". In this operational mode, a constant electrical current is applied through the cell during the adsorption step,

which produces effluent with a constant and unchangeable concentration. Furthermore, by adjusting the current level or the flowrate, the concentration of the product can be tailored according to the needs of various applications. Despite the operational mode, another important aspect for (M)CDI and also for other desalination techniques is the energy consumption. In **Chapter 4**, the energy consumption of MCDI for both the "constant current mode" and the "constant voltage mode" is compared with that of CDI, which showed that MCDI consumes much less energy to remove one salt ion than CDI in both cases. Those advantages by using the ion-exchange membranes drive the research towards how to optimize the operation of MCDI in order to obtain maximum salt adsorption per unit time.

Following this line of thought, **Chapter 5** defined a new term "ASAR" (average salt adsorption rate). Together with the water recovery (WR), they evaluate the salt adsorption performance in one MCDI cycle. ASAR depicts the amount of salt removal in one MCDI cycle per cycle time, and WR shows the ratio of produced fresh water to total saline water volume. In this chapter, a series of input parameters, namely influent salt concentration, water flowrate, adsorption and desorption current, desorption voltage, and adsorption and desorption time has been systematically varied in turn. As a result the ASAR and the water recovery (WR), respective to each input parameter, are shown. In the future, the optimization of parameter settings can be advanced in order to obtain the highest ASAR and WR for the operation of a particular MCDI system, where all the parameter settings are varied together at the same time.

In **Chapter 6**, many points which deserve future modifications were discussed, including those properties which are possible to be measured using proper methods, e.g. the two porosities of carbon electrodes, the membrane charge density, and the chemical adsorption term. Furthermore, this chapter suggested a modified

analyzing procedure for salt adsorption and energy consumption. Additionally the energy consumption of MCDI was compared with the energy consumption of Reverse Osmosis as a function of influent salt concentration. It is concluded that at lower salt range, MCDI can be more energy-efficient. Besides the discussions, some future perspectives were provided, followed by general conclusions: Using the combination of the modified Donnan theory and the transport model leads to in-depth understanding of the salt adsorption and charge transfer process, and it is proved from both the salt adsorption and the energy consumption sides that Membrane Capacitive Deionization works better than the conventional Capacitive Deionization.

Samenvatting

Bij capacitieve deionisatie (CDI) worden poreuze elektrodes van koolstof gebruikt om geladen ionen uit zout water te adsorberen, met als resultaat zoet water. Deze manier van ontzouten heeft een relatief lage energieconsumptie vergeleken met het ontzouten van brak water met omgekeerde osmose. Een groot vraagstuk dat samenhangt met CDI is het zoutadsorptiemechanisme. Eerdere studies waren gebaseerd op de klassieke dubbellaag-theorie en relateerden de zoutadsorptie-capaciteit met het effectieve oppervlak van de elektrode. De selectie van het koolstofmateriaal die werden gebruikt voor CDI was in deze eerdere studies gebaseerd op het gemeten oppervlakte van de materialen. Deze aanpak had een ingebouwde fout, namelijk dat in het klassieke Gouy-Chapman-Stern model de dikte van de diffusielaag groter is dan de grootte van de microporiën van de poreuze koolstof en dit leidde tot een sterke overlapping van de dubbellagen. Deze fout kan worden rechtgetrokken door een uniform potentiaalverschil aan te nemen tussen elke plek in de microporiën (onafhankelijk van de afstand van het oppervlak van de microporie tot de locatie in de microporie), en de macroporiën (welke elektrisch neutraal zijn) van de elektrodes. Een nieuw model met de hierboven genoemde aanname is hiervoor ontwikkeld in **hoofdstuk 2.** Dit is het gemodificeerde Donnan (mD) model, welke een realistischer beeld geeft van de zoutadsorptie en verdeling van de lading over de interne structuur van de elektrode.

In **hoofdstuk 2** worden evenwichtsberekeningen van zoutadsorptie en lading, verkregen met het mD model, vergeleken met experimenteel verkregen data. Door het fitten van de theoretische resultaten met de experimentele resultaten kan een beter inzicht worden verkregen in de structuur van de elektrische dubbellaag en kunnen de volgende parameters worden verkregen: de capaciteit van de Stern laag, het potentiaalverschil over de dubbellaag, en de microporositeit en lading van de

microporiën. In **hoofdstuk 2** wordt het mD model niet alleen gebruikt voor het beschrijven van 1:1 zout (bijv. NaCl), maar wordt het ook gebruikt voor 1:2 zout (bijv. $CaCl_2$) en mengsels (bijv. $NaCl/CaCl_2$). Het uitgebreide gebruik van het mD-model bewijst aan de ene kant de betrouwbaarheid ervan, en bevestigt aan de andere kant de aanname dat de poreuze elektrodes inderdaad uit een structuur met een dubbele porositeit bestaan (microporositeit en macroporositeit).

Capacitieve deionisatie, met of zonder membranen, is een proces waarin transport een grote rol speelt. Alleen het modelleren van evenwichtscondities is daarom niet genoeg om het hele adsorptie/desorptie-proces te begrijpen. In **hoofdstuk 3** is het mD-model samengevoegd met een transportmodel, met inbegrip van de eigenschappen van geladen membranen. Met deze inspanning werd het mogelijk een beter inzicht te verkrijgen in de processen van zout-adsorptie/oplading en zout-desorptie/ontlading, bijvoorbeeld de zoutconcentratie in de macroporiën als functie van tijd. Het transportmodel helpt ook om een beter inzicht te verkrijgen in de voordelen van het gebruik van geladen membranen in CDI. Zo wordt gedurende de adsorptiestap de zoutconcentratie in de macroporiën verhoogd tot boven de zoutconcentratie in het spacerkanaal, met andere woorden, in de macroporiën komt extra ruimte beschikbaar voor de adsorptie van zout naast de elektrische dubbellagen in de microporiën. Naast het theoretische werk wordt ook de capaciteit voor zoutadsorptie van CDI en MCDI met elkaar vergeleken. Hieruit blijkt dat MCDI 20% meer zout kan adsorberen dan CDI in de "constante spanningstechniek". Verder blijkt dat zoutadsorptie verder kan worden verbeterd wanneer de celspanning wordt omgekeerd gedurende de zoutdesorptiestap.

In **hoofdstuk 4** wordt verder ingegaan op manieren van operatie van CDI. In de klassieke techniek, welke al een paar decennia wordt gebruikt om (M)CDI te bedrijven, wordt een constante spanning aangebracht over de CDI-cel gedurende de zoutadsorptiestap, waarna tijdens de desorptiestap de cel wordt kortgesloten, of een omgekeerde spanning wordt over de CDI-cel aangebracht. Deze methode van

bedrijf produceert een uitstroom met een sterk fluctuerende zoutconcentratie gedurende de adsorptiestap. Om dit probleem op te lossen wordt een nieuwe methode van operatie voor MCDI voorgesteld in **hoofdstuk 4**, de "constante stroomtechniek". In deze methode wordt een constante elektrische stroom door de cel geleid gedurende de zoutadsorptiestap, waardoor een uitstroom met een constante zoutconcentratie wordt geproduceerd gedurende de adsorptiestap. Door het aanpassen van de elektrische stroom of het waterdebiet kan de zoutconcentratie in de uitstroom worden aangepast aan de eisen van verschillende toepassingen. Een ander belangrijk aspect voor (M)CDI en andere ontzoutingstechnieken is de energieconsumptie. In **hoofdstuk 4** wordt de energieconsumptie van de "constante spanningstechniek" en "constante stroomtechniek" van MCDI en CDI vergeleken. De energieconsumptie is in beide gevallen gunstiger voor MCDI. MCDI verbruikt dus minder energie voor de verwijdering van zoutionen vergeleken met CDI. Het voordeel van het gebruik van geladen membranen wordt toegepast bij het optimaliseren van MCDI om een maximale zoutadsorptie per tijdseenheid te behalen.

Voortbouwend op deze gedachte wordt in **hoofdstuk 5** een nieuwe term "ASAR" (gemiddelde zoutadsorptiesnelheid) gedefinieerd. Samen met de term "water recovery" (WR) kunnen deze termen worden gebruikt om het adsorptievermogen van één MCDI-cyclus te evalueren. ASAR beschrijft de hoeveelheid zout die wordt verwijderd in één MCDI-cyclus en WR geeft de verhouding aan tussen het volume zoet water en geconcentreerd zout water dat wordt geproduceerd. Een aantal parameters, namelijk de zoutconcentratie van de instroom, het waterdebiet, de elektrische stroom, de desorptiespanning en de adsorptie- en desorptie-tijd zijn individuele en systematisch gevarieerd, met als resultaat uitsluitsel over de invloed van elke parameter op ASAR en WR. Met deze resultaten kunnen in de toekomst alle parameters samen worden gevarieerd om de optimale parameterinstelling te verkrijgen met de hoogst mogelijke waarden voor ASAR en WR.

In **hoofdstuk 6** worden onderwerpen besproken waar in de toekomst aandacht aan moet worden besteed, zoals de meetbare eigenschappen van bijvoorbeeld de grootte van micro- en macroporiën van koolstofelektrodes, de ladingsdichtheid van membranen en de chemische adsorptieterm. Verder wordt in dit hoofdstuk voorgesteld om de analyseprocedure van zoutadsorptie en energieconsumptie te verbeteren. De energieconsumptie van MCDI wordt vergeleken met de energieconsumptie van omgekeerde osmose als functie van de zoutconcentratie van de instroom. De conclusie luidt dat voor lagere zoutconcentraties MCDI het meest energie-efficiënt is. Na deze onderwerpen worden enkele toekomstperspectieven geschetst met de volgende conclusies als resultaat: Het gebruik van de gemodificeerde Donnantheorie en het transportmodel leidt tot een beter inzicht in zoutadsorptie en het proces van ladingtransport, en het is bewezen dat gebruik van membranen leidt tot meer zoutadsorptie en minder energieconsumptie.

提要

电容去离子技术使用多孔活性炭电极从盐水中吸附带电的离子，继而产出淡水。如果在其活性炭电极上附加离子交换膜，则可提升去离子的能力，被称之为膜电容去离子。在用于苦咸水脱盐处理中，电容去离子技术与反渗透等脱盐技术相比能耗较低。然而，长久以来，其对盐分的吸附机理暂无定论。过往基于经典的双电层理论的研究和学习一直将活性炭电极的盐分吸附总量与之有效的比表面积对应、关联起来。因此在电容去离子的应用中，对于活性炭材料的选择和评价一直以来主要基于测量出的比表面积，但是使用比表面积建立模型有其先天的缺陷：在经典的双电层模型之中，扩散层具有一定的厚度，而电容去离子使用的多孔活性炭材料的微孔的孔径要比双电层模型中的扩散层小，这样双电层会有严重的重叠。这个物理上的缺陷是可以弥补的。我们只需要假设活性炭电极微孔中任何地方到电极里呈现电中性的大孔之间的电势差是一致的。

所以，**第二章**建立了一个基于上述假设的全新的模型，从而为盐分吸附和电极中电荷的分布提供一个更加合理的解释。它被称作改良的唐南模型。**第二章**详细描述了改良后的唐南模型，并且基于该模型计算得到了平衡态中盐分的吸附和电量的数据。这些数据与实验中测定得到的是一致的。通过拟合由模型获得的理论结果和实验取得的数据，新的双电层的结构可以被刻画出来：斯特恩层电容，双电层的电势差，微孔孔径，微孔电荷都可以通过拟合的途径得到。改良后的唐南模型

不仅仅可以用于模拟阳离子为一价的盐（如氯化钠）的吸附量，也可以用在阳离子为二价的盐（如氯化钙）和一、二价盐的混合物上。这样对改良后的唐南模型的深度应用一方面证明了它自身的可靠性，另一方面也证实了对于多孔活性炭电极双孔（微孔、大孔）结构的假设。但是由于电容去离子是一个动态传输过程，平衡态的模型不足以让人们理解吸附和解吸附的过程。

因此，**第三章**将改良后的唐南模型嵌入一个传输模型以方便我们可以更好的理解盐分吸附或反吸附的过程，例如，大孔内的盐浓度随时间的变化。同时这个传输模型还包括了离子交换膜的部分从而可以帮助我们理解使用离子交换膜的优点，例如，在吸附阶段，大孔内的盐浓度可以远远的超过液流通路中的盐分的浓度，也就是在使用离子交换膜的前提下，大孔可以被用作除了双电层之外的另一个离子吸附的空间。除了理论的工作，**第三章**也比较了电容去离子系统与膜电容去离子系统的盐吸附量。通过比较得出在恒定电压模式中，膜电容去离子系统可以比电容去离子系统多吸附高达百分之二十的盐分。除此之外，在解吸附的阶段，如果反转工作电压，还可以进一步的提升下一个循环中的盐吸附总量。

作为**第三章**的后续工作，**第四章**主要论述了操作模式。经典的（膜）电容去离子系统的操作模式已经被应用了数十年，它在盐吸附阶段给电容去离子原件施加一个恒定的电压，在解吸附阶段将原件短路或者给原件施加反向电压。然而，这种方法不能在吸附阶段保证出水

浓度恒定不变。所以在第四章里，我们引入膜电容去离子系统的另一种操作模式，也就是恒定电流模式。在这种操作模式的吸附阶段，一个恒定的电流被施加在原件上，这样出水浓度就可以一直保持在稳定状态。另外，通过调节电流强度或进水流速，生产出的脱盐水的浓度可以依照不同应用的需求被调节至最适合的程度。除了操作模式，另一个（膜）电容去离子技术的重要方面是它们的能耗。

第四章比较了在恒定电流和恒定电压两种操作模式下的膜电容去离子系统与电容去离子系统的能耗。我们发现膜电容去离子系统每吸附一个盐离子的能耗在两种操作模式下都要比电容去离子系统低。使用离子交换膜得到的这些优势驱使着我们的研究转向对膜电容去离子系统的操作方法的优化，从而在一定时间内得到最大的盐吸附量。

顺着这个思路，**第五章**引入了一条新术语：平均盐吸附速率。与产水率一起，它们可以对一个膜电容去离子系统的工作循环中的盐吸附的表现进行评价。平均盐吸附速率反映了在一个膜电容去离子系统的工作循环中单位时间的盐吸附量，而产水率则展示了生产出的脱盐水占总进水量的比重。在这一章里，进水盐浓度，水流速，吸附与解吸附电流，解吸附电压，吸附与解吸附时间等一连串的输入参数都被系统地一一测试。这样一来，针对于各个参数的平均盐吸附速率与产水率的变化趋势都被展示出来。将来，所有的参数可以同时被调试，为一个特定的膜电容去离子系统寻找最优的参数配置，以获得最高平均盐吸附速率和产水率。

　　第六章讨论了很多值得在今后研究中改进的方面，包括了一些可以被测量的特性，比如，活性炭的两种孔隙的大小、离子交换膜的电荷密度以及化学吸附单位。接着，这个章节提出了一种经过改进的对于盐吸附和能耗的分析过程，并且比较了在不同入水浓度条件下膜电容去离子技术与反渗透技术的能耗。我们发现，用于处理低浓度盐水时，膜电容去离子技术比反渗透技术更节能。此外，作者还讨论了未来的研究方向，然后对全文做出了总结：改良的唐南模型和传输模型，可以让我们对盐吸附、电荷转移有更好更深的理解；膜电容去离子技术从盐吸附和能耗两方面来讲都比传统的电容去离子技术更好。

Acknowledgements

It was again a rainy day when I was writing the final part of my thesis. I never thought that I could have finally finished this alone. Herein, I would like to thank everyone who has helped and supported me in finishing this thesis during the last four years, and I wish you all the best.

Dear dr. Maarten Biesheuvel, thank you for being my mentor, for leading me into the world of science and for showing me the beauty of CDI, and thank you for being a friend. Without you, I would not have been able to finish my thesis in time. I learned so much from you, and I will always admire your enthusiasm in discovering new things in science, and worship your ability in working with Excel without (almost) clicking the mouse.

Professor Bert van der Wal, thank you very much for being my promotor and for giving me this precious opportunity to work with you on CDI. I will never forget the fruitful discussions with you in Leiden, in Sassenheim, in Wageningen and in Leeuwarden. Professor Huub Rijnaarts, thank you for being my co-promotor and for so many valuable advices. Professor Cees Buisman and Mister Johannes Boonstra, thank you for allowing me to work in Wetsus. It is such a wonderful place! Dr. Henk Miedema, thank you for being my supervisor in the first year and for encouraging me all the time. Dr. Bert Hamelers, thank you for your guidance when I was an MSc student, and for the suggestions on my propositions.

Slawek, my Polish Ziomus, it is my pleasure to have worked with you in Wetsus, and I enjoyed all the happiness we had in our shared time. Johannes Kuipers, Bruno Bastos Sales, and Fei Liu, thank you for all the selfless help, for all the entertainments, and for sharing your wisdom. My office mates, Natalia, Lina and Lieven, thank you for making HX0.01 such a wonderful place in Wetsus, and thank you for all the chats. I also want to thank my colleagues Aga, Maria, Oane, Anna,

Martina, Florian, Adam, Kamuran, Martijn, Joeri, Philipp, Ingo, Luewton, Nadine, Lucia, Daniel, Olivier, Harm, Jan, Jelmer, Roel, Suman, Urania, Bart, Piotr, and many others.

My students, Onanoung, Marta, Alexandra, He Yang, thank you for helping me with the experiments and the literature research.

Yiwen, thank you for your love and for always being at my side. In the end, I want to thank my family, especially my parents, for their support, understanding and love.

About the author

Ran Zhao was born on 7th September 1985 in Ma'anshan, China, where almost everybody was working for the steel industry. He studied in Red Star middle school (1997-2000), and then in Ma'anshan No. 2 high school (2000-2003). After finishing his secondary education, he joined a joint education program between China Agricultural University and Wageningen University, the Netherlands. From 2003 to 2005, he studied in China Agricultural University in Beijing, and from 2005 to 2007, he continued his study in Wageningen University, and got his Bachelor diploma in environmental science. In the same year, he was rewarded the WUR scholarship, with which he was able to continue studying environmental technology in Wageningen University, and he graduated in 2009. From July 2009, he was appointed as a PhD student at the Sub-department of Environmental technology of Wageningen University, and he started the research of Capacitive Deionization in Wetsus, centre of excellence for sustainable water technology, in Leeuwarden.

Netherlands Research School for the
Socio-Economic and Natural Sciences of the Environment

C E R T I F I C A T E

The Netherlands Research School for the
Socio-Economic and Natural Sciences of the Environment
(SENSE), declares that

Ran Zhao

born on 7 September 1985 in Ma'anshan, China

has successfully fulfilled all requirements of the
Educational Programme of SENSE.

Wageningen, 10 September 2013

the Chairman of the SENSE board

Prof. dr. Rik Leemans

the SENSE Director of Education

Dr. Ad van Dommelen

The SENSE Research School declares that **Mr. Ran Zhao** has successfully fulfilled all requirements of the Educational PhD Programme of SENSE with a work load of 45 ECTS, including the following activities:

SENSE PhD Courses
- o Environmental Research in Context
- o Research Context Activity: Co-organizing Wetsus Water Challenge (25-28 May 2010) and creating a Wikipedia page on "Capacitive Deionization" (in English and Chinese)
- o The Art of Modelling

Other PhD and Advanced MSc Courses
- o Techniques for Writing and Presenting Scientific Papers
- o Bath Electrochemistry Winter School
- o Information Literacy PhD including EndNote Introduction
- o Process Dynamics and Control
- o Working Safely in Laboratories, Avans+ school for professionals
- o In-company training of English writing, Eurolangues
- o Intermediate Dutch Lesson, DC Taleninstituut

Management and Didactic Skills Training
- o Organizer of the Wetsus-Kuraray Carbon Workshop
- o Supervision of one MSc thesis, one BSc thesis and two internships

Oral Presentations
- o *How to improve the performance of capacitive deionization by using ion-exchange membranes.* 13th NYM international conference, 21-23 July 2011, Enschede
- o *Time-dependent ion selectivity in capacitive charging of porous electrodes by capacitive deionization.* 10th International Symposium on Electrokinetic, 20-24 May 2012, Tsukuba, Japan
- o *Charge efficiency as a functional tool to probe the double layer structure of capacitive deionization.* Wetsus Internal Congress 2009, 10 November 2009, Leeuwarden
- o *The role of ion exchange membrane in Capacitive Deionization.* Wetsus Internal Congress 2011, 24 November 2011, Leeuwarden

SENSE Coordinator PhD Education

Drs. Serge Stalpers